NTNU – Trondheim
Norwegian University of
Science and Technology

Wet Gas Compressor Performance

A Numerical Investigation of
Thermal-Equilibrium in a Centrifugal
Compressor Exposed to Wet Gas

Erik Mele

Master of Science in Product Design and Manufacturing
Submission date: June 2012
Supervisor: Lars Erik Bakken, EPT
Co-supervisor: Trond Gruner, EPT
Øyvind Hundseid, EPT

Norwegian University of Science and Technology
Department of Energy and Process Engineering

O NTNU

Norges teknisk-
naturvitenskapelige universitet

Institutt for energi- og prosessteknikk

MASTEROPPGAVE

for

Stud.techn. Erik Mele

Våren 2012

Våtgass kompressorytelse

Wet Gas Compressor Performance

Bakgrunn

De fleste store felt i Nordsjøen er utbygd med tradisjonell teknologi. Fokus har i de senere år skiftet mot mindre og mer fjerntliggende felt med begrenset infrastruktur. Utvikling og drift av slike felt krever ny kostnadseffektiv teknologi. Et helt sentralt element her er havbunnsbasert brønnkompresjon for å frakte brønnstrømmen direkte til land, eller mer fjerntliggende prosesseringsanlegg offshore.

Teknologien kan i enkelte tilfelle eliminere behovet for offshore prosessanlegg, noe som kan gi en formidabel kostnadsreduksjon. De fleste leverandører av turbomaskiner satser derfor på utvikling av havbunnsbaserte våtgasskompressorer. Noen få prototype konsepter eksisterer og det foregår i dag utstrakt testing og validering av teknologien.

Ved NTNU er det bygd opp en rigg for å teste våtgass kompressorer og analysere de grunnleggende mekanismene relatert til våtgass kompresjon. Riggen er unik og sentral i blant annet analyse av innvirkningen ulik instrumentering har på ytelsene.

Mål

Ved hjelp av litteratur og eksperimentaldata er det et mål å etablere og validere teknologi for beregning av ytelser til våtgasskompressorer. Herunder inngår spesielt innvirkningen av termisk likevekt, samt plassering og validering av utløpstemperatur i et våtgass strømningsregime.

Oppgaven bearbeides ut fra følgende punkter:

1. Dokumentere relevant litteratur på termisk likevekt ved kompresjon av våtgass fluid.

2. Prosjektering og installering av optimal sensor og system for måling av tørr og våtgass inn og utløpstemperatur.

3. Etablere og validere tørr og våtgass ytelsesmodell mot eksperimentaldata. Herunder inngår validering av effektbalense mellom kompressor og drivenhet..

” - ”

I

Senest 14 dager etter utlevering av oppgaven skal kandidaten levere/sende instituttet en detaljert fremdrift- og eventuelt forsøksplan for oppgaven til evaluering og eventuelt diskusjon med faglig ansvarlig/veiledere. Detaljer ved eventuell utførelse av dataprogrammer skal avtales nærmere i samråd med faglig ansvarlig.

Besvarelsen redigeres mest mulig som en forskningsrapport med et sammendrag både på norsk og engelsk, konklusjon, litteraturliste, innholdsfortegnelse etc. Ved utarbeidelsen av teksten skal kandidaten legge vekt på å gjøre teksten oversiktlig og velskrevet. Med henblikk på lesning av besvarelsen er det viktig at de nødvendige henvisninger for korresponderende steder i tekst, tabeller og figurer anføres på begge steder. Ved bedømmelsen legges det stor vekt på at resultatene er grundig bearbeidet, at de oppstilles tabellarisk og/eller grafisk på en oversiktlig måte, og at de er diskutert utførlig.

Alle benyttede kilder, også muntlige opplysninger, skal oppgis på fullstendig måte. For tidsskrifter og bøker oppgis forfatter, tittel, årgang, sidetall og eventuelt figurnummer.

Det forutsettes at kandidaten tar initiativ til og holder nødvendig kontakt med faglærer og veileder(e). Kandidaten skal rette seg etter de reglementer og retningslinjer som gjelder ved alle (andre) fagmiljøer som kandidaten har kontakt med gjennom sin utførelse av oppgaven, samt etter eventuelle pålegg fra Institutt for energi- og prosessteknikk.

Risikovurdering av kandidatens arbeid skal gjennomføres i henhold til instituttets prosedyrer. Risikovurderingen skal dokumenteres og inngå som del av besvarelsen. Hendelser relatert til kandidatens arbeid med uheldig innvirkning på helse, miljø eller sikkerhet, skal dokumenteres og inngå som en del av besvarelsen.

I henhold til "Utfyllende regler til studieforskriften for teknologistudiet/sivilingeniørstudiet" ved NTNU § 20, forbeholder instituttet seg retten til å benytte alle resultater og data til undervisnings- og forskningsformål, samt til fremtidige publikasjoner.

Besvarelsen leveres digitalt i DAIM. Et faglig sammendrag med oppgavens tittel, kandidatens navn, veileders navn, årstall, instituttnavn, og NTNUs logo og navn, leveres til instituttet som en separat pdf-fil. Etter avtale leveres besvarelse og evt. annet materiale til veileder i digitalt format.

NTNU, Institutt for energi- og prosessteknikk, 16. januar 2012

Olav Bolland
Instituttleder

Lars E Bakken
Faglig ansvarlig/veileder

Medveileder(e)
T Gruner, NTNU
Ø Hundseid, NTNU

Preface

This master thesis was developed between January 16th and June 11th 2012 at the Department of Energy and Process Engineering at the Norwegian University of Science and Technology, NTNU-Trondheim. The master thesis will form the basis for a doctorial project sponsored by Statoil ASA and General Electric.

Trondheim, 08.06.2012

Erik Mele

Abstract

Wet gas compression and subsea compression technology has gained increased focus in the recent years. With aging fields on the Norwegian continental shelf and new discoveries in arctic regions, subsea compression could boost aging gas fields and make remote fields profitable where extraction is difficult. Wet-gas compression could reduce the need for expensive scrubbers and separators and this would be a major economic enhancement to subsea processing. There is currently no standard for wet gas compression as the ASME PTC 10 [1] offers no guidance on this. The complex phenomena encountered in wet-gas compression is not yet fully understood. The present work is concerned with the thermal discharge equilibrium of a wet-gas compressor, as this will strongly influence the performance calculations of the compressor. If there is thermodynamic equilibrium at the discharge, then measurements and calculations become relatively simple. If not, then everything becomes more complex.

A numerical simulation model was established, both for dry and wet gas. An open loop test rig at NTNU was used to compare calculations with experiments to validate the model. This was done with great success for dry gas. For wet gas accurate measurements were not obtained. The working fluid was an air-water mixture, where water was injected into almost saturated air.

To calculate the possible gas discharge temperature under heavily wet conditions, a power balance was also set up. The uncertainties in the frequency converter and the torque meter were too great for reliable power calculations. A new measurement technique has been proposed to be able to measure the gas temperature, utilizing a cyclone to separate the gas prior to the measurements. This technique has not been tested.

The numerical model showed small signs of non-equilibrium conditions at GMF 0,8. The discharge temperature proved as large as 0,16°C or 0,15°C depending on the droplet diameter. These differences are still significant when calculating the polytropic efficiency. Evaporation proved to be virtually non-existent in the calculations, due to almost saturated conditions at the inlet. Still, validation against wet-gas experiments is needed to confirm the findings.

Sammendrag

Våt-gass kompresjon og subsea kompresjon teknologi har fått økt fokus i de siste årene. Med aldrene felt på norsk sokkel og nye funn i arktiske strøk, kan subsea kompresjon gi økt utvinning og gjøre fjerntliggende felt lønnsomme der utvinning er vanskelig. Våt-gass kompresjon kan redusere behovet for dyre scrubbere og separatorer. Dette vill i så fall kunne føre til en stor økonomisk fortjeneste ved subsea prosessering. Det er foreløpig ingen standard for våtgass kompresjon. ASME PTC 10 [1] tilbyr ingen instrukser på dette. Forståelsen av komplekse fenomener som oppstår i våt-gasskompresjon er ennå ikke helt forstått. Det foreliggende arbeidet er opptatt av termisk utløps likevekt av en våt-gass kompressor. Dette er noe som sterkt vil påvirke ytelsesberegningene til kompressoren. Hvis det er termodynamisk likevekt ved utløpet vil målinger og beregninger være forholdsvis enkle. Dersom det motsatte er tilfelle så begge prosessene mer komplekse.

En numerisk simuleringsmodell ble etablert, både for tørr og våt gass. En åpen sløyfe testrigg ved NTNU ble brukt til å sammenligne beregninger med eksperimenter og deretter å validere modellen. Dette stemte oppsiktsvekkende bra for tørrgass. For våtgass ble nøyaktige målinger ikke oppnådd. Arbeidsmediet var en luft-vann-blanding, hvor vann ble sprøytet inn nesten mettet luft.

For å beregne mulig utløpstemperatur på gassen under tungt våte forhold, ble en kraftbalanse også satt opp. Usikkerhetene i frekvensomformeren og momentmåler var for store for pålitelige effektberegninger. En ny måleteknikk har blitt foreslått for å kunne måle utløpstemperaturen på gassen. Denne tar i bruk en syklon for å skille gassen før målinger. Denne teknikken er enda ikke blitt testet.

Den numeriske modellen viste små tegn til ikke-likevekt forhold på GMF 0,8. Utløpstemperaturen viste forskjeller på 0,16°C eller 0,15°C, avhengig av dråpe diameteren. Disse forskjellene er fortsatt betydelige når man beregner polytropic effektivitet. Fordampning viste seg å være praktisk talt ikke-eksisterende i beregningene. Dette skyldes at luften inn i kompressoren er tilnærmet mettet. Likevel er validering mot våt-gass eksperimenter avgjørende for å bekrefte funnene.

Table of Contents

Table of figures

List of tables

Nomenclature

Basic symbols and units

Symbol	Description	Unit
A	Flow area	m^2
Aa, Ba, Ca	Antoine equation constants	
b	Width	m
B	Bearing width	m
Bi	Biot number	Dimensionless
C	Absolute velocity of fluid	$m\ s^{-1}$
Cp,Cv	Specific heat constants	$J\ K^{-1}$
ct	Response coefficient	Dimensionless
D	Diameter	m
d_h	Hydraulic diameter	m
d_m	Bearing mean diameter	m
d_s	Seal counter face diameter	m
DH	Hub Diameter	m
DS	Shroud diameter	m
E_b, $E_{b\lambda}$	Heat radiation	$W\ m^{-2}$
f	Head correction factor	Dimensionless
Fr	Frössling number	Dimensionless
g	Air mass fraction	Dimensionless
Grr	Frictional variables	
Gsl	Frictional variables	
h	Heat transfer coefficient	$W\ m^{-2}\ K^{-1}$
h_{ev}	Heat of evaporation	$J\ mol^{-1}$
H	Head	J
k	Thermal conductivity	$W\ m^{-1}\ K^{-1}$
Kroll	Frictional variable	
Ks1	Frictional variable	
Ks2	Frictional constants	N m
L	Length	m
$\dot{m}$	Mass flow	$kg\ s^{-1}$
M	Frictional moment	N m
$M_{rr}\ M_{sl}\ M_{seal}\ M_{drag}$	Frictional moments	N m
MW	Molecular weight	$g\ mol^{-1}$
n	Polytropic exponent	Dimensionless
N	Compressor speed	rpm
Nb	Number of blades	Dimensionless
Nu	Nusselt number	Dimensionless
p	Pressure	bara
Pr	Prandtl number	Dimensionless
Q	Volume flow	$m^3\ s^{-1}$

r	Radius	m
$\bar{R}$	Specific gas constant	J kg^{-1} K
R$_0$	Universal gas constant	J K^{-1} mol^{-1}
Rc	Resistance constant	s^{-1}
Re	Reynolds number	Dimensionless
Rt	Resistance	s^{-1}
S	Entropy	J K^{-1}
SH	Specific humidity	Dimensionless
SP	Volute sizing parameter	Dimensionless
St	Stokes number	Dimensionless
T	Temperature	K or °C
U	Impeller velocity	m s^{-1}
V	Volume	m^3
Vm	Oil level variable	
W	Relative velocity	m s^{-1}
We	Weber number	Dimensionless
X	Schultz compressibility factor	Dimensionless
$\bar{X}$	Sample mean	Dimensionless
Xi	Mole fraction	Dimensionless
Xs	Vapour mole fraction	Dimensionless
y	Wetness fraction	Dimensionless
Y	Schultz compressibility function	Dimensionless
Z	Compressibility factor	Dimensionless

Greek symbols

α	Flow angle	°
α_c, β_c, δ_c	Van-Dusen equation constants	Dimensionless
α_f, ε_f,	Flow constants	Dimensionless
β	Flow angle	°
β_s	Frictional constants	Dimensionless
Γ	Diffusion constant	m^2 s^{-1}
δ	Liquid film thickness	m
δ_s	Streamline deflection distance	m
η	Efficiency	Dimensionless
κ	Isentropic coefficient	Dimensionless
λ	Thermal conductivity	W m^{-1} K^{-1}
λ_i	Interface friction	Dimensionless
λ_w	Wavelength	m
μ	Viscosity	Kg m^{-1} s^{-1}
μ_{sl}	Sliding friction coefficient	Dimensionless

ν	Kinematic viscosity	$m^2\ s^{-1}$
ρ	Density	$m^3\ kg^{-1}$
σ	Slip factor	Dimensionless
σ_b	Stefan-Boltzman constant	T^{-4}
σ_s	Surface tension	$N\ m^{-1}$
τ	Torque	N m (check)
τ_H	Head coefficient	Dimensionless
ϕ	Flow coefficient	Dimensionless
ω	Compressor speed	$Rad\ s^{-1}$
ϖ	Head loss coefficient	Dimensionless

Subscripts

1-inlet

2-impeller outlet

3-diffusor outlet

4-volute outlet

c-critical

d-droplets

e-exit

eff-effective

g-gas (inert gas)

i-index

l-liquid

m-mixture (refers to inert gas plus vapour)

o-stagnation quantity

p-polytropic

P-pressure

r-radial

ref-reference

s-isentropic

sg-superficial gas

sl-superficial liquid

T-temperature

u-tangential

v-vapour

V-volume

w-woods corrected

Abbreviations

ASME-Association for mechanical engineers

ASP-Anti Surge Protection

API-American petroleum institute

CFD-Computational fluid dynamics

FT-Flow transmitter

GE-General electric

GVF-gas volume fraction

GMF-gas mass fraction

IFB-Inlet fog boosting

ML-Matlab

NGL-Natural Gas liquid

PTC-Performance test code

PT-Pressure transmitter

RTD-Resistance temperature detector

TT-Temperature transmitter

1 Introduction

1.1 Background

The Norwegian Petroleum Directorate states that as of 2010, 5,5 billion Sm^3 of oil equivalents have been produced from the Norwegian continental shelf. The estimated remaining recoverable resources are in the range of 7 billion Sm^3 o.e. Since the Norwegian oil and gas production started in 1971, 81 fields have contributed to this production[2].
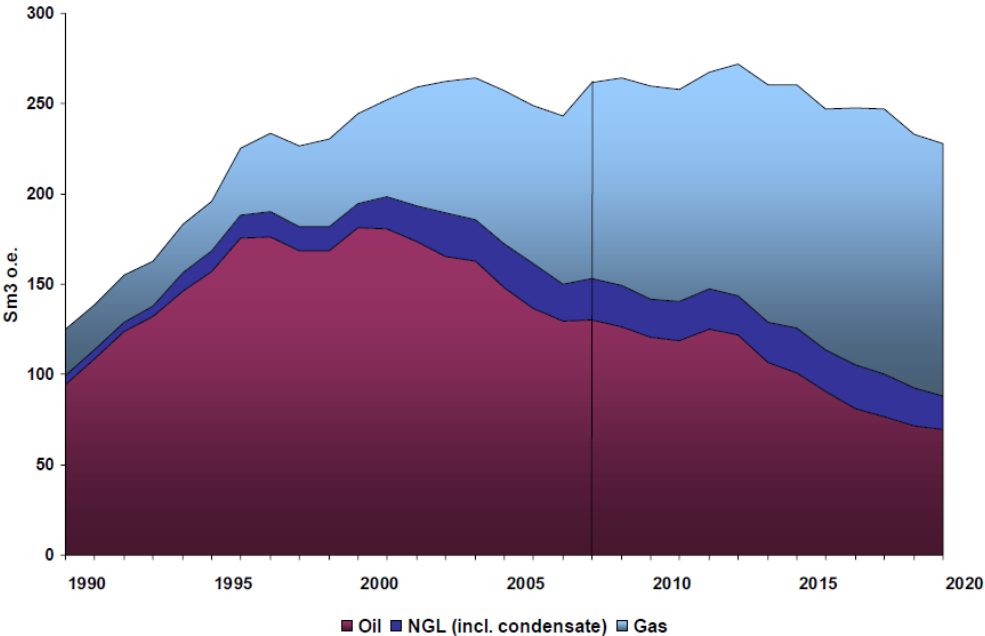
Figure 1-1 Norwegian petroleum production

Figure 1-1 shows the projected Norwegian petroleum production until 2020. It shows that as the oil production is declining, the gas production will continue to grow. As conventional resources are depleted the remaining resources might be more challenging to acquire. The U.S. Energy Information Administration estimates that 22% of the world's oil and gas resources are located in the arctic [3]. In such remote locations new subsea developments are vital.

For typical compressors the liquid components are separated from the gas stream entering the compressor. This is done with a scrubber or separator. These installations are large and heavy, which would increase costs for subsea projects. Wet gas compression is a topic that has gained increased focus during recent years. Brenne et al. (2008) [4] discusses the potential of this new technology. It poses new opportunities, by the means of sub-sea bosting and can increase recovery for existing fields.

Statoil and Petoro have recently agreed to install subsea gas compressors on Gullfaks. Two 5MW Framo counter rotating axial compressors have been chosen. They will lie at a water depth of 135m to be completed in 2015. The Åsgard subsea compression project has also been

1

approved. It is believed that this project will increase the recovery by 280 millions of barrels of o.e. Furthermore at Nyhamna a GE, Nuovo Pignone 12,5MW compressor is tested for the Ormen Lange field. This field is located 120km of the coast at water depths of 800-1100m.

Unfortunately the ASME PTC10 [1] offers no guidance on wet gas compression testing and the performance of wet gas compressors is difficult to determine. This is due to the fact that it is heavily influenced by the discharge temperature which is difficult to measure.

Due to the possible non-equilibrium condition of the mixture at the discharge, the temperature of the liquid and the gas phase may differ. The gas temperature increases during the compression process and the liquid temperature may not change quickly enough to keep up. It is a trivial task to measure the temperature of the liquid as the droplets will have a significantly larger heat capacity than the gas. The droplets in the gas phase prevent any measuring of the gas temperature as water droplets will hit the thermocouples and this will strongly affect the measurements.

1.2   Tasks and limitations

The tasks of this report can be summarized as follows:

- Document relevant literature on thermal equilibrium on wet-gas compression
- Project and install optimal sensors for measurements of dry and wet-gas discharge temperature
- Establish and validate a dry and wet gas performance model against experimental data. Including validation of a power balance between compressor and power unit.

Relevant literature has been discovered on the subject, for axial and centrifugal compressors. The literature is presented in chapter 5. Other areas such as turbocharges and steam turbines have also been inspected for a deeper understanding on multiphase temperature measurements, but little information has been found on this subject. A temperature measurement technique has been proposed in chapter 7. In accordance with professor Bakken it was decided that the purchase and installation of this would be postponed because of scheduled maintenance of the test rig.

A numerical performance model has been created by the author in Matlab. Even though numerous simplifications were made, the model turned out to be more complicated than anticipated. The liquid film in the compressor was disregarded and all the liquid transport was assumed to be in the form of droplets. This was done because the author's computational capacity was limited, and this would be considerably more demanding computationally. The next improvement in the model should be the introduction of liquid film. But further experiments needs to be done to understand how much of the liquid will travel in the form of droplets and film. The model was validated against dry gas measurements, but sufficient wet-gas tests were not performed due to breakdown of the compressor.

A power balance was set up, and the uncertainty regarding this was analysed. The uncertainties of the measurements were too great for appropriate use of the power balance. Finally improvements for the test rig were proposed.

1.3   Structure of the report

This report begins with fundamental thermodynamic relations. Chapter 3 and 4 are description of centrifugal compressors and multiphase flow respectively. Chapter 5 is the literature review and following is a description of the NTNU test rig and the instrumentation setup. The temperature sensor projected is described in chapter 7 along with general measurement temperature measurement techniques. The numerical model developed is described and validated in the two following chapters. The final results are presented in chapter 11.

The entire report is written in English, with the exception of Appendix D and Appendix L, an email correspondence between the author and Cameron and the HAZOP for the test rig. This has not been translated to avoid unnecessary bias from the author.

2 Thermodynamics

2.1 Equations of State

In thermodynamics, an equation of state (EOS) describes the relation between two or more state variables such as pressure, temperature, specific volume or internal energy. These can help describe system properties and are vital for calculations in compression and expansion processes. The simplest of these is the ideal gas relation, but as this becomes increasingly inaccurate at high pressures it is not suitable for process compressors.

2.1.1 Ideal gas

An ideal gas is described as a gas that obeys the equation of state shown in Eq 2-1. From this it follows that specific internal energy only depends on temperature.

$$p = \rho \bar{R} T$$

Eq 2-1

Since most gases do not obey Eq 2-1 the validity of this usually depends on the acceptable error in a given calculation.

2.1.2 Real gas

Real gases as opposed to ideal or perfect gases cannot be described accurately by the ideal gas equation. Eq 2-1 has therefore been corrected to take into account the compressibility factor Z [5].

$$p = Z\rho \bar{R} T$$

Eq 2-2

In this thesis a low pressure air-water wet gas compressor is examined, so the compressibility factor will be negligible and the ideal gas equation is used.

2.2 The polytropic analysis

Centrifugal compressor performance calculations have been based on polytropic analysis rather than isentropic analysis for a long time. Different methods have been proposed for the polytropic analysis. The most famous being of course the one proposed by Schultz (1962) [6] and utilized both by the ASME PTC 10 [1] and the ISO 5381 [7]. Huntington (1985) [8], questioned this calculation method and proposed a more accurate but also more complex method.

The polytropic compression path follows the actual compression path, but has infinitesimal small isentropic compression steps along this path. The definition of a polytropic process is:

$$pv^n = \text{constant} \qquad \text{**Eq 2-3**}$$

In Schultz (1962), two additional compressibility functions are introduced to facilitate the calculations of the temperature and volume exponents.

$$X = \frac{T}{Z}\left(\frac{\delta Z}{\delta T}\right)_P = \frac{T}{V}\left(\frac{\delta V}{\delta T}\right)_P - 1 \qquad \text{**Eq 2-4**}$$

$$Y = 1 - \frac{P}{Z}\left(\frac{\partial Z}{\partial P}\right)_T = -\frac{P}{V}\left(\frac{\partial V}{\partial P}\right)_T \qquad \text{**Eq 2-5**}$$

With these the polytropic temperature and volume exponents become:

$$\frac{n_T - 1}{n_T} = \frac{\left(\dfrac{\kappa - 1}{\kappa}\right)\left(\dfrac{1}{\eta_p} + X\right)Y}{\left(1 + X\right)^2} \qquad \text{**Eq 2-6**}$$

$$n_V = \frac{(1 + X)}{Y\left[\dfrac{1}{\kappa}\left(\dfrac{1}{\eta_p} + X\right) - \left(\dfrac{1}{\eta_p} - 1\right)\right]} \qquad \text{**Eq 2-7**}$$

From this, expressions for the isentropic exponents can be obtained by setting the efficiency equal to one. Integrating vdp along a path of constant efficiency, i.e. a polytropic process, while setting the polytropic volume exponent constant, the polytropic head is obtained.

$$H_p = \int_1^2 vdp = \frac{n_V}{n_V - 1}\left[p_2 v_2 - p_1 v_1\right] \qquad \text{**Eq 2-8**}$$

$$H_p = \frac{n_V}{n_V - 1}\frac{Z_1 R_0 T}{MW}\left[\left(\frac{p_2}{p_1}\right)^{\frac{n_V}{n_V - 1}} - 1\right] \qquad \text{**Eq 2-9**}$$

It is important to notice that Eq 2-8 and Eq 2-9 are only equal if the polytropic volume exponent is defined as:

$$n_V = \frac{\ln\left(\dfrac{p_2}{p_1}\right)}{\ln\left(\dfrac{v_1}{v_2}\right)} \qquad \text{**Eq 2-10**}$$

If not, then the two methods can give very different results. Hundseid et al. (2006), showed a discrepancy of 1.7% by using the different calculations. Schultz also proposed a head factor, f, to account for this variation in the exponent along the compression path.

$$f = \frac{h_{2s} - h_1}{\dfrac{\kappa_V}{\kappa_V - 1}\left[p_2 v_{2s} - p_1 v_1\right]} \qquad \text{**Eq 2-11**}$$

With the polytropic head factor Eq 2-8 becomes:

$$H_p = f \frac{\kappa_v}{\kappa_v - 1} \left[p_2 v_{2s} - p_1 v_1 \right]$$

<div align="right">**Eq 2-12**</div>

The polytropic efficiency is defined as:

$$\eta_p = \frac{H_p}{H}$$

<div align="right">**Eq 2-13**</div>

3 Theory for centrifugal compressors

The overall job of the centrifugal compressor consists of increasing the pressure of the gas-stream. The compressor is basically composed of an outer casing, of a stator (diaphragm bundle) and a rotor. The rotor can have one or more impellers, includes the balance drum and the thrust collar, and it is connected to the driver by a coupling.

3.1 Compression gas path

The gas enters the compressor through a suction nozzle, an annular chamber (inlet volute) then forces the gas to flow towards the centre of the compressor and into the first impeller. The impeller consists of disk, shroud and vanes as in Figure 3-1. The gas flows into the impeller and the rotational speed of the impeller increases the velocity of the gas as well as its pressure. It then enters a diffusor, a circular chamber in the diaphragm bundle, where the gas velocity decreases and thereby increasing the pressure further. Next the gas enters the return channel and flows to the next impeller. At the end of the last diffusor the gas enters an annular chamber known as discharge volute. This guides the gas from the diffuser to the discharge nozzle. The test compressor at NTNU only consists of a single stage, meaning that after the first diffusor, the gas enters straight into the volute.

3.1.1 Impeller performance

When the fluid enters the impeller, it comes in at an absolute velocity C_1. If the impeller moves at a velocity U_1, the relative velocity to the impeller will be the vector $C_1-U_1=W_1$. These three vectors together form the inlet velocity triangle as can be seen in Figure 3-1. The gas will then follow the vanes and exit the impeller with a velocity C_2. This velocity will have a radial component C_{2R} and a whirl component C_{2U}. The exit components depend on the impeller tip speed and the velocity of the fluid, but also the slip and the angle of the guide vanes.
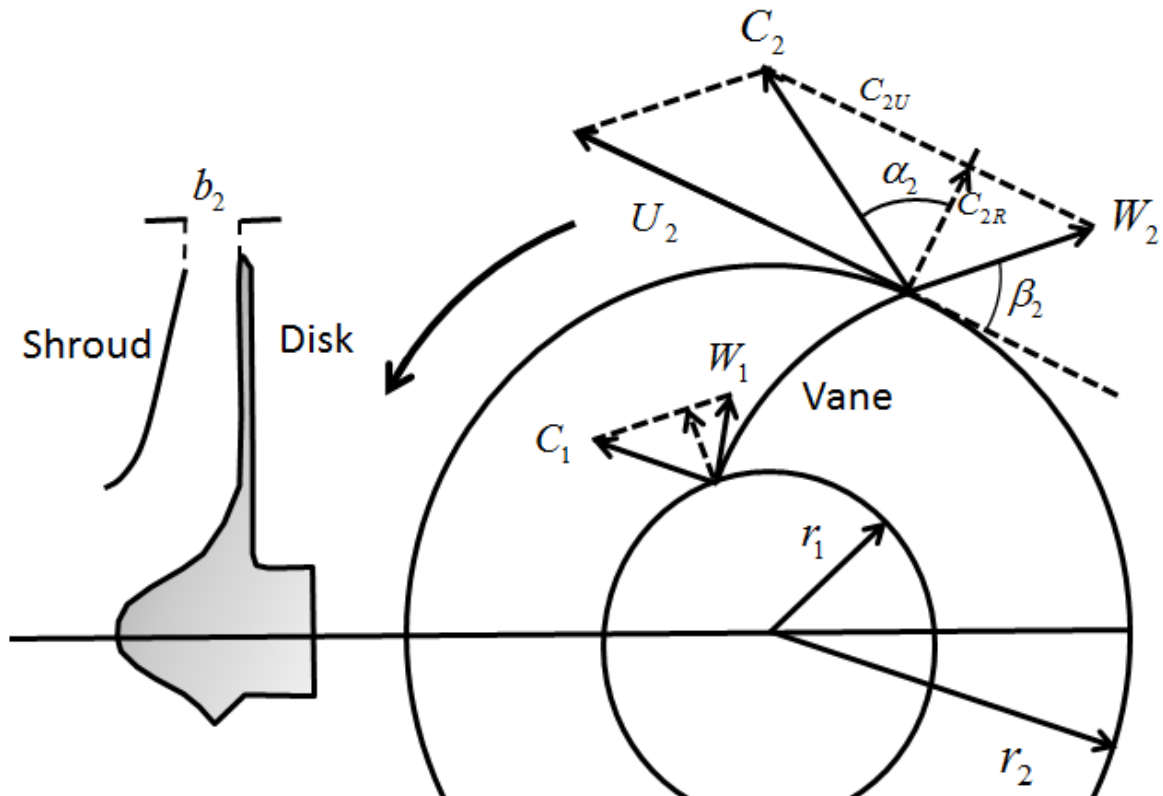
Figure 3-1 Velocity triangles in an impeller with backwards swept vanes.

Applying the conservation of angular momentum between the outlet and the inlet, we note that the torque must be:

$$\tau = \dot{m}(r_2 C_{2U} - r_1 C_{1U})$$

<div align="right">Eq 3-1</div>

Utilizing the fact that the work per mass of fluid is given by:

$$W = \frac{\omega \tau}{\dot{m}} = \omega(r_2 C_{2U} - r_1 C_{1U})$$

<div align="right">Eq 3-2</div>

The first principle of thermodynamics states that work per mass flow is equal to enthalpy for an adiabatic flow.

$$\Delta H = (U_2 C_{2U} - U_1 C_{1U})$$

<div align="right">Eq 3-3</div>

Eq 3-3 is known as the Euler equation for turbo-machines and is of fundamental importance for compressors. It is useful to characterize the operating conditions of centrifugal compressors in terms of dimensionless parameters. The most important dimensionless parameters in this dissertation are the flow coefficient and the coefficient of head shown in Eq 3-4 and Eq 3-5 respectively.

$$\phi_2 = \frac{4Q_2}{\pi D_2^2 U_2} = \frac{C_{2R}}{U_2}$$ **Eq 3-4**

$$\tau_H = \frac{\Delta H}{U_2^2} = \frac{C_{2U} - C_{1U}}{U_2}$$ **Eq 3-5**

It can be assumed for most centrifugal compressors that there is no preswirl. So Eq 3-5 can be simplified.

$$\tau_H = \frac{C_{2U}}{U_2}$$ **Eq 3-6**

Eq 3-4 could be used to make the coefficient of head explicitly dependent on flow rate and discharge blade angle. From the velocity triangle at the impeller outlet, Figure 3-1, it can be shown that:

$$C_{2U} = U_2 - \frac{C_{2R}}{\tan \beta_2}$$ **Eq 3-7**

If the equation above is divided with the impeller discharge speed while recalling the equations for the flow and head coefficients Eq 3-8 is obtained.

$$\tau_H = 1 - \phi_2 \cot \beta_2$$ **Eq 3-8**

Because of inertial and coriolis forces, the relative particle velocity at the outlet W2 in Figure 3-1 will not follow the exact same path as the vanes.
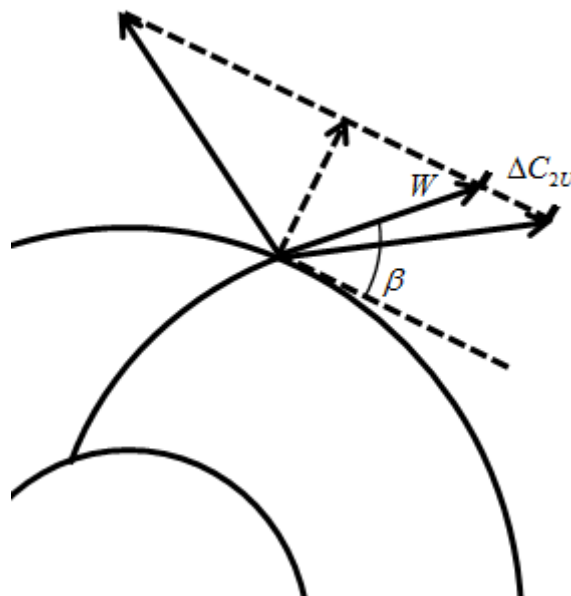
Figure 3-2 Slip at the impeller exit

This effect is known as the slip and can be seen in the figure above. The slip is defined as:

$$\sigma = 1 - \frac{\Delta C_{2U}}{U_2}$$

Eq 3-9

The equation for the head coefficient then becomes.

$$\tau_H = \sigma - \phi_2 \cot \beta_2$$

Eq 3-10

Currently many formulas for the slip factor have been proposed, based on the geometry of the impeller. In this dissertation a correlation proposed by Stanitz has been used.

$$\sigma = 1 - \frac{0,63\pi}{Nb} \left(1 - \frac{U_2}{C_{2R} \cot(\beta_2)} \right)$$

Eq 3-11

In this expression Nb refers to the number of blades in the impeller.

3.1.2 Diffusor performance

Although the additional energy in the gas stream is added in the impeller, a large part of the pressure increase takes place in the diffusor. This is because the gas velocity is reduced in the diffusor. Introducing the concept of the stagnation pressure and temperature will help explain this. Stagnation pressure is the sum of the static pressure and the dynamic pressure as seen in Eq 3-12. This means that the stagnation pressure is the pressure you would measure if the fluid was brought to rest adiabatically, it can be derived directly from Bernoulli's equation.
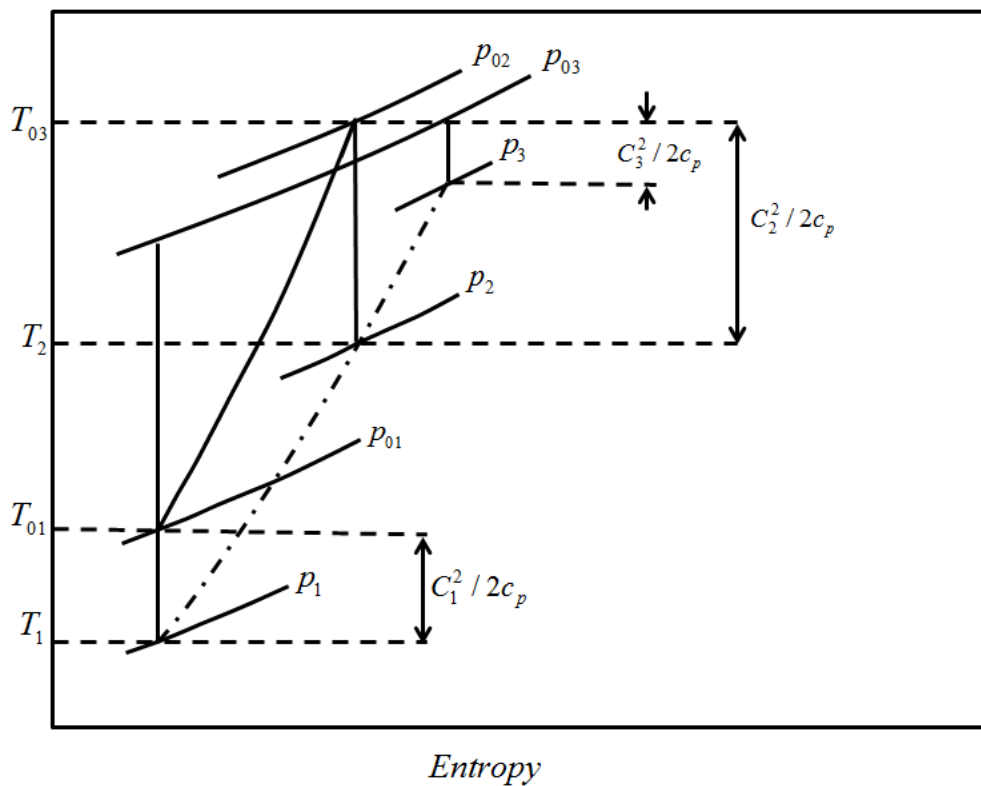
Figure 3-3 Temperature-entropy diagram of an impeller and diffusor [9]

12

$$p_o = \frac{1}{2}\rho v^2 + p$$

$$T_o = \frac{C^2}{2C_p} + T$$

Figure 3-3 shows that the stagnation temperature and pressure increase takes place from the impeller inlet (1) to the impeller discharge (2). From the diffuser inlet (2) to discharge (3), there is an increase in static temperature and pressure, but only because the velocity is reduced. The stagnation temperature remains constant (provided that the compressor is properly isolated) because of zero work input and the stagnation pressure decreases slightly due to fluid friction.

Stanitz (1952) [10] created a numerical analysis method for NACA to examine flow in vaneless diffusers. He used a cylindrical coordinate system with r, U and z to describe the radial, tangential and axial positions. For a constant height diffusor, a reasonable assumption is that the boundary layer remains roughly constant so the z coordinate can be ignored when calculating the mean flow. The velocity is then the sum of the radial and tangential component.

$$C = \sqrt{C_U + C_R}$$

The angle α describes the flow direction between the velocity components as seen in the figure below.
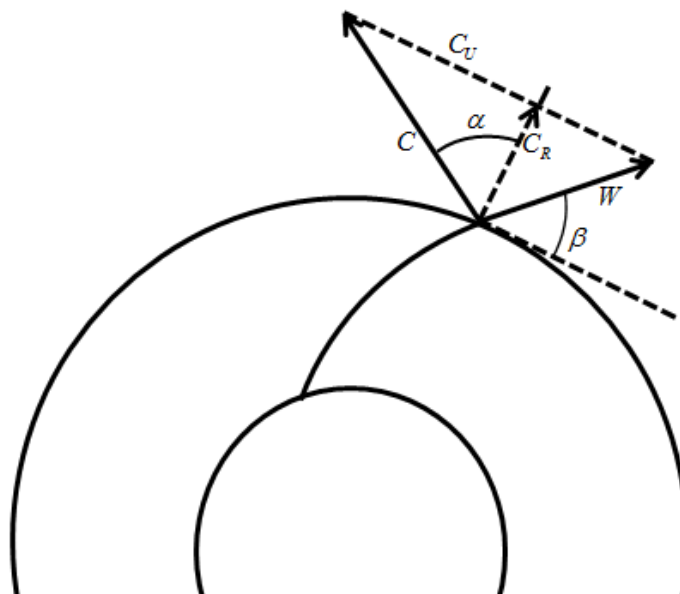
Figure 3-4 Flow direction in the diffuser

13

$$\alpha = \tan\frac{C_U}{C_R}$$
Eq 3-15

In Appendix B the differential equations for the iterative process in the diffusors are shown.

3.1.3 Volute performance

The discharge volute collects the radial gas flow from the diffusor of the last compression stage and sends it to the pipeline. Weber and Koronowski (1986) have developed a simple one dimensional analysis to describe the losses in the volute. This method was improved by Aungier (2003) [11] and is the basis that has been used in this thesis.
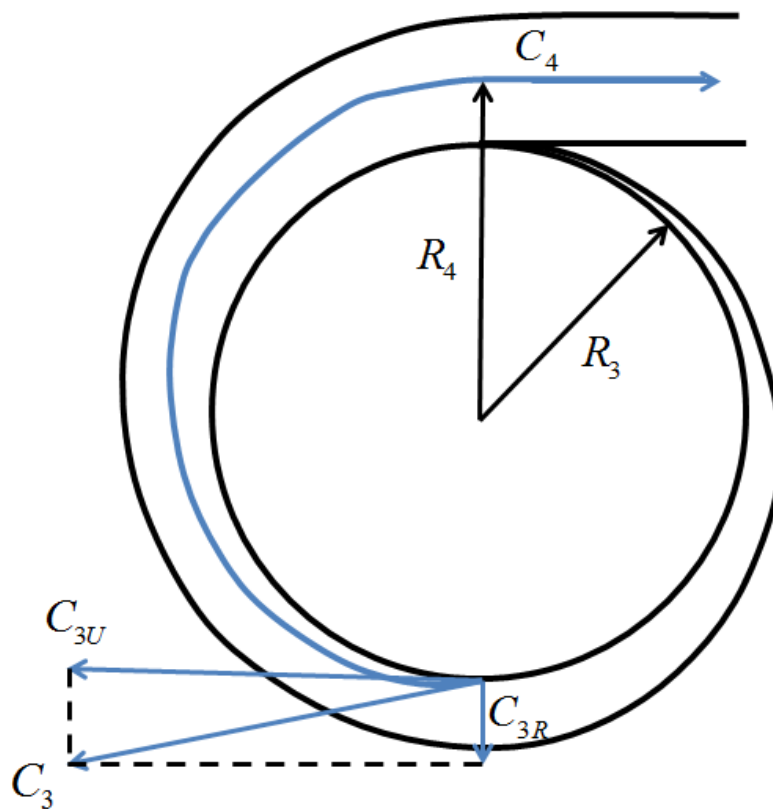
Figure 3-5 Flow path in the volute

Figure 3-5 shows the flow path in the discharge volute. According to Aungier (2003), the radial velocity C3R turns into a swirl component that will be dissipated in the pipe downstream, meaning that all the radial velocity head will be lost. This is shown in Figure 3-6. The dimensionless head loss of the radial velocity is calculated from Eq 3-16.

$$\varpi_R = \left(\frac{C_{3R}}{C4}\right)^2$$
Eq 3-16

There is also a loss associated with the tangential velocity component. This loss depends on the volute sizing parameter, defined as:

$$SP = \left(\frac{r_3 C_{3U}}{r_4 C_4} \right)$$

Dependent on this parameter, the head loss can be calculated. If the volute sizing parameter is greater than 1, then the head loss is given by:

$$\varpi_U = \frac{1}{2} \frac{r_3 C_{3U}^2}{r_4 C_3^2} \left[1 - \frac{1}{SP^2} \right]$$

If not then the head loss is provided with the following equation.

$$\varpi_U = \frac{r_3 C_{3U}^2}{r_4 C_3^2} \left[1 - \frac{1}{SP} \right]^2$$
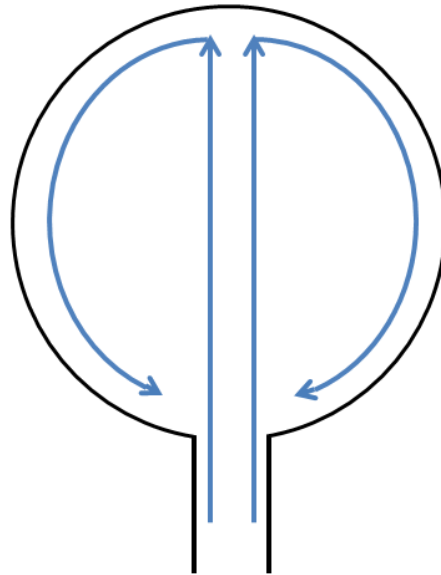
Figure 3-6 The radial component of velocity in the volute, entering from the diffusor

The loss from the wall skin friction can also be computed with:

$$\varpi_{SF} = 4 \cdot c_f \left(\frac{C_4}{C_3} \right)^2 \frac{L}{d_H}$$

L is the average path length of the flow and dH is the hydraulic diameter.

$$L = \frac{\pi (r_3 + r_4)}{2}$$

$$d_H = \sqrt{\frac{4 A_4}{\pi}}$$

All the previously mentioned the dimensionless loss parameters can be added to obtain the total pressure loss.

$$p_{o4} = p_{o3} - (p_{o3} - p_3)\sum \varpi \qquad\qquad \textbf{Eq 3-23}$$

With these equations the pressure loss can be obtained with an iterative process as the inlet conditions in the volute are known. The velocity at the outlet is first assumed and then adjusted with the continuity equation while calculating the other properties at the outlet.

3.2   Degradation

The causes of degradation can be many, but the results are always that the compressor will not perform according to the design specifications. At best this can result in an increased workload on the electric motor or power turbine, at worst it may disturb the entire process. The major causes of degradation are fouling, erosion and corrosion [12]. For wet-gas compression erosion is a significant problem and should be studied to a great extent.

Fouling is the accumulation of unwanted material on the impeller and diffuser surface. This can roughen the surface and create a smaller area for the gas flow, increasing the gas velocity as well as the losses due to friction.

Erosion takes place when particles such as sand, dust or liquid droplets hit the impeller, this may damage the impeller and wear the material. Centrifugal compressors are generally more resistant to erosion than axial compressors. Still the droplet diameter allowed in a wet gas compressor should be as small as possible.

Corrosion on the other hand is generally dependant on the concentration of acid-forming gases, moisture and material selection of the compressor [13].

4 Physics of multiphase flow

4.1 Flow regimes

Multiphase flow is a complex field of study. When studying wet gas compressors it is important to be aware of the different possible flow regimes one may encounter, to be able to physically describe the process in the best possible way. Some important definitions for multiphase flow are superficial gas and liquid velocity.

$$U_{sg} = \frac{Q_g}{A}$$

Eq 4-1

They are defined as the volume flow of the gas or liquid divided by the total area of the pipe.

$$U_{sl} = \frac{Q_l}{A}$$

Eq 4-2

Horizontal flow is roughly divided into four separate regimes, stratified, annular, bubble and slug flow. It is usual to treat the stratified and annular flow differently from the bubble and slug flow as the first are classified as separated flows, while the latter are mixed flows. This can be seen in the figure below. Regarding thermodynamic imbalance between the gas and liquid the actual flow regime is of fundamental importance. Imbalance will happen with greater simplicity in separated flows for obvious reasons.
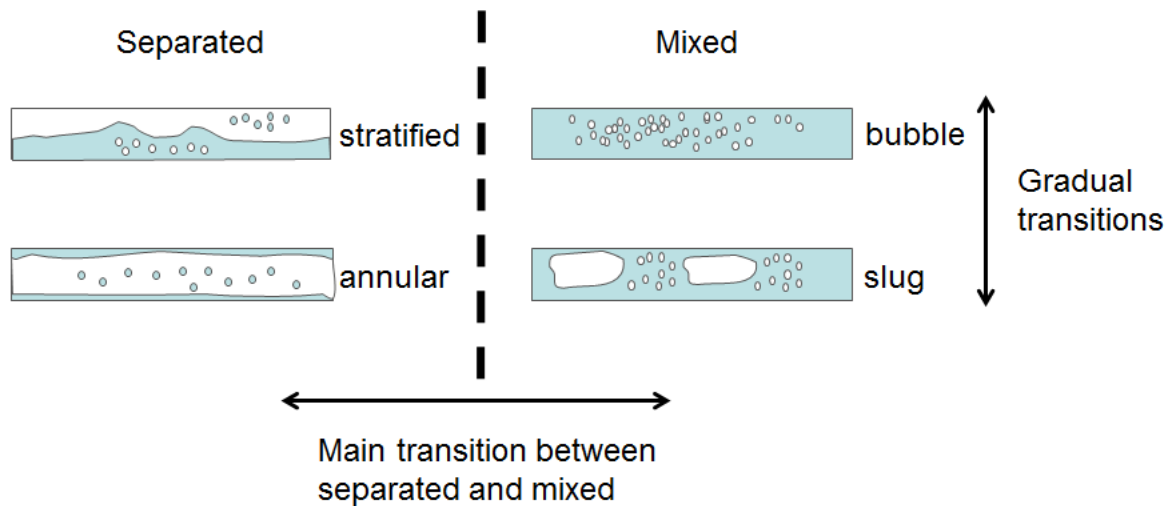
Figure 4-1 Flow regimes in horizontal flow

It has been tried to make generalized flow regime maps, this has proven difficult as the flow regime depends on many factors, including, flow rates, pipe geometry, fluid properties and inlet conditions. Mandhane, Gregory and Aziz [14] proposed a generalized flow map for gas-liquid flow (Figure 4-2). Still this flow map has a limited validity. Due to the high flow velocity and low liquid content in the wet-gas compressor, it seems likely that the flow will be either annular or a dispersed droplet flow.

4.1.1   Annular flow

Annular flow is characterized as a separated flow, even if the liquid flow can be dominated by droplets. For vertical pipes the liquid distribution is often in the form of very thin films, while it is a-symmetric for horizontal flows.

4.1.2   Bubble flow and dispersed bubble flow

Bubble flow takes place at high liquid velocities and low superficial gas velocities. This can be divided into two types of flows. Dispersed bubble flow, where turbulence is the dominating factor or buoyant bubble flow, where buoyancy is the governing factor for the bubble transportation. It is also possible to have a dispersed droplet flow, this is basically the same as for the bubble flow, but here the gas occupies the majority of the volume.
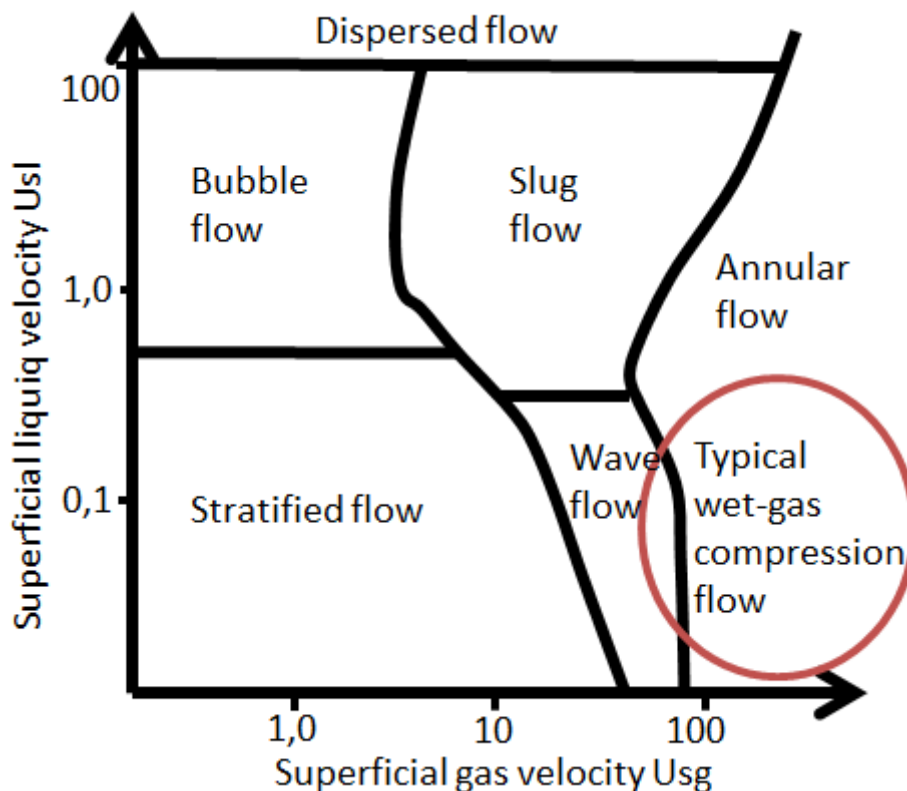
Figure 4-2 Generalized flow map for horizontal pipes, Mandhane Gregory and Aziz (1974) [14]

Flow regimes in vertical flow are similar to horizontal, with the exception that stratified flow is no longer possible, due to the fact that gravity will not separate the fluid in the same manner. A flow that only takes place in vertical pipes is churn flow. This is a highly unstable flow, where neither phase is continuous, churn flow takes place at relatively high gas velocities and will often develop into annular flow.

4.2 Modelling two-phase flow

There are three main ways to model two phase flows, the homogeneous model, the two phase model or the three phase model. The homogeneous model consists of averaging the fluid properties of the flow, while using one equation for the momentum-, mass- and energy-balance. There are many empirical correlations for pressure drop and friction factor in the homogeneous model of two phase flow, e.g. Lockhart-Martinelli and Beggs and Brill. The problem with the homogeneous model for wet-gas compressors is that it does not allow for the gas temperature to vary from the liquid temperature. For this reason it is not favourable to use when modelling the wet-gas compression in this thesis.

The two-fluid model uses two mass-, momentum- and energy-balances. Besides this its structure will depend on the type of flow encountered. This allows for the gas and liquid temperature to vary. In this thesis, a two-fluid model describing a gas-droplet multiphase flow has been developed , using the equations derived by Young (1994) [15]. This model neglects the liquid film as well as the relative velocity between the gas and droplets. The model is described more thoroughly in section 9.1.

The inarguably most accurate, but also most complex model for two phase flow is the three phase model. It models the gas, the liquid film but also the liquid droplets, and it uses separate equations for the momentum-, mass- and energy-balances. It also allows the gas, liquid film and droplets temperature to vary from each other. The greatest difficulty with this model is the droplet deposition and the tear-up of liquid film.

4.3 Liquid film

A liquid film will always wet the wall in a high velocity two phase flow as droplets are deposited on the pipe walls. Liquid droplets will continuously be entrained from this thin liquid film as the shear force from the gas will tear up the liquid film. This inception was investigated by Ishii and Grolmes (1975) [16]. Entrainment methods can be seen in Figure 4-3. The thin liquid film will also influence the interfacial friction factor. The friction of the gas is similar to the friction the gas would experience in a rough pipe. Wallis (1969) [17] came up with a Darcy-Weisbach friction factor for this.

$$\lambda_i = 0,02\left(1+300\frac{\delta}{D}\right)$$

Eq 4-3

Where δ is the liquid film thickness and D the pipe diameter. The friction between the liquid film and the wall is more problematic to model. It can be modeled as single flow using the hydraulic diameter or it can be modeled using velocity profiles, e.g. the law of the wall. In either case the friction factor is highly inaccurate.
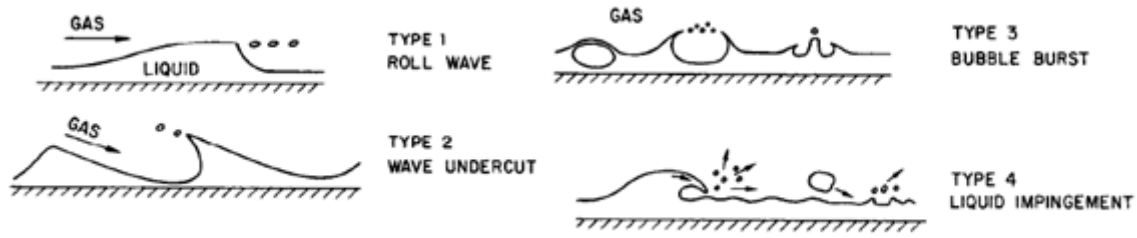
Figure 4-3 Entrainment methods in concurrent liquid film (Ishii and Grolmes 1975 [16])

Schubring (2003) [18], found an empirical formula for the liquid height that fits well with several experiments for an air-water mixture.

$$\frac{\delta}{D} = 4.7 \frac{\dot{m}_m + \dot{m}_l}{m_m} \left(\frac{\rho_g}{\rho_l} \right)^{1/3} \left(\frac{(\dot{m}_m + \dot{m}_l)D}{A \cdot \mu_l} \right)^{-2/3}$$

Eq 4-4

From this formula, the liquid film height can easily be calculated iteratively.

4.4 Gas-droplets slip

When droplets are ripped from the liquid film they are likely to have a velocity equal to the interface between the gas and liquid. As they move into the gas core, they are likely to be accelerated by the greater velocity of the gas phase which will create drag forces on the droplets. Brenne (2004) [19] found that the diffuser performance decreases when liquid droplets are entrained into a continuous gas flow. He explained this by an insufficient acceleration of the high-inertial droplet phase. A negative droplet phase slip was observed when increasing the flow area in the diffusor, meaning a failure to decelerate the droplets properly. This causes a drag on the gas by the droplets and the gas will not decelerate properly. As the diffuser area is still increasing, the effective flow area has to be decreased for continuity to hold. A boundary layer separation will occur.

The Stoke number is an appropriate non-dimensional number that describes the droplets response to an abrupt change in the gas flow path or velocity. It is defined as the acceleration period between a droplet and the gas surrounding it. For a spherical particle the Stokes number is defined as:

Eq 4-5

$$St = \frac{d^2 \rho_l \Delta u}{18 \mu_g \delta_s}$$

Here δs is the streamline deflection distance. Particles with a Stokes number much smaller than unity will follow the gas fluctuations completely. On the other hand, particles with a Stokes number much greater than one will not be much influenced by changes in the gas flow path, as can be seen in Figure 4-4.
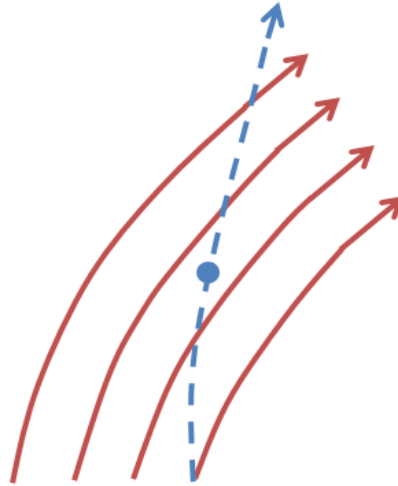
Figure 4-4 Flow path of a particle with St>>1

Later in this thesis a numerical model for presenting the two phase flow in a compressor is presented. The model assumes no slip between the gas and the droplets. To check this assumption it is important to investigate the Stokes number.

4.5 Droplet size

The droplet size is an important factor to determine the heat and mass transfer between the two phases. Currently several methods exist for measuring the droplet size distribution in a pipe, but droplet breakup is expected in the high speed impeller.

Hinze (1955) [20] and (1975) [21] documented two mechanisms responsible for droplet breakup, average velocity differences and turbulent eddies. It is possible to calculate a critical Weber number for these two mechanisms. The maximum stable droplet diameter can then be found by calculating which of these limits would be reached first.

Nigmatulin (1991) [22] observed the break-up of droplets above the critical Weber number.

$$We_C = 12 + 18\left(\frac{\rho_l \sigma_s d_C}{\mu_l^2}\right)^{-0,37}$$ **Eq 4-6**

The critical Weber number is based on the assumption that droplets break up because of average velocity differences and not turbulent eddies. The critical diameter can then be found iteratively, by using the regular equation for the Weber number.

$$We = \frac{d\rho_g(u_g - u_d)^2}{\sigma}$$ **Eq 4-7**

For this the largest velocity difference between the gas and liquid is needed, it can be assumed that this takes place when the droplets are injected. The second mechanism that might be responsible for droplet breakup is known as the Kolomogrov-Hinze mechanism. Alipchenkov

21

et al. (2004) [23] wrote the expression for the critical Weber number due to turbulent eddies as:

$$We_C = \frac{3}{c_t \left(1 + 2\rho_l / \rho_g\right)} \qquad \textbf{Eq 4-8}$$

Where ct is the coefficient of response of the particles to turbulent fluctuations and can be found in Alipchenkov et al. (2004) [23].

5 Literature review

Most previous work on this field is related to water injection on axial compressors to reduce the necessary power input for gas turbines. This goes all the way back to the 50s, proposed originally by Wilcox and Trout (1951) [24] to decrease the compressor power consumption. The purpose of this was to move towards isothermal compression from adiabatic compression.

Since then, White and Meacock (2004) [25] evaluated the injection of water droplets into axial compressors as a mean for boosting the power for industrial gas turbines. This feature is known as inlet fog boosting (IFB) or High-Fogging. Typical water injection rates are much lower than for wet compression and can be as low as 1% of the air mass flow and typical droplet sizes can even be 5 μm. These features are quite different from the ones encountered in wet gas compression where GMF can be 50% and droplet sizes are usually considerably higher. Härtel and Pfeiffer (2003) [26] analysed the effect of High-Fogging on the compression work. They used two models to evaluate this, the ideal model of thermodynamic equilibrium and a "droplet model". The ideal model assumes that the temperature will lie on the saturation line in the Mollier diagram. The "droplet model" is based on simple heat and mass transfer equations. However, the equations have to be solved numerous times during the compression process and a large accuracy is required to avoid instabilities. Abdelwahab (2006) [27] developed a similar model for centrifugal compressors to investigate the use of direct water injection to reduce the power requirements of a centrifugal compressor. Fabbrizzi et al. (2009) [28] investigated the effect of thermal non equilibrium on a wet gas compressor with typical subsea conditions. They narrowed the performance differences from dry compression down to three main effects, aerodynamic distortion, increased flow density and intercooling effect. The increased flow density and the intercooling effect will have a result in increased performances for wet gas compression, however, the aerodynamic effects will have opposite effects on the performance. Bettocchi et al. (2010) [29] investigated a multistage compressor exposed to wet conditions and discovered that the temperature measured at the outlet by thermocouples was not the actual gas temperature.

For process compressors under wet gas conditions, Hundseid and Bakken [30] advices that direct integration should be used when calculating the polytropic head and efficiency. Brenne et al. (2005) [31], discovered that the pressure increased and the specific power consumption was reduced when liquid was injected. Furthermore, they did not find any significant evidence of erosion. Hundseid et al. (2008) [32] developed a correction factor for the specific polytropic head reduction, titled the Wood's correction factor. This correction factor is based on the speed of sound in a multiphase flow. This is shown in Figure 5-1. D. Ransom et al. (2011) [33] investigated an air-water compressor with up to 20bar inlet pressure. Their findings showed that the pressure ratio was increased with liquid injection. and they attributed this to the increased thrust load and increasing Mach number at the discharge. The increasing Mach number is described with Wood's law.
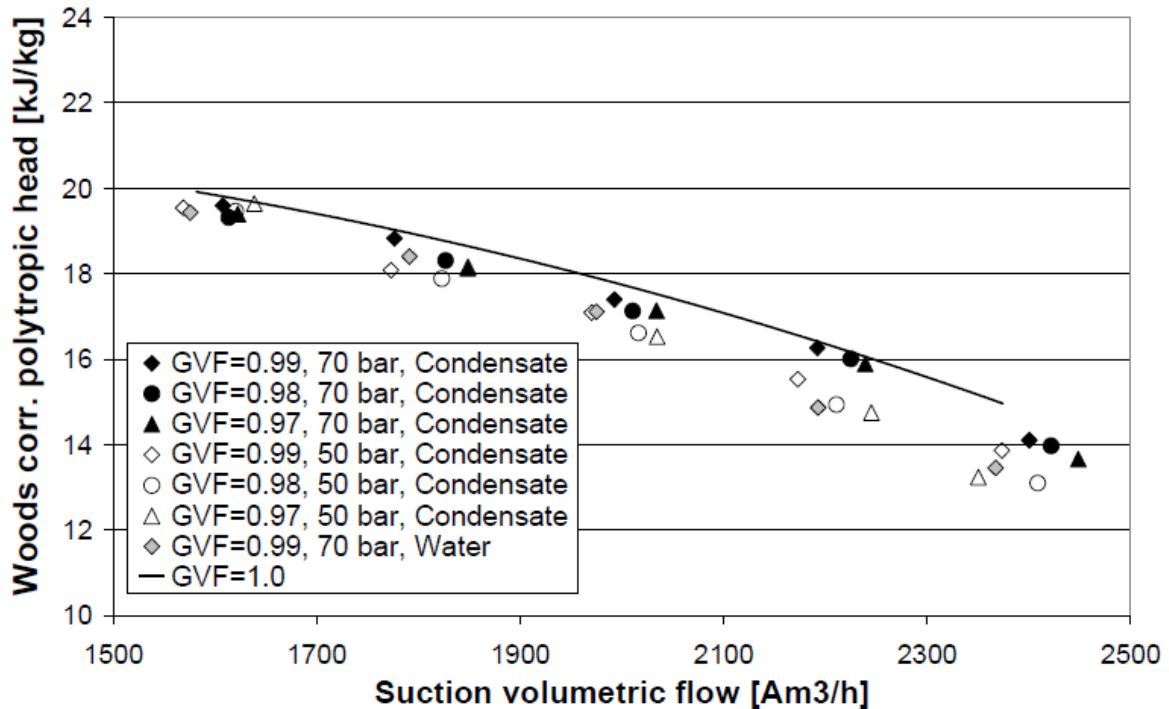
Figure 5-1 Polytropic head plotted against volumetric flow, corrected with Woods correctional factor (Hundseid et al. 2008)

Brenne (2004) [19], investigated diffuser performance with the addition of liquid in the form of film and droplets. Grüner (2012) [34], investigated the aerodynamic stability of a compressor exposed to liquid and actually discovered that the stability increased when liquid was injected.

Literature regarding steam turbines and turbo expanders has also been studied to discover if there is any instrumentation available for measuring the gas temperature of a multiphase flow not in equilibrium. Gyarmathy (1966) [35] and Moore and Sieverding (1976) [36] did not know of any measurement techniques for measuring the gas temperature in heavily wetted conditions. This was expected as both sources are substantially outdated when it comes to measuring temperature. According to Kleiz and Dorey (2004) [37] hardly any probes for measuring thermal non-equilibrium of wet steam have been pertinent. Schleicher et al (2008) [38] developed a high reaction time thermocouple, for use in highly transient multiphase flows. It is unclear if this would work for centrifugal compressors.

6   NTNU compressor test rig

The NTNU test rig is a single compression stage, driven by a high-speed electric motor capable of speeds up to 11000 rpm. The impeller is a shrouded backswept blade impeller, with 18 blades. It has an axial inlet as shown in Figure 6-1. The diffusor is vaneless and the volute is a spiral volute with an increasing cross-sectional area. Some data about the impeller and diffuser geometries is shown in Table 6-1. The design point at 10000 rpm is at $1\text{m}^3/\text{s}$.
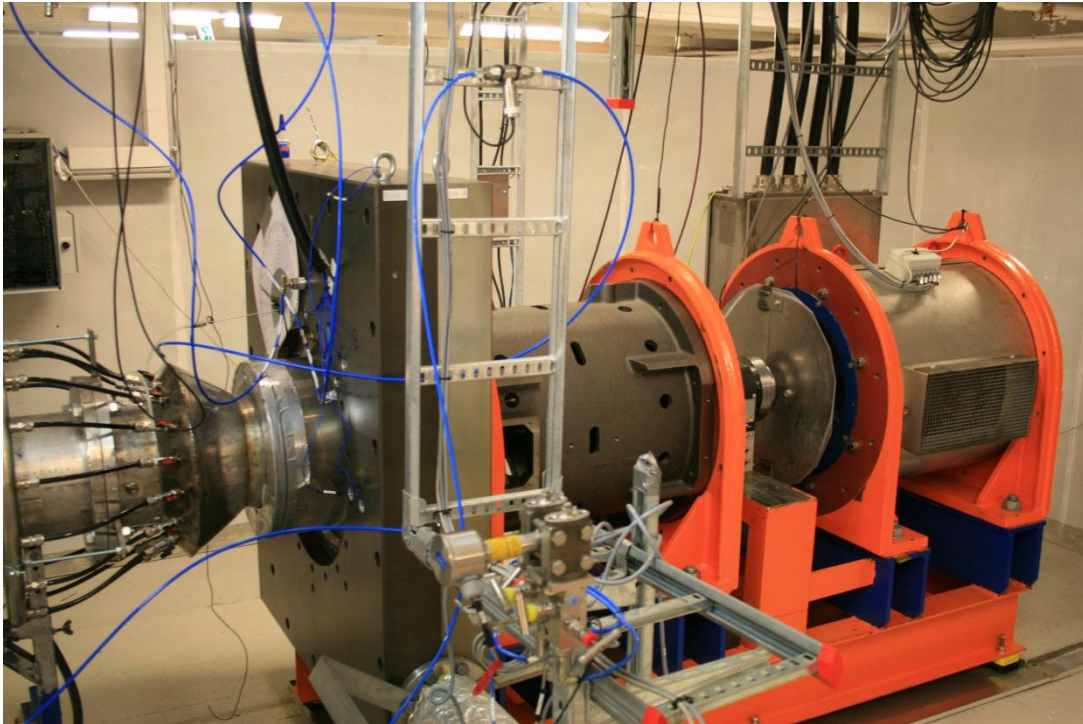
Figure 6-1 NTNU test centrifugal compressor

Table 6-1 Impeller and diffusor geometries

Inlet hub diameter (DH)	0,180 m
Inlet shroud diameter (DS)	0,2517 m
Impeller outlet diameter (D2)	0,455 m
Impeller outlet blade angle (β2)	50°
Impeller blades (Nb)	18
Impeller width (b2)	0,014 m
Diffusor width (b3)	0,014 m
Diffusor outlet diameter (D3)	1,7 * D2

6.1   Instrumentation

Liquid is injected by 16 nozzles positioned annularly. They are positioned 0,4m upstream of the impeller. The flow is measured by an inductive flow meter and the liquid temperature is measured by a Resistance Temperature Detector.

Across an orifice plate upstream of the compressor, the differential pressure is calculated. With the inlet pressure and this differential pressure the flow can be calculated with Eq 6-1. The differential pressure is measured with an Apilsen pressure transmitter.

Eq 6-1

$$Q = \alpha_f \cdot \varepsilon_f \cdot \frac{\pi}{4} \cdot d^2 \sqrt{2 \cdot \Delta p \cdot p_1}$$

The inlet pressure is measured by an LD300 pressure transmitter from SMAR. The total pressure increase across the compressor is measured with an Apilsen pressure transmitter.

The inlet and outlet temperature is measured with two AFL F500 resistance temperature detectors. They have been calibrated prior to use as well as calibrated onsite.

To perform a power balance, it is important to measure the power output from the electric engine. This is measured by a torque meter, situated between the impeller and the electric motor. The model is Smart Torque T12 by HBM and it makes it possible to calculate the power output by the electric motor. The speed of the compressor is controlled with a frequency converter. The torque and speed are related to the power with the following formula:

Eq 6-2

$$P = M \cdot \omega \cdot \frac{\pi}{30}$$

The layout of the instrumentation in the compressor test-rig is shown in Figure 6-2.
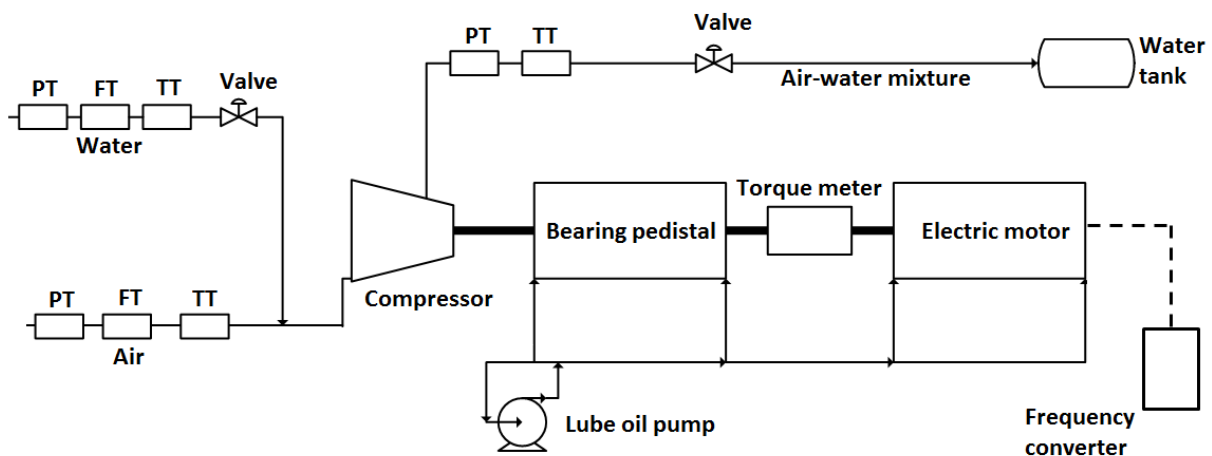
Figure 6-2 Instrumentation in test facility

6.2 Losses

Between the torque meter and the impeller a bearing pedestal is placed, held by two SKF angular contact ball bearings. The electric motor is also mounted on two identical bearings. This setup is seen in Figure 6-3. The bearings produced by SKF are custom made. A constant supply of lube oil is provided by a small pump for each of the bearings. The losses in the bearings were calculated using the SKF model for bearing losses. This is based on adding the rolling and sliding frictional moment, as well as the frictional moment of the seals and the drag.
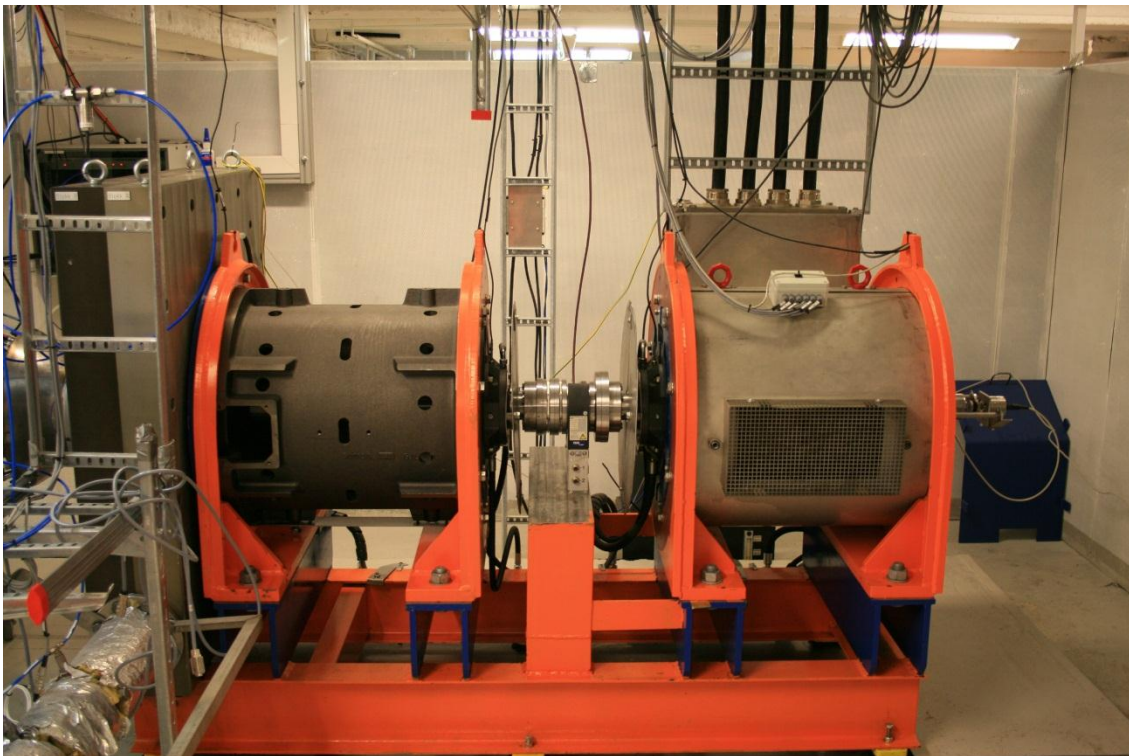
Figure 6-3 Electric motor and torque meter connected with the impeller

$$M_{tot} = M_{rr} + M_{sl} + M_{seal} + M_{drag}$$ **Eq 6-3**

These frictional moments are defined as:

$$M_{rr} = G_{rr} \cdot (\omega \cdot v)^{0,6}$$ **Eq 6-4**

$$M_{sl} = \mu_{sl} \cdot G_{sl}$$ **Eq 6-5**

$$M_{seal} = K_{s1} \cdot d_s^{\beta s} + K_{s2}$$ **Eq 6-6**

$$M_{drag} = 10 \cdot V_M K_{roll} \cdot B \cdot d_m^4 \cdot \omega^2$$ **Eq 6-7**

As some of the frictional constants were not known by the author for the custom bearings in the compressor, Henrik Tveit from SKF was contacted. He helped calculate the frictional loss at different speeds, shown in Table 6-2.

Table 6-2 Frictional losses at different speeds

Speed (rpm)	Power(W)
6000	172
7000	200
8000	228
9000	254
10000	282

6.3   Uncertainty in the NTNU-test rig

The procedure for calculating the uncertainty for the test rig is shown in Appendix A. The temperature sensors in the test rig are highly accurate and have a fixed error of 0,005°C. They are not designed for multiphase flow, and the accuracy may drop due to this.

As the flow of the compressor is calculated with Eq 6-1, the uncertainty in the flow is the square root of the product of the uncertainty in the differential pressure times the inlet pressure. The data sheet for the differential pressure transmitter is shown in Appendix K.

The Apilsen pressure transmitters have an accuracy of 0,4% and the LD300 have an accuracy of 0,04%. The accuracy of the torque meter is 0,03%. The frequency converter, measuring the compressor speed, has an accuracy of 3%.

6.4   Necessary improvements for the impeller test-rig

The fluctuations in the torque meter are somewhat larger than its nominal accuracy, suggesting that the accuracy might be less than expected. There have also been a number of problems previously with the torque meter. To verify the calculations for the test-rig it is important to achieve a correct power balance. To this date the inaccuracies in the torque meter and the frequency converter along with the poorly isolated compressor casing makes this problematic. The lack of isolation in the compressor casing also results in the need for an approximately one hour warm-up to make it stabilize. The slow bearing lubrication replenishment combined with this warm-up means a limited runtime at desirable conditions, before the bearing temperatures reaches intolerable limits.

A new and improved torque meter needs to be purchased, the compressor casing needs to be better isolated and the bearing lubrication should be improved. The frequency converter also needs to be more accurate to achieve tolerable calculation errors. For the author's investigation of the thermal equilibrium, droplet sizes should be measured both at the inlet and outlet. The inlet droplet temperature is vital to understand the heat and mass transfer between the gas and liquid. The droplet measurements at the outlet would verify the heat and mass transfer calculations, but is not vital to do calculations.

The inductive liquid flow meters should also be improved to get a higher accuracy in the liquid mass flow, as these have proved unreliable before.

7 Temperature sensors

Accurate temperature measurements are vital to determine the compressors performance. For dry gas, small inaccuracies in the measurements can alter the polytropic head, efficiency and power calculations notably. Figure 7-1 shows the sensitivity of the single stage compressor located at NTNU (at dry conditions 10000rpm Q=0,9m^3/s) versus errors in the temperature measurements. For heavily wetted gas flow accurate measurements are more challenging and the uncertainties will be even greater.
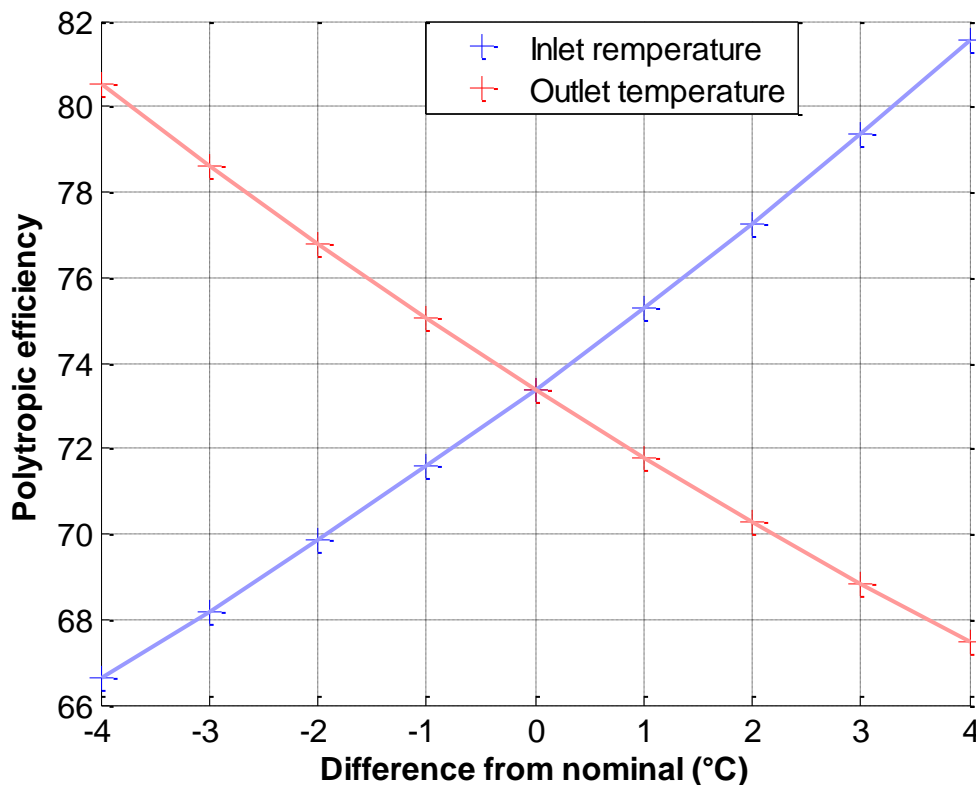
Figure 7-1 Sensitivity of the polytropic efficiency with regards to the temperature

7.1 Thermocouples

If two conductors are connected, they will produce a voltage between them. This voltage is a function of the temperature of the junction. This can be used to directly measure the temperature of the junction. This device is called a thermocouple and is a widely used temperature sensor. The voltage is the sum of two voltage effects called the Peltier effect and the Thompson effect. The main limitation of thermocouples is their accuracy [39].

7.2 Resistance temperature detectors

Metals have an electrical resistance that is a function of the temperature. Therefore a length of a metal wire, combined with an apparatus, measuring the resistance in the metal can measure the temperature of the metal. A Temperature sensor based on this effect is known as a resistance temperature detector (RTD). RTDs are generally more accurate than thermocouples and tend to be more stable. Most RTD sensors are made of platinum, and the temperature is calculated with the Calendar-Van Dusen equation [39].

$$R_T = R_c \left(1 + \alpha_c \left[T - \delta_c (0,01T - 1)(0,01T) - \beta_c (0,01T - 1)(0,01T)^3 \right] \right)$$ **Eq 7-1**

The constants in Eq 7-1 depend on the purity of the platinum and have to be determined by calibration. At the NTNU compressor test-rig two platinum resistance thermometers have been installed. One of them is placed at the compressor inlet and one at the outlet.

7.3 Pyrometers

Noncontact devices for measuring temperature are called Pyrometers, they measure temperature by sensing the radiation emitted from a body. The power and wavelength distribution of this radiation can be used to calculate the temperature of the body. The power from a blackbody is calculated by the Stefan-Boltzmann law. A blackbody is an ideal radiating body, emitting more power at a certain temperature than any other body.

$$E_b = \sigma_b T^4$$ **Eq 7-2**

The wavelength distribution of this radiation can be described as:

$$E_{b\lambda} = \frac{C_1 \lambda_w^{-5}}{e^{C_2/\lambda_w T} - 1}$$ **Eq 7-3**

From this a pyrometer has two ways to determine the temperature. Not only the power emitted, but also the spectral distribution. Most bodies are unfortunately not blackbodies. They will only emit a fraction of the power emitted by blackbodies at the same temperature. This fraction is known as the emissivity and is important to know to be able to accurately measure the temperature with a pyrometer [39]. This would not be possible for gas measurements.

7.4 Fiber optic sensors

An optical fiber transmits light between the two ends of the fiber. A fibre optic sensor either uses the optical fibre for measurements or for transmitting the signal measured by a coating device at the tip of the optical fiber. This is known as intrinsic and extrinsic sensors

respectively. For measuring temperature the same physical laws as for pyrometers are often used [40]. This measurement technique is not very practical as fiber optic sensors are expensive and difficult to install. It could be a realistic option for the NTNU test rig, but for process compressors in general, the costs and the complexity are not beneficial.

7.5 Measuring temperature in two-phase flow

For wet gas compression the compressor exit temperature is vital to know the compressors performance and efficiency. If the compressor pressure and temperature increase fast the evaporation will not be able ensure that the liquid-gas mixture will remain in thermodynamic equilibrium. This will make any attempts to measure the gas temperature extremely challenging. Liquid droplets with higher specific heat coefficient will hit the thermometer and thereby alter the measurements of the gas temperature. What will be measured in practice will be the temperature of the liquid. The need for accurate measurements will also increase in wet-gas compression, Figure 7-2 show how the temperature sensitivity increases with water injection. This concurs well with the findings of Hundseid (2008) [32].
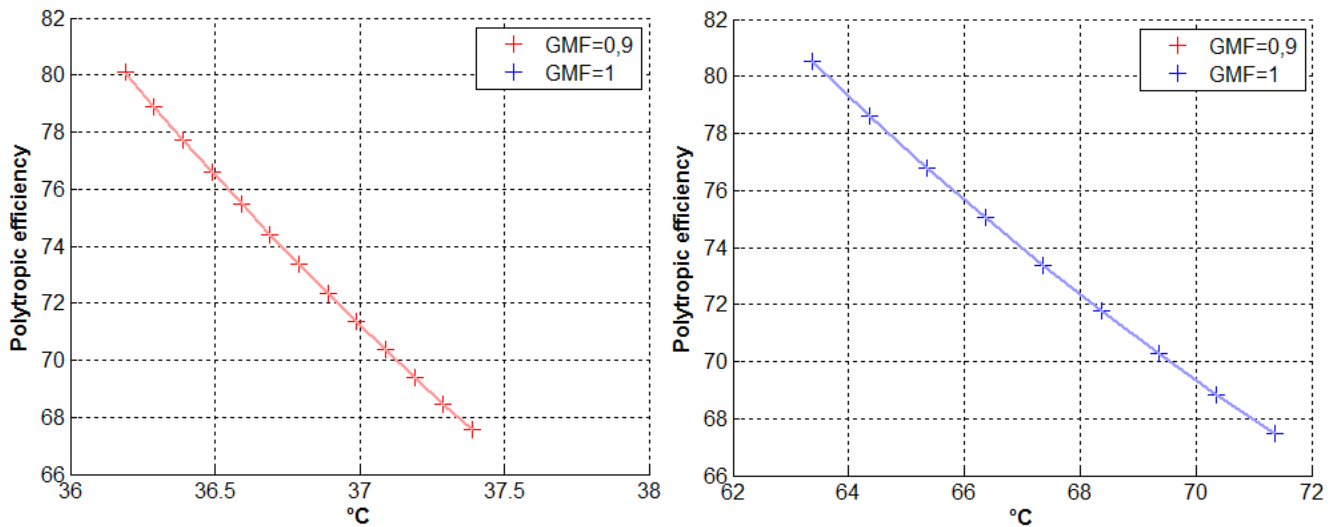
Figure 7-2 Sensitivity of the outlet temperature with a different GMF

7.6 Proposed new measurement techniques

To be able to measure the temperature of the gas without any interference from the liquid, a simple solution would be to separate the two phases without altering the gas properties significantly. A challenge with this is that exit velocities from the compressor are high at the NTNU test rig, typically 60-80m/s, dependent on the speed and volume flow. Several simple separators have been looked at, but few can handle good separation efficiencies at such high flows. The author has proposed a cyclone separator prior to measuring the gas temperature.

7.6.1 Cyclone gas separator

A cyclone is a gas-liquid separation device that puts the mixture into a spiral movement in a cylinder. The heavier droplets, with greater inertia are flung out towards the outer walls, while the gas will continue towards the centre of the cylinder. The droplets will deposit on the walls, and will be drained. In the middle of this cyclone, there will be only gas, and the temperature could be measured, from a regular thermometer.
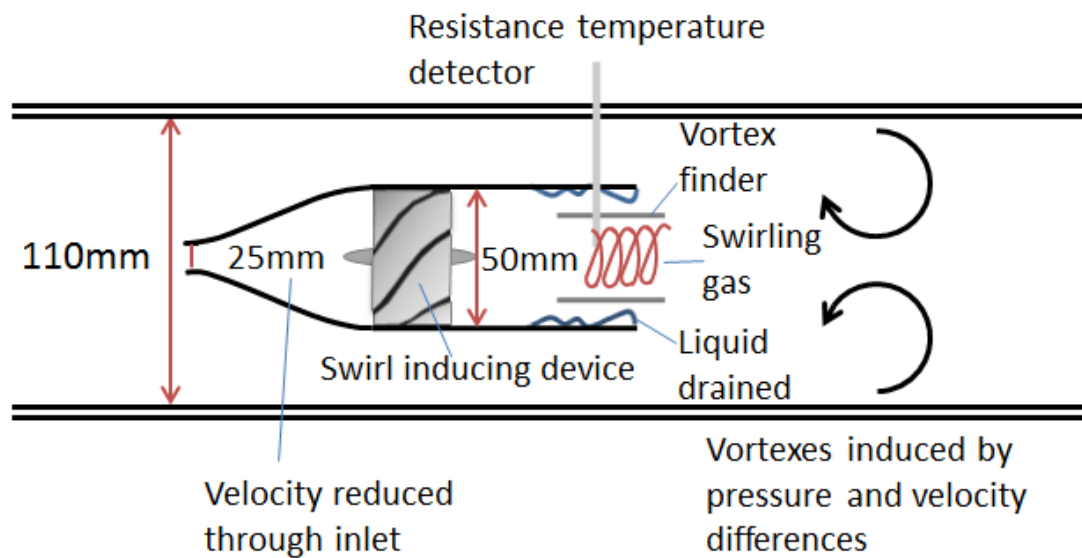
Figure 7-3 Proposed cyclone for gas temperature measurements

Figure 7-3 shows the cyclone proposed at the outlet of the NTNU compressor test rig. Some simple calculations have been done to understand if this idea is feasible. Using data from the tests performed, with 10000rpm and a volume flow of 0,9m³/s at the inlet. The compressor will have a volume flow of about 0,7m³/s at the outlet using the ideal gas law. This is equivalent to 2520m³ per hour. With an inlet of 25mm diameter, assuming the flow is evenly distributed, approximately 130m³/h will enter the cyclone. From the experiments done by Verlaan (1991) [41], seen in Figure 7-4 this cyclone should have a separation efficiency of 97%. Some calculations on the pressure drop across the cyclone are presented in Appendix C.
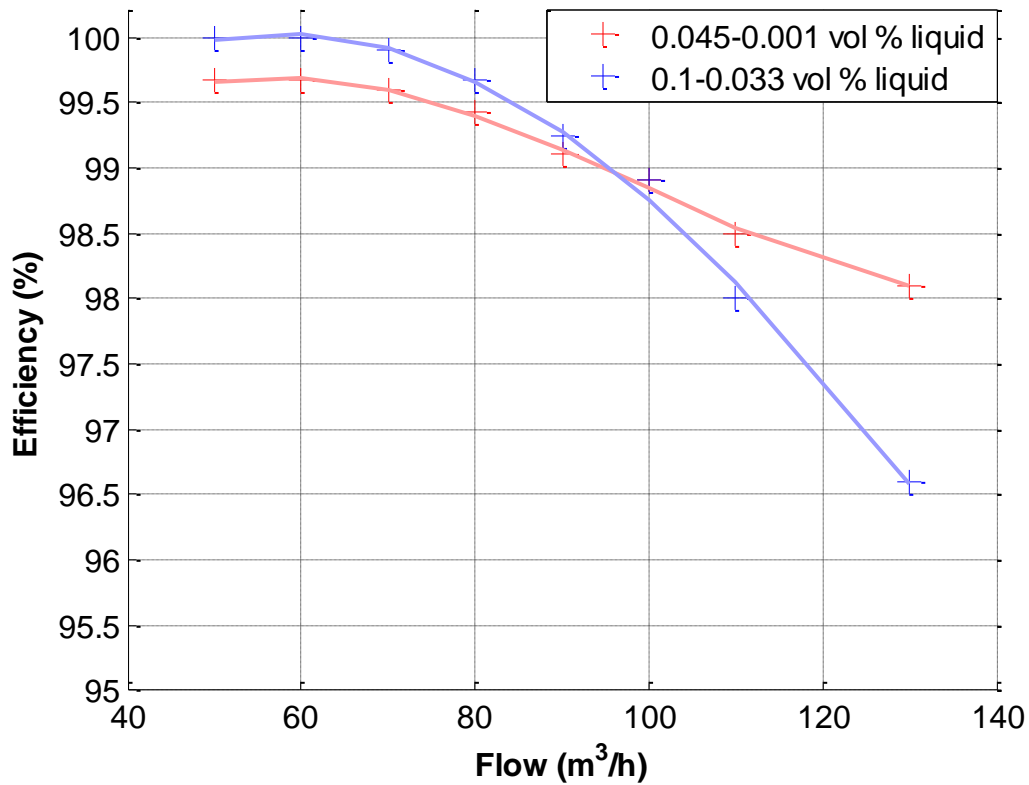
Figure 7-4 Experiments done by Verlaan on cyclone performance at low pressures

It is important to verify that the temperature measured by the resistance temperature detector is in fact correct. To discover how the gas temperature has been altered by the cyclone, a test rig has been proposed, shown in Figure 7-5. Hot air is induced into a pipe before liquid is injected. The gas and the liquid will have different temperatures, and the cyclone will have to be placed close to the liquid injectors so evaporation and heat transfer between the gas and liquid will be limited.
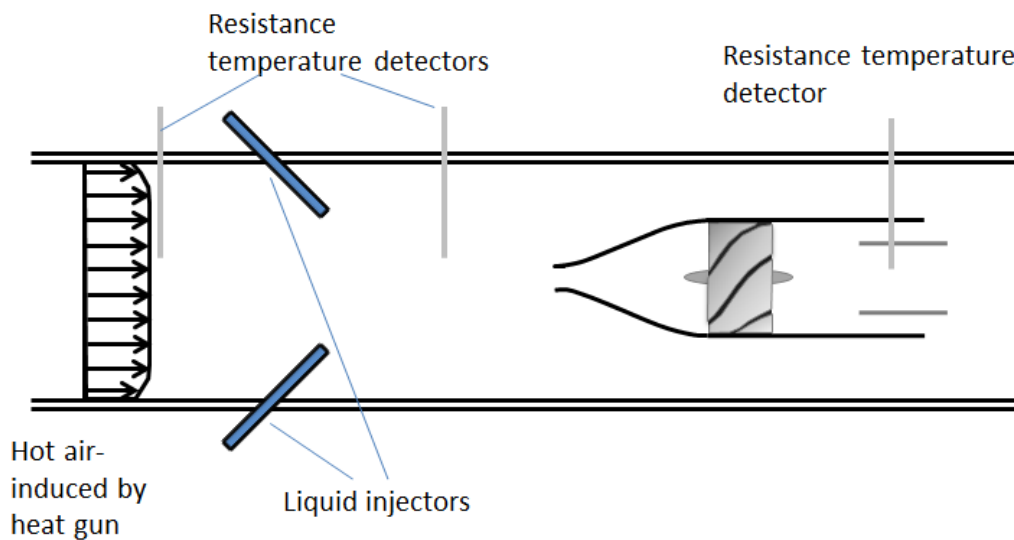
Figure 7-5 Proposed test rig for Cyclone

The RTD after the liquid injectors will verify that the temperature measured by the RTD in the cyclone is different than it would be without the cyclone.

The author has been in contact with Cameron for the delivery of their Consept Demisting Cyclones, and they have shown their interest in this project. They have agreed to lend NTNU one of their Cyclones for an extended period of time. Due to maintenance activity on the compressor test-rig, it was agreed with professor Bakken to postpone this project. A summary of the discussion with Fredrik Carlson, Process Engineer from Cameron, is included in Appendix D.

8 Numerical compression model

A useful tool when modelling, designing or modifying compressors is numerical methods to calculate performance calculations. In recent years 3-D commercial computational fluid dynamics packages have become more easily available as computer power has increased drastically. Still these 3-D CFD codes are time consuming and accuracy is not guaranteed. Therefore other tools have been developed for centrifugal compressors that have been simplified considerably. Many of these use one dimensional calculations and empirical relations developed particularly for centrifugal compressors. For these codes, validation is vital to justify the simplifications and empirical models used. It is very common to have to calibrate these models with experimental results. Correctly calibrated 1-D codes are considerably faster than commercial CFD packages and can often lead to more accurate results. Many companies, including GE, Alstom and Rolls-Royce, are developing their own 1-D models to be able to get fast and accurate results about projected compressors at different speeds and flows[42].

The author has developed a 1-D model for both dry and wet-gas compression. In this chapter the description of the dry calculation are explained, the implications of the wet gas will be discussed in the following chapter. To model the impeller, the Euler equation for turbo-machinery (Eq 3-5) has been used as the base, and knowledge about the machine geometry is necessary.

$$H_{eff} = H_p - \left(\frac{C_2^2}{2} - \frac{C_1^2}{2} \right) + H_{loss}$$

Eq 8-1

The effective head is calculated with the Euler turbo-machinery equation.

$$H_{eff} = \tau U_2^2$$

Eq 8-2

Where τ is the head coefficient calculated from Eq 3-10. The velocities at the inlet and outlet of the impeller are calculated using the velocity triangles. At the outlet of the compressor, the flow coefficient is not known prior to simulation as this depends on the density of the gas. The flow coefficient is therefore calculated iteratively as seen in Figure 8-1. The losses in the impeller can be attributed mainly to friction, incident losses and losses due to blockage. The enthalpy and temperature increase is related with the simple equation:

$$dh = Cp \cdot dT$$

Eq 8-3

Enthalpy and entropy is then related to the pressure increase with Gibbs equation.

$$dh = TdS + vdp$$

Eq 8-4

Along the polytropic process the efficiency is described as:

$$\eta_p = \frac{vdp}{dh}$$

Eq 8-5
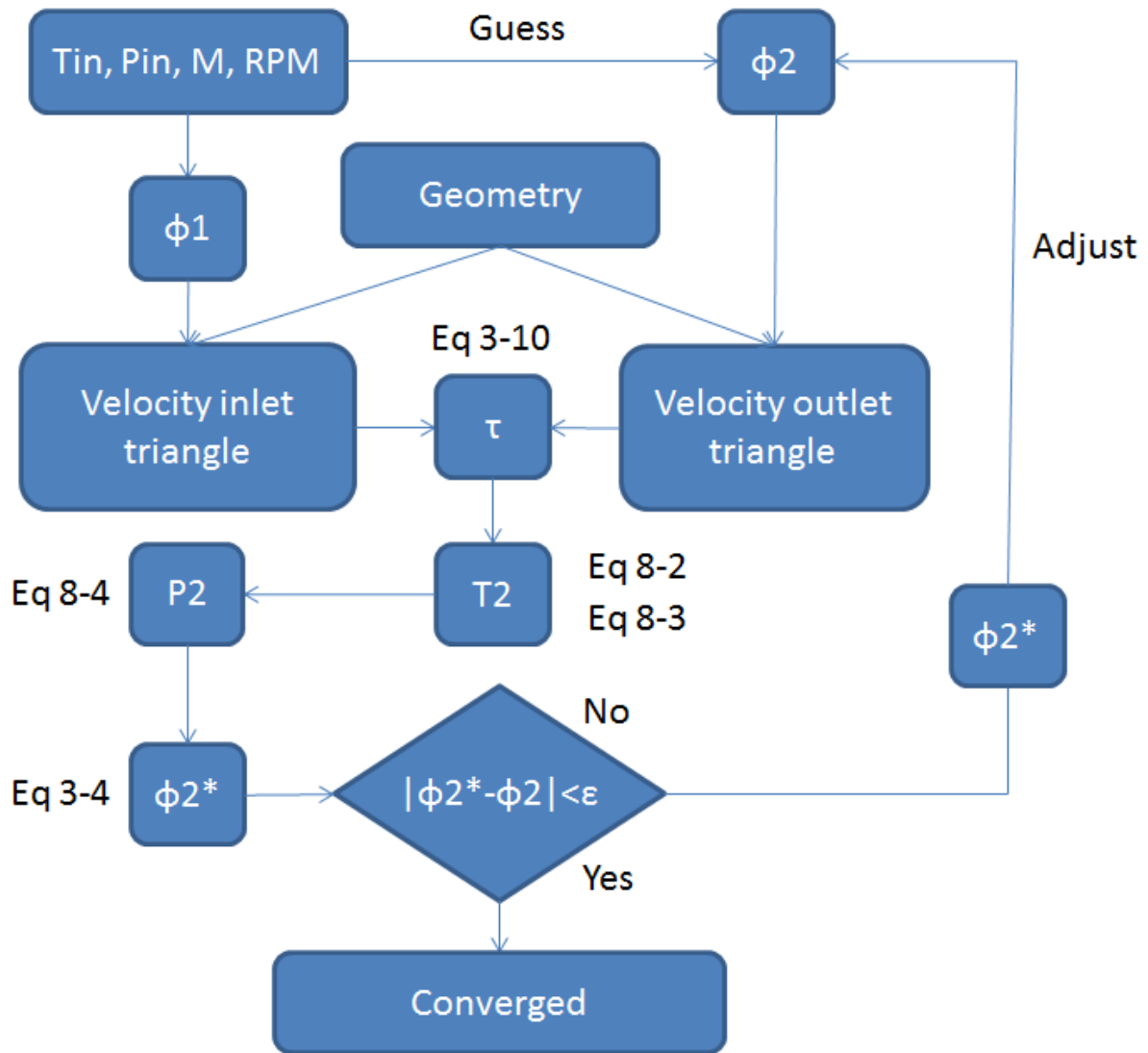
Figure 8-1 Impeller iteration flow chart

The diffusor design is calculated by the method of Stanitz, described in section 3.1.2. This is also an iterative process where the density is assumed at first, then adjusted by iteration.

For the volute, the process is described in section 3.1.3. The method used is that of Aungier (2003), as for the other compressor parts the process is iterative. Here the outlet velocity is first assumed, the losses are then calculated with the assumed outlet velocity as a reference. At the end of the calculations the outlet velocity is checked with the continuity equation.

9 Numerical model for wet gas compression

This chapter explains the implications of wet gas compression in the numerical model created. It is based on the work done by Fabbrizzi et al. (2009) [28] as well as Härtel and Pfeiffer (2003) [26] and Abdelwahab (2006) [27]. All of these articles have examined compression with liquid injection and the basis for all of these articles has been a droplet model. Developed by Spalding (1979) [43] for combustion, it is based on the fact that each droplet is surrounded by a saturated vapour layer as seen in Figure 9-1.
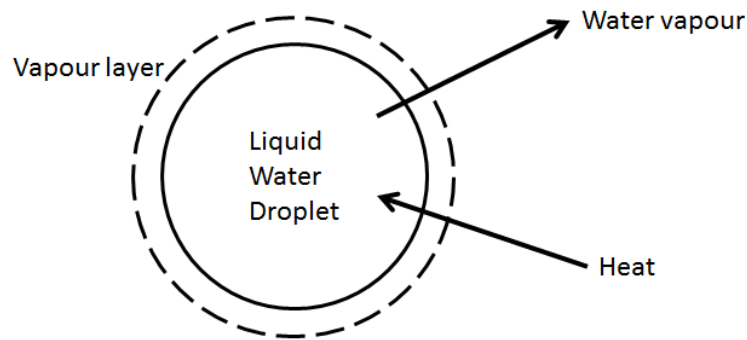
Figure 9-1 Droplet model for prediction of the thermodynamic non-equilibrium

The model developed is described by a gas-droplet flow by Young (1995) [15]. This model does not allow for a liquid film, or droplet-droplet interactions and this is a great flaw in the model. Nevertheless, it provides an estimate of the temperature differences in a wet-gas compressor. For a wet-gas compressor with a low GMF, this is believed to be representative. Still experiments should be done to completely comprehend the dynamics of the multiphase flow in a wet-gas compressor.

9.1 Young's description of the gas-droplet flow

Young's model for the multiphase flow is only based on gas-droplet flow. It allows for numerous droplet groups of different sizes, but in this dissertation only a single size has been used.

The description applies to a gas-droplet mixture, where the gas phase consists of an inert gas and a condensable vapour. The liquid phase is a discontinuous dispersed population of spherical droplets. If the mass of inert gas, per total mass is defined as g, then the mass of vapour plus liquid would be (1-g).

$$g = \frac{m_g}{m_g + m_l + m_v}, \quad 1 - g = \frac{m_v + m_l}{m_g + m_l + m_v}$$

Eq 9-1

The mass of liquid per unit mass of vapour plus liquid is defined as y.

$$y = \frac{m_v}{m_l + m_v}$$

Consequently:

$$g + (1-g)(1-y) + (1-g)y = 1$$

An advantage with this description method is that g will remain constant. The specific humidity is easily described by:

$$SH = \frac{(1-g)(1-y)}{g}$$

This model allows for variation of the temperature of the gas phase and droplets. By Dalton's law the pressure of the mixture phase can be described as the partial pressure of the gas and vapour.

$$p = p_v + p_g$$

The partial pressure for perfect gasses is given by:

$$p_i = p \cdot X_i$$

The partial densities of the gas and vapour can then be calculated:

$$p_v = \rho_v \cdot R_v \cdot T$$

$$p_g = \rho_g \cdot R_g \cdot T$$

From these definitions many of the properties of the gas phase are easily described by Eq 9-9, illustrated here with the specific heat capacity and the gas constant.

$$cp = \frac{g \cdot cp_g + (1-g)(1-y)cp_v}{g + (1-g)(1-y)}$$

$$\bar{R} = \frac{g \cdot \bar{R}_g + (1-g)(1-y)\bar{R}_v}{g + (1-g)(1-y)}$$

9.2   Droplet model

For this purpose a number of simplifying assumptions are used, stated below.

- All droplets are spherical
- There is no slip between the gas and liquid phase
- The properties of the gas and liquid are homogenous throughout their phases.
- There are no droplet-droplet interactions
- Droplets are surrounded by a saturated vapour layer

During compression, the gas temperature will rise. This will lead to a head flux from the gas to the droplets. The temperature of the droplets will start to increase and evaporation will take place. Evaporation will results in cooling of the droplets. The driving force for the evaporation will be the difference in humidity between the vapour layer surrounding the

droplets and the ambient gas. The mass rate transfer between the droplets and the air is described as:

$$\dot{m}_v = 4\pi \cdot \rho_{ref} \cdot \Gamma_{ref} \frac{D}{2} \ln\left(\frac{1 - X_{v,\text{inf}}}{1 - X_{v,surf}}\right)$$

<div align="right">**Eq 9-11**</div>

The molar concentrations of the vapour at the ambient gas and the surface of the droplets can be described by:

$$X_{v,surf} = \frac{p_{v,surf}}{p}, \quad X_{v,\text{inf}} = \frac{p_{v,\text{inf}}}{p}$$

<div align="right">**Eq 9-12**</div>

The saturation pressure at the droplet surface $p_{v,surf}$ is calculated by the Antoine equation. The Antoine equation is shown in Eq 9-13.

$$\log_{10} p = A_a - \frac{B_a}{C_a + T}$$

<div align="right">**Eq 9-13**</div>

The pressure p_{inf} is the partial pressure in the ambient gas and can easily be found by Dalton's equation. The simplifying assumption about gas and droplets having homogenous properties throughout their phases means that the droplet temperature is uniform everywhere inside the droplet. From Eq 9-11 the variation of droplet diameter can be found.

$$\frac{dD}{dt} = \frac{4\rho_{ref} \cdot \Gamma_{ref}}{\rho_l \cdot D} \ln\left(\frac{X_{v,\text{inf}} - 1}{X_{v,surf} - 1}\right)$$

<div align="right">**Eq 9-14**</div>

The liquid temperature variation is described below:

$$\frac{dT_l}{dt} = \frac{6Nu}{\rho_l \cdot D^2 \cdot cp_l}\left[Nu \cdot \lambda_{ref}\left(T_{\text{inf}} - 1\right) - 2h_{ev} \cdot \rho_{ref} \cdot \lambda_{ref} \ln\left(\frac{X_{v,\text{inf}} - 1}{X_{v,surf} - 1}\right)\right]$$

<div align="right">**Eq 9-15**</div>

9.3   Validity of the assumptions

It is important to check if these assumptions are fairly accurate or if they are outside their range of legitimacy at the NTNU compressor test rig. To see if the no-slip condition holds it is useful to check the Stokes number. The Stokes number is described in section 4.4. To calculate the Stokes number the greatest velocity difference in the test rig was assumed to be the tangential velocity component at the impeller inlet. The streamline deflection difference was then assumed to be the middle radius (between disk and shroud) at the impeller inlet. The Stokes number was then plotted against different possible droplet diameters in Figure 9-2. The figure shows that the Stokes number is sufficiently small for the no-slip condition to hold at the NTNU impeller test-rig.
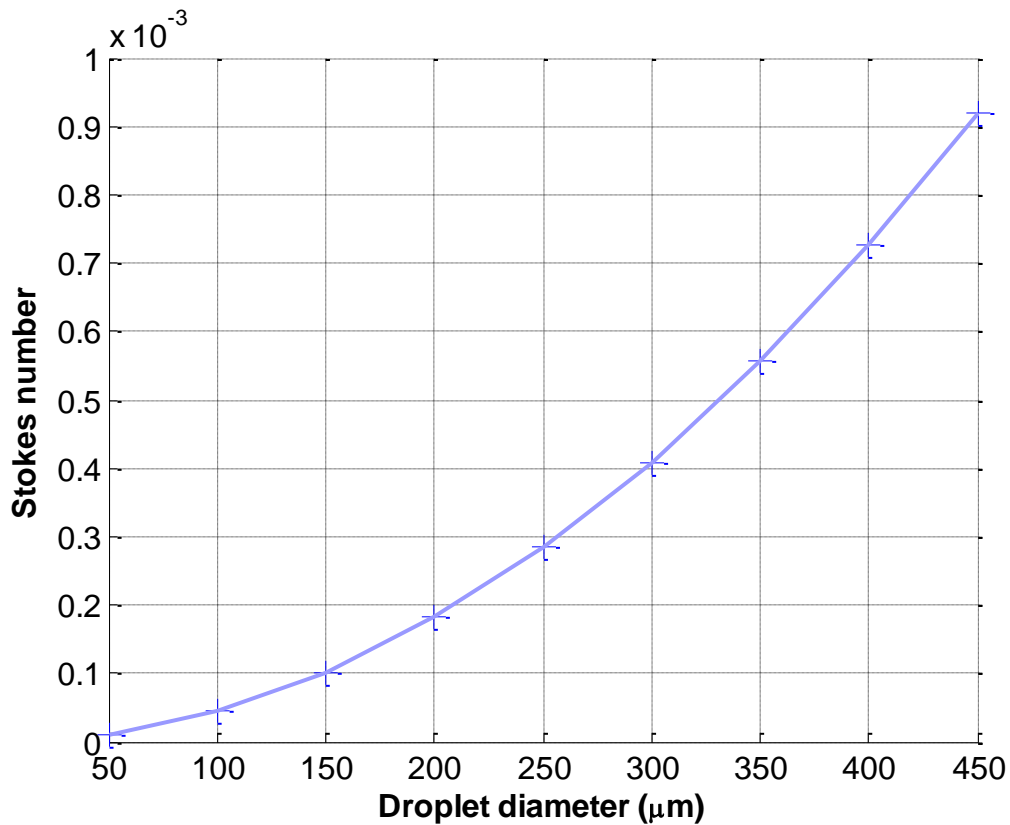
Figure 9-2 Stokes number for different droplet diameter

The assumption regarding the homogeneity of the phases was examined with the Biot number. This number determines if the temperature inside a body will vary significantly and it is defined as:

$$Bi = \frac{hL_c}{\lambda}$$

Eq 9-16

From Incropera et al. (2007) [44], it can be assumed that the temperature inside a body is uniform if the Biot number is below 0,1. Figure 9-3 shows that the droplet Biot number at the compressor inlet is significantly smaller than 0,1. It can therefore be assumed that the temperatures inside the droplets at the NTNU test rig are uniform.
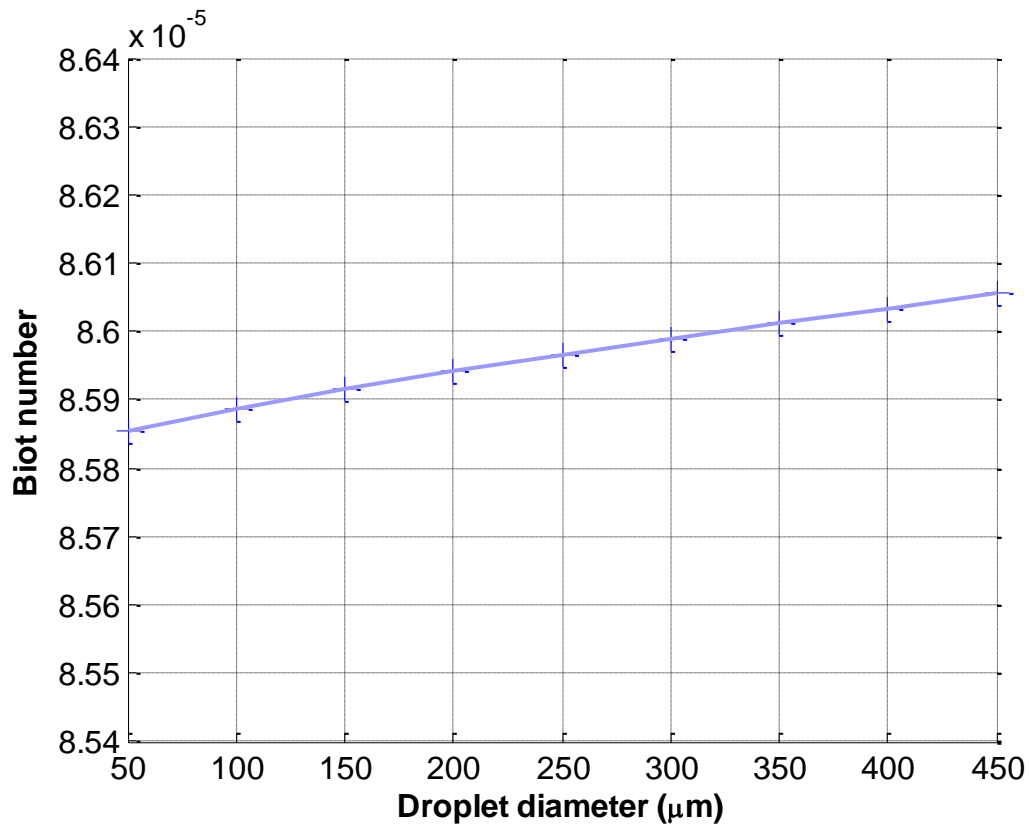
Figure 9-3 Biot number at the compressor inlet with different droplet diameters

The assumption of no droplets-droplets interactions is an uncertain simplification, in reality droplets will collide and be torn apart. Nevertheless, if the gas mass fraction is small, then for an air-water mixture at ambient conditions, the volume occupied by the droplets is minimal. When the volume occupied by the droplets is small, then the number of collisions between them will also be limited. The volume occupied by the gas at different mass fractions at ambient conditions is shown in Table 9-1.

Table 9-1 Mass of droplets and volume occupied by droplets

GMF	GVF
0,9	0,9999
0,8	0,9997
0,7	0,9995

The absence of the liquid film in the model is certainly the largest uncertainty. How much the absence of the liquid film in this model will affect the result is unclear. Modeling the liquid film is complicated and requires a great numerical capacity. It is also currently unknown how much of the liquid will be in the form of droplets and how much will be deposited as liquid film. These are the reason why the author has chosen to neglect it at this present time. To get more exact numerical results additional tests should be done to understand how much of the liquid will be in the form of liquid film. This can be done by flush mounting a high speed camera in the diffusor or even in the impeller. Another option would be to build a diffusor in

acrylic glass and to identify the flow pattern with a high speed camera. Both methods will be technically challenging and costly. If the liquid film proves to be important, then it should incontestably be added to the model.

9.4 Numerical method

Given the base equations in the previous chapter, the temperature at each time-step throughout the compressor can be calculated iteratively. The overall structure of the impeller code is still as in Figure 8-1, but at each time-step, both the pressure and temperature is calculated iteratively. This is done because heat and mass transfer affect these properties continuously.

The code begins by adjusting the specific polytropic head in Eq 8-2 for wet conditions. The adjustment is done with Wood's correctional factor, derived by Hundseid et al (2008) [32].

Eq 9-17

$$h_{p,w} = h_p \cdot \sqrt{\left(1 + \frac{1-GVF}{GVF}\right) / \left(GVF\left[1 + \frac{1-GVF}{GVF}\frac{\rho_l}{\rho_g}\right]\right)}$$

The temperature of the gas is first guessed at a time-step (i+1), then the droplet diameter, temperature and mass transfer is calculated. The gas temperature is then adjusted with the following equation, developed from the energy conservation equation.

Eq 9-18

$$T_g(i+1) = T_{g,guess} - \frac{\dot{m}_v \cdot h_{ev}}{cp_m \cdot m_m} - \frac{m_l \cdot cp_l\left(T_l(i+1) - T_l(i)\right)}{cp_m \cdot m_m} - \frac{m_l\left(P(i+1) - P(i)\right)}{\rho_l \cdot cp_m \cdot m_m}$$

If this is a solution to Eq 9-19, then the iteration process is stopped, if not, then a new guess for the gas temperature have to be made.

$$dh = g \cdot cp_g dT_g + (1-g)(1-y)cp_v dT_g + (1-g)y \cdot cp_l dT_l + h_{ev} \cdot \dot{m}_s$$ **Eq 9-19**

Eq 9-14 and Eq 9-15 are differential equations and are calculated with a Runge-Kutta fourth order scheme, made by the author in Matlab. Some info about this iterative procedure is shown in Appendix E. Figure 9-4 shows the iteration loop for the temperature at each time-step. The equations Eq 9-1 to Eq 9-10 are updated continuously throughout the calculations to update the fluid properties.
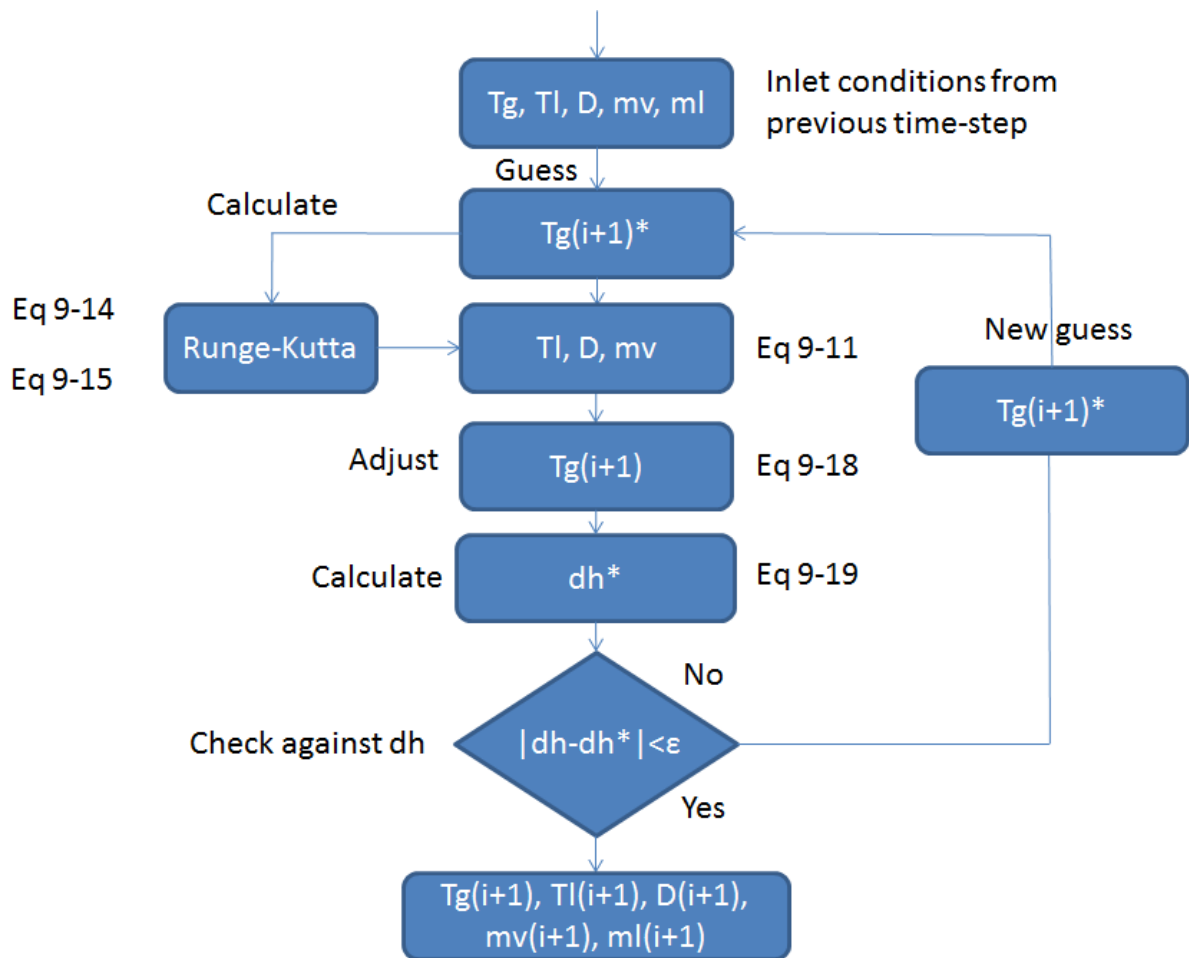
Figure 9-4 Impeller iteration flow chart, wet conditions

In the diffuser, the process is different. First the properties of the dry gas are calculated as in section 3.1.2. This gives the supposed temperature, pressure density velocity and Mach number at "dry" conditions. Then between each time-step, the dry temperature of the gas is adjusted by the differential equations for the gas-droplet heat transfer. This is known as a predictor-corrector step, where the gas temperature is predicted with the use of equations for dry conditions. It is then adjusted with the Runge-Kutta scheme described previously. The entire iteration setup in the diffusor is seen in Figure 9-5.
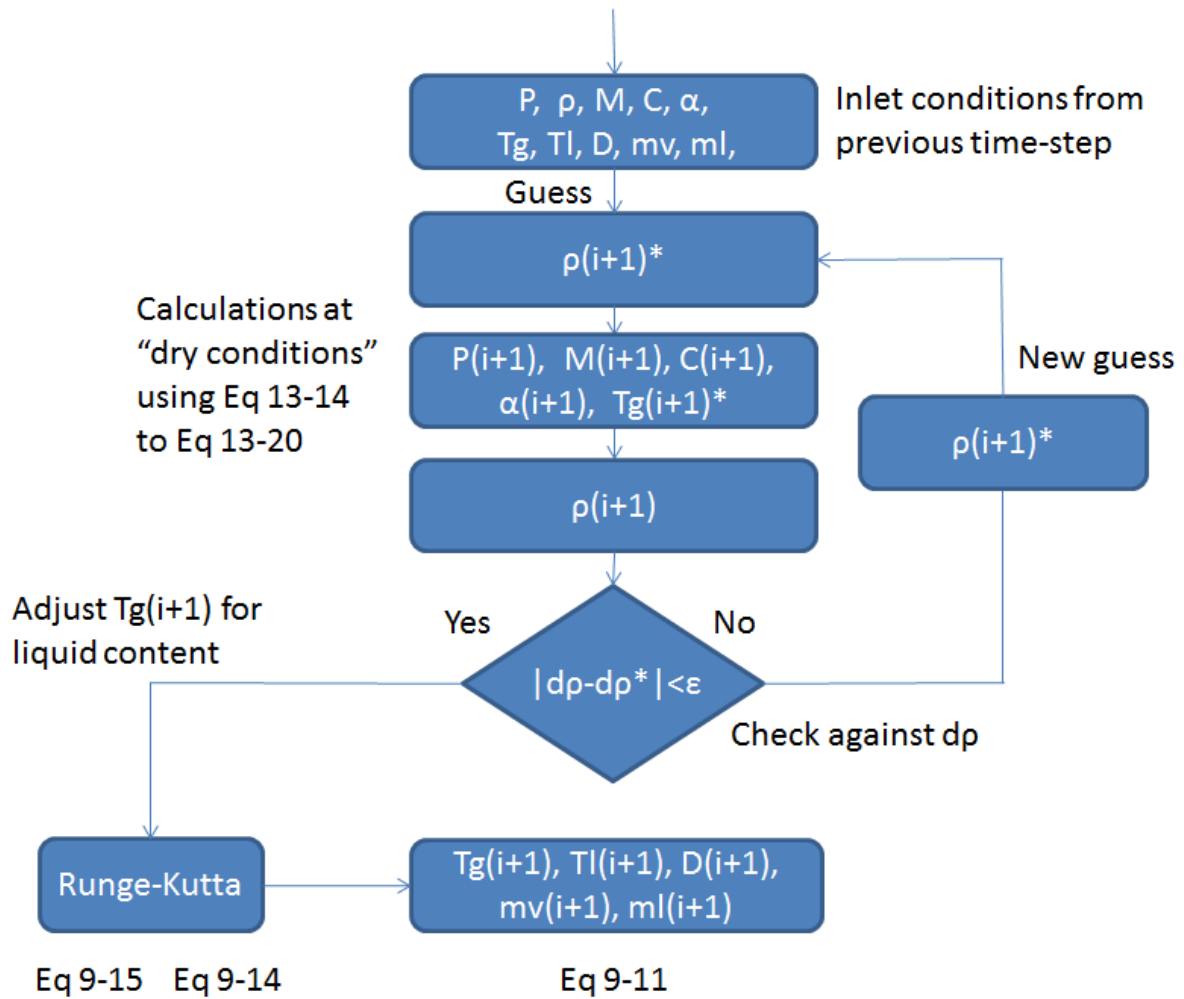
Figure 9-5 Predictor-corrector iteration flow chart in the diffusor

For the discharge volute, the procedure of section 3.1.3 is used, with the exception that the temperature is adjusted for the liquid content. The iteration is very similar to that of the impeller, with the exception that the velocity is used as a criterion for convergence. The procedure is shown in Figure 9-6.
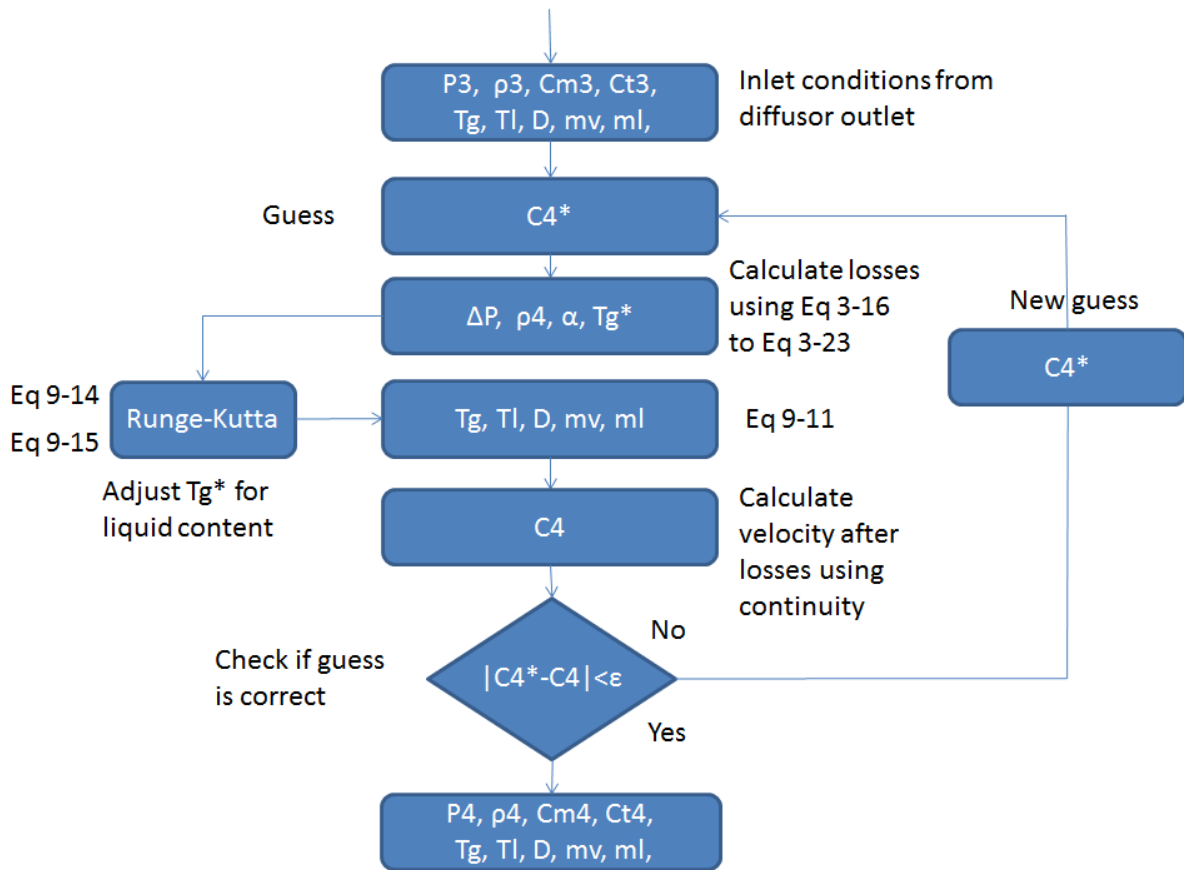
Figure 9-6 Iteration flow chart in the volute, wet conditions

It is very challenging to perform the wet-gas calculations, as a small droplet size makes the need for accuracy quite large. This is due to the fact that Eq 9-15 has the square of the droplet diameter in the denominator. The liquid temperature then gets increasingly sensitive as the droplet diameter decreases. This is referred to as a stiff ordinary differential equation. For very small droplet diameters, the author's computational capacity is too limited to achieve the desired accuracy.

9.5   Part conclusion

Some of the assumptions made to create the model have been verified while some could not be validated. The assumption that all the liquid will be in the form of droplets is one of those and it was not possible to evaluate how much this will affect the final result. The assumption that all the droplets are spherical and that there are no droplet-droplet interactions is also dubious, but it is expected that the final result would not be altered much by this. For further work, the flow pattern in the compressor test-rig must be examined. This can be done with a high speed camera. If the liquid film proves to be an important part of the liquid flow, then it should be modelled.

10 Validating the model for dry gas

To get qualitative results regarding wet gas compression it is vital to perform experiments to support calculations. When it comes to verifying the numerical Matlab model this is not different.

It was discovered that although the pressure stabilized rapidly for the NTNU test compressor, the temperature stabilisation was slow. Therefore the early tests were deemed worthless for everything except the pressure ratio. Unfortunately, it was not possible to perform all the tests desired due to a breakdown of the compressor in mid may, then scheduled maintenance.

It was also discovered that the time to stabilize the compressor was approximately one hour, due to the fact that the compressor casing is not properly isolated. The gas is cooled by the compressor casing, resulting in an appearance of increased efficiency. Figure 10-1 shows how the apparent compressor efficiency changes over time.
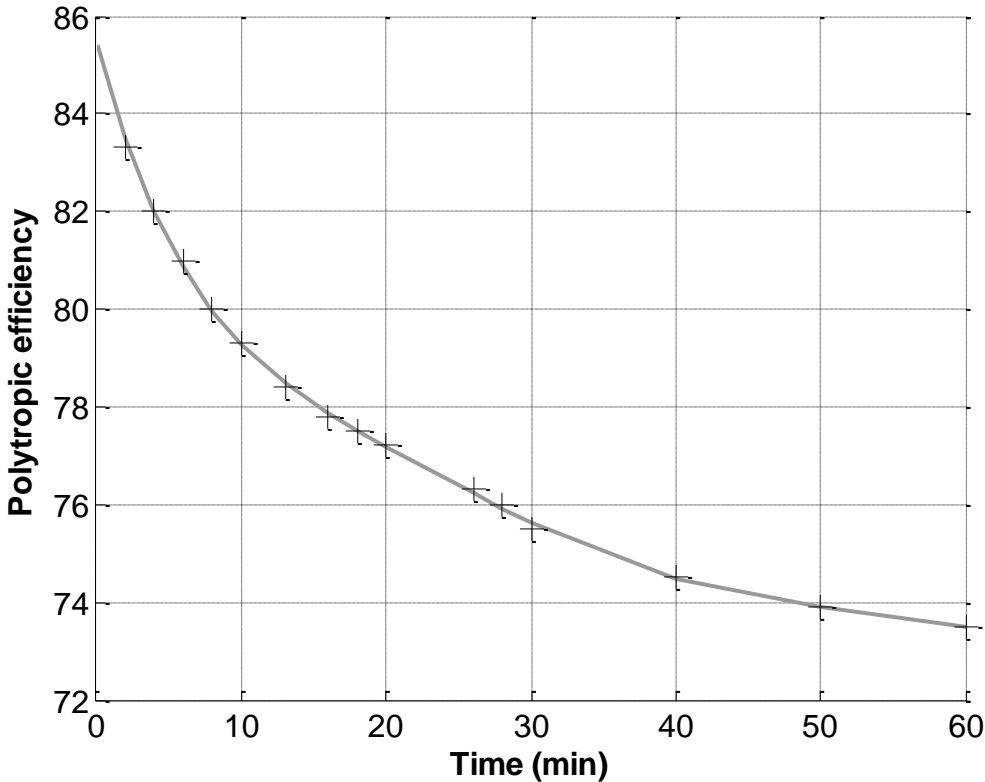
Figure 10-1 Stabilizing time at 10000rpm and Q=0,9m3/s

For the Matlab script constructed to model the possible thermodynamic non-equilibrium, the most important thing to verify against the experimental results is the outlet temperature. This has been done for two different flows at 10000rpm. The author desired a larger set of data for comparison, but unfortunately this was not possible.

Table 10-1 Comparison of experimental measurements of the outlet temperature with the calculated temperature

Test	Flow	Rpm	P1	T1	P2	P2 (ML)	T2	T2 (ML)	T Diff
1	0,91	10000	0,857	24,9	1,207	1,208	67,36	64,85	0,74%
2	1,01	10000	0,84	25,3	1,176	1,176	65,2	63,02	0,73%

Table 10-1 shows that the inaccuracy between the numerical model and experimental results. This is only 0,73-0,74% for the outlet temperature. This may not seem like much, however we see from Figure 7-2 that a difference of 2,5°C means a difference in polytropic efficiency of 4,3pp (percentage points). This inaccuracy is too great for polytropic efficiency calculations. Nevertheless, this model is not intended for polytropic efficiency calculations, but is supposed to give a clear indication of the possible non-equilibrium effects at the compressor discharge. The inlet conditions are set equal to the test conditions.

The calculation procedure described in Appendix A along with the listed uncertainties from section 6.3 has been used to calculate the error in the result. The error was 2,44 and 2,46°C for test 1 and test 2 respectively. This error is large enough to solely explain the deviation between the calculations and the measurements for test 2. For test 1, the discrepancies are 0,07°C. The large error in the temperature calculations is due to the large uncertainty in the frequency converter.

To validate the experimental results, they were checked against the power measurements, with the following equation:

$$\dot{P}_{elec} - \dot{P}_{mech} - \dot{Q}_{env} = \frac{Hp}{\eta_p} \cdot \dot{m}$$

Eq 10-1

The power from the electric motor was then subtracted the mechanical losses and heat losses, to result in the total power provided to the flow. The heat losses to the environment were calculated by using heat transfer equations for radiation and free convection. The calculations were performed in Matlab, and the script is shown in Appendix G. The coefficients used are collected from Incropera et al. (2007) [44]. The mechanical losses were calculated with the procedures mentioned in section 6.2.

This power is supposed to match the power calculated with the polytropic equations. A discrepancy between the measured power and the calculated power was discovered. This means that the instrumentations may not be as accurate as assumed.

Table 10-2 Power balance at dry conditions

Test	Flow	Pelec (kW)	Pmech (W)	Q (W)	Pflow (kW)	Pcalc (kW)	Diff (kW)
1	0,91	44,19	282	2897	41,01	38,45	2,56 (6,2%)
2	1,01	45,05	282	2897	41,87	39,30	2,57 (6,1%)

The uncertainty of the power measurements have been calculated using the same procedure as

for the temperature. This error resulted in 1,33kW for both test points. This means that the discrepancies are outside the margin of error provided by uncertainties in the measurements.
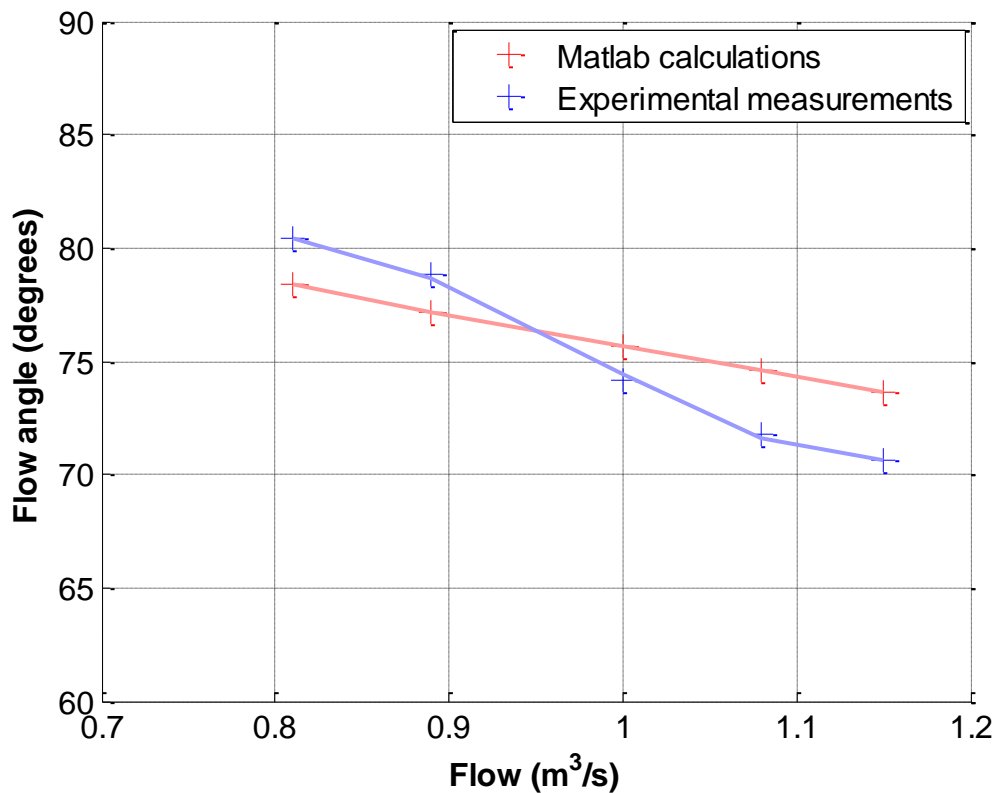
Figure 10-2 Comparison of calculations with experimental measurements

Another way of validating this numerical model for dry gas is to check if the flow pattern provided by the model gives realistic results. The flow angle in the diffusor α (seen in figure Figure 3-4), was measured experimentally by rotating a pitot tube and locating where the maximum pressure appeared. This was done by Sørvik (2012) [45], and the results were then checked against the numerical model, seen in Figure 10-2. This shows that the Matlab model gives a realistic picture of the flow for dry gas as the discrepancies are not large.

10.1 Part conclusion

The outlet temperature discrepancy of the numerical model is too large for accurate polytropic efficiency calculations. To examine if there is a non-equilibrium condition at the discharge it seems sufficient. However, the discrepancies in the power balance are larger than desirable. This means that the experiments should be repeated, to assure that the measured properties are correct. In either case, more experiments are needed at different flows and compressor speeds to fully verify the model. The flow pattern in the diffusor concurs well with experimental results, this is a small assurance for the numerical model, but still more tests must be done to asses this model.

11 Results

Early tests in the NTNU test rig showed an increase in pressure ratio with the injection of liquid in the compressor. Figure 11-1 shows the pressure ratio plotted against the actual flow coefficient divided by the design point flow coefficient. This is consistent with the findings of Brenne et al. (2008) [31]. Fabbrizzi et al. (2009) [28] showed an increased pressure ratio for LMF=5-10% at a low flow coefficient, while for higher LMF and flow coefficients the pressure ratio dropped below that of dry gas. They attributed this to the fact that at low flow coefficients increased flow density and the intercooling effect is greater than the aerodynamic distortion caused by the liquid. Grüner and Bakken (2010) [46], investigated the pressure ratio of a single stage centrifugal impeller exposed to wet gas conditions. Their findings suggested that even with a GMF of 0,48 the pressure ratio increased with comparison to dry conditions at low volume flows. The findings of Grüner and Bakken are consistent with the findings in this thesis, as would be expected, since they are performed at the same test rig, but with a different impeller.
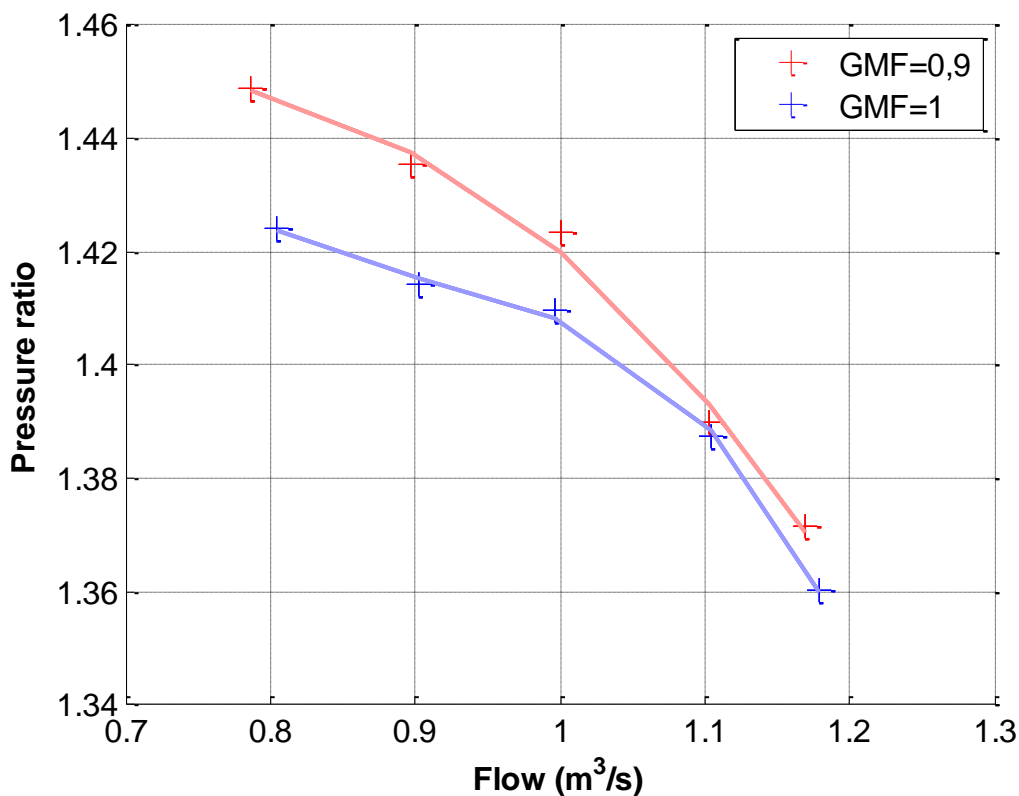
Figure 11-1 Pressure ratio with liquid injection

The temperature measurements for the wet-gas tests are not deemed reliable enough, therefore it is not possible to compare the wet-gas simulations with experimental results. Early simulations showed that the outlet temperature varied strongly with the droplet size. This was expected since the heat transfer area changes with the droplet size. The critical droplet size at the inlet was calculated using Eq 4-6 and Eq 4-7. As this is a simple iterative procedure

calculated with a Matlab script shown in Appendix H. The result was a maximum stable droplet diameter of 340µm.

Simulations run on a flow of 0,91 m³/s with temperature equilibrium between the gas and liquid shows little signs of non-equilibrium conditions at the outlet. The mean line temperature of the gas and liquid at the simulations are shown in Figure 11-2. The different compressor parts in the figure should not be compared against each other as the x-axis is of equal length for the impeller, diffusor and volute. This is not correct as the flow path in the volute is significantly larger than in the impeller and diffusor. The simulations resulted in a temperature difference of 0,16°C between the gas and the liquid at the outlet. This might seem insignificant, but it would still provide noteworthy errors when calculating the efficiency of the compressor. Recalling Figure 7-2, the error would be approximately 2pp. in the polytropic efficiency.
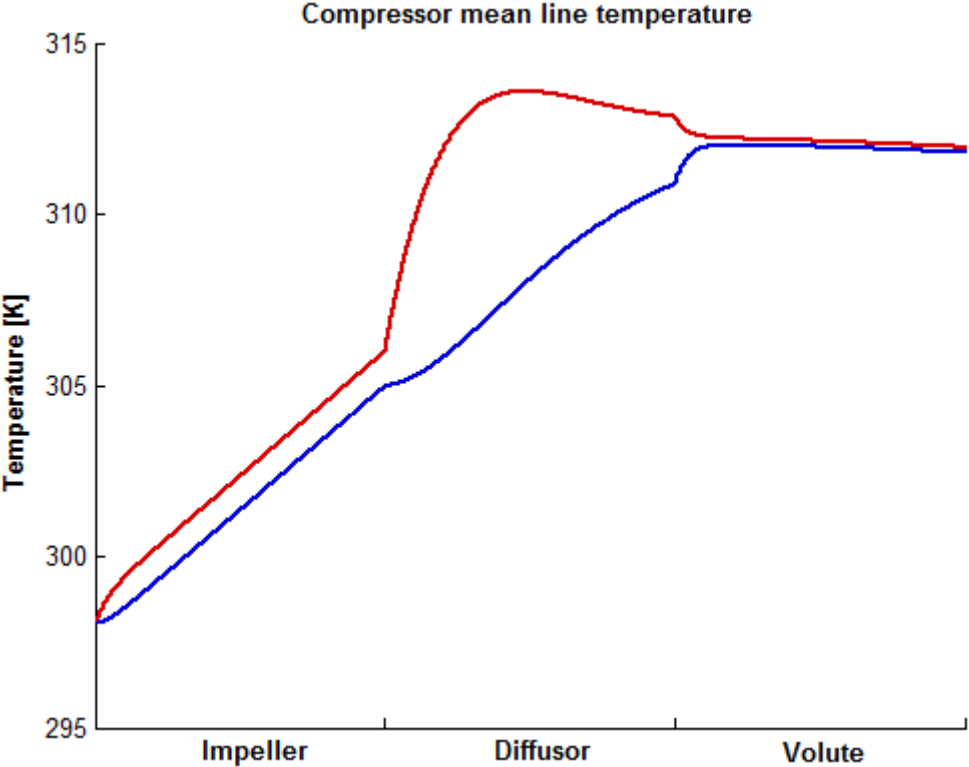
Figure 11-2 Compressor mean line temperature for gas (red) and liquid (blue), 0,91 m³/s, 0,8GMF, 340µm droplet size
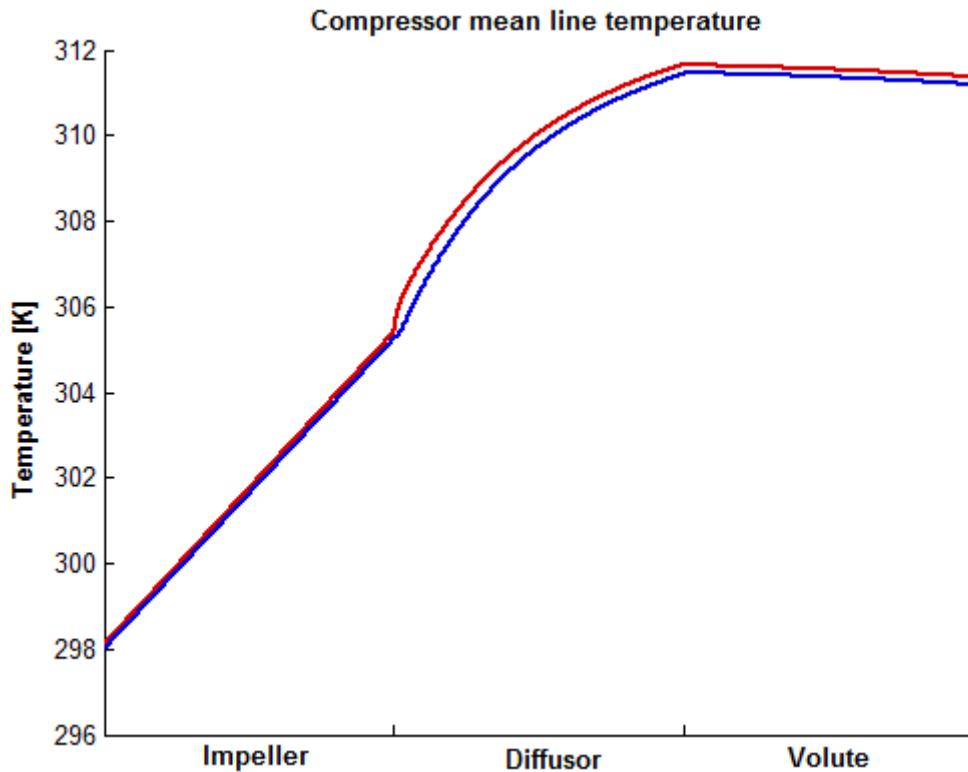
Figure 11-3 Compressor mean line temperature for gas (red) and liquid (blue), 0,91m^3/s, 0,8GMF, 70μm droplet size

Simulations were also run with a smaller droplet diameter, to see the effect. It showed that not only is the droplet diameter of fundamental importance to the temperature differences in the compressor, but it also affects the mean discharge temperature of the flow. This can be seen by comparing Figure 11-2 and Figure 11-3. Fabbrizzi et al. [28] examined the importance of the injected droplet diameter on compressor performance and discovered that this was of little importance. This may be due to the droplet-droplet interactions in the impeller, i.e. coagulation and breakup. The actual droplet diameter inside the compressor may not be governed by the injection nozzle size. Measuring the droplet size on both the inlet and outlet will validate this hypothesis. If the droplet size on the compressor outlet is greater than at the compressor inlet, then the droplet size depends on the critical droplet diameter and not the injection nozzles.

Evaporation inside the compressor was also examined. Figure 11-4 shows that the evaporation increases with increasing droplet diameter. This can be explained directly from Eq 9-11, that shows that the mass evaporated is proportional to the droplet diameter. Nevertheless, it is clear that this evaporation is negligible. The air into the compressor is almost saturated at the inlet and this inhibits evaporation significantly. At the compressor discharge all the water flows into a tank. By measuring how much water is injected into the compressor and measuring the amount of water present in the tank at the end of the run the evaporation in the numerical model can be tested.
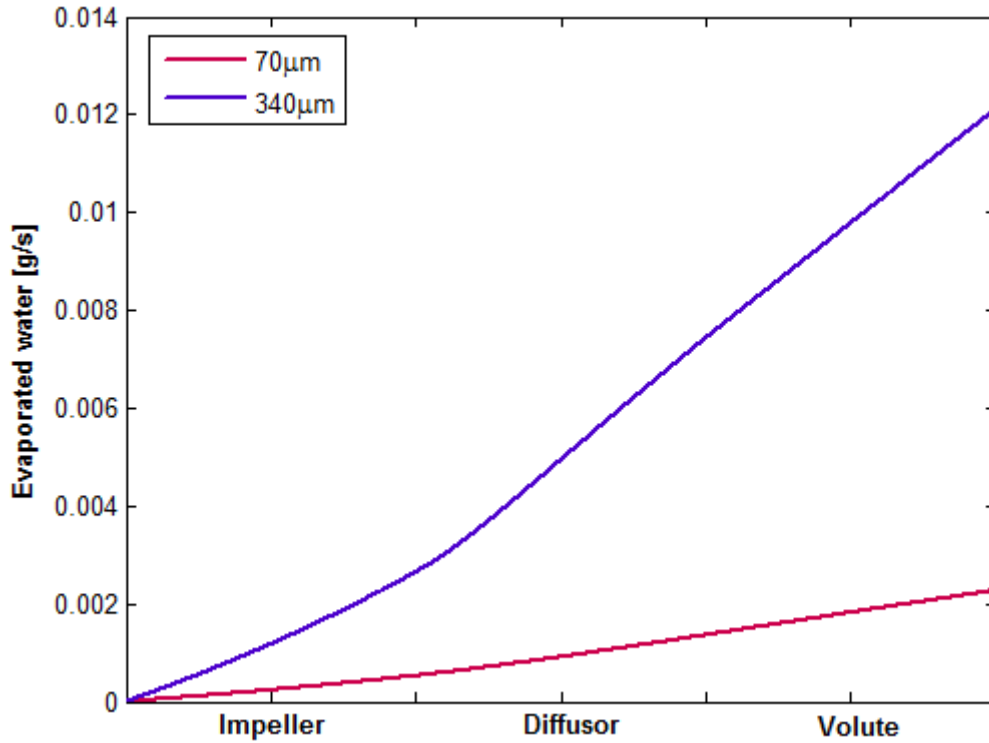
Figure 11-4 Evaporation inside the compressor, 0,91m³/s, 0,8GMF

Another way to determine if there is thermodynamic equilibrium at the droplet discharge is by the power balance. From Härtel and Pfeiffer [26], the work of compression can be calculated from an enthalpy balance.

$$\dot{P} = \dot{m}_m (h_{m2} - h_{m1}) + \dot{m}_l (h_{l2} - h_{l1}) + \dot{m}_{ev} \cdot h_{ev} \qquad \textbf{Eq 11-1}$$

As previously mentioned, the evaporation process is negligible for the compressor performance in this case and the equation can therefore be simplified.

$$\dot{P} = \dot{m}_m C_{p,m} \left(T_{2,m} + \frac{\kappa - 1}{2} \left(M_2^2 - M_1^2 \right) - T_1 \right) + Q_l \left(p_2 - p_1 \right) \qquad \textbf{Eq 11-2}$$

$$+ \dot{m}_l C_l \left(T_{2l} - T_1 \right)$$

If the compression power, the inlet and outlet pressure, inlet temperatures along with the temperature of the liquid is measured accurately enough, then the gas temperature can be calculated with Eq 11-2. As of now, the power balance for dry gas does not match, so to try to evaluate the liquid temperature based on the compressor power would be irrational.

11.1 Part conclusion

It is clear from the numerical simulations that the outlet temperature is dependent on initial droplet diameter. Because of the long particle path inside the volute, both simulations show approximately thermal-equilibrium at the outlet. This is despite the fact that the larger droplet simulations show a significant discrepancy at the diffusor outlet. Simulations also show that the amount of water evaporated in the compressor is negligible. This is attributed to the fact that at the inlet the gas is almost saturated.

Wet-gas experiments have to be done to verify this model. Droplet measurements should be made and the power measurements should be more accurate than they currently are. The inductive flow meters for measuring the liquid inlet flow should also have a high accuracy as this is a significant parameter. Evaporation should be checked with water measurements in the discharge tank and compared to results from the numerical model.

12 Conclusion and further work

For wet gas performance measurements, temperature sensors need to be extremely accurate. A fraction of the errors tolerable in dry gas measurements will give significant deviations for the polytropic efficiency. Measuring multiphase temperature at non equilibrium conditions is a challenging task. Both a numerical simulation model and a temperature measurement solution have been proposed for this problem. Additional experiments should be done to assess both solutions. A calculation method involving the power measurement of the electric motor has also been suggested. The calculated uncertainties for the power were deemed too great for calculation of the gas temperature.

Numerical simulations done for wet gas show a dependence of the droplet diameter for the outlet temperature and thus also the polytropic efficiency. Both simulations showed that because of the long mean particle path in the volute, there will be virtually thermodynamic equilibrium. The mass of evaporated water is insignificant because the air entering the compressor is almost saturated.

Many improvements must be done in the test rig for accurate measurements. The accuracy of the frequency converter, controlling the compressor speed should be increased. The compressor should be properly isolated to avoid large heat losses to the environment. This would also reduce the time required for experiments. Droplet sizes should be measured both at the inlet and outlet and the inductive liquid flow meters should be improved to get a higher accuracy in the liquid mass flow. This should be checked against the water in the discharge tank to see if evaporation is in fact negligible.

To improve the numerical calculation model, the liquid film must be included in the simulation. Some of the liquid will likely deposit on the will and this may have an impact on the outlet temperature. Visual experiments should be done with a high speed camera to asses this.

13 References

1.   ASME, *Compressors and Exhausters*, in *Performance Test Code 10*-1998.
2.   *Petroleum Resources on the Norwegian Continental Shelf*, 2011, The Norwegian Petroleum Directorate: Stavanger.
3.   Budzik, P., *Artic Oil and Natural Gas Potential*, U.S.E.I. Agency, Editor 2009.
4.   Brenne, L., et al., *Prospects for Sub Sea Wet Gas Compression.* ASME Conference Proceedings, 2008. **2008**(43178): p. 671-677.
5.   Moran, M.J. and H.N. Shapiro, *Fundamentals of engineering thermodynamics*2006: John Wiley & Sons.
6.   Schultz, J.M., *The polytropic analysis of Centrifugal Compressors.* ASME Journal of Engineering for Power, 1962.
7.   ISO-5381, *Turbocompressors*, in *Performance Test Code*2005.
8.   Huntington, R.A., *Evaluation of Polytropic Calculation Methods for Turbomachinery Performance.* Journal of Engineering for Gas Turbines and Power, 1985. **13**.
9.   Saravanamuttoo, H., et al., *Gas Turbine Theory*2009: Pearson Education Limited.
10.   Stanitz, J.D., *One Dimensional Compressible Flow in Vaneless Diffusers of Radial- and Mixed-flow Centrifugal Compressors, Including Effects of Friction, Heat Transfer and Area Change.* NACA, 1952. **Technical note 2610**.
11.   Aungier, R.H., *Axial-flow compressors: a strategy for aerodynamic design and analysis*2003: ASME Press.
12.   Boyce, M.P., *Centrifugal Compressors, A Basic Guide*2003: PennWell Corporation.
13.   Haskell, R.W., *Gas Turbine Compressor Operating Environment and Material Evaluation*, in *Power Generation*, G. Company, Editor 1989: New York.
14.   Mandhane, J.M., G.A. Gregory, and K. Aziz, *A flow pattern map for gas—liquid flow in horizontal pipes.* International Journal of Multiphase Flow, 1974. **1**(4): p. 537-553.
15.   Young, J.B., *The Fundamental Equations of Gas-Droplet Multiphase Flow.* International Journal of Multiphase Flow, 1995. **21**(2): p. 175-191.
16.   Ishii, M.a.G., M. A., *Inception criteria for droplet entrainment in two-phase concurrent film flow.* AIChE J, 1975. **21**(2): p. 308–318.
17.   Wallis, G.B., *One-dimensional two-phase flow*1969, New York: McGraw-Hill.
18.   Schubring, D. and T.A. Shedd, *Critical friction factor modeling of horizontal annular base film thickness.* International Journal of Multiphase Flow, 2009. **35**(4): p. 389-397.
19.   Brenne, L., *Straight- Walled Diffuser Performance*, in *EPT*2004, NTNU: Trondheim.
20.   Hinze, J.O., *Fundamentals of the hydrodynamic mechanism of splitting in dispersion processes.* AIChE J, 1955. **1**(3): p. 289–295.
21.   Hinze, J.O., *Turbulence*1975: McGraw-Hill.
22.   Nigmatulin, R.I., *Dynamics Of Multiphase Media*1990: Hemisphere Pub. Corporation.
23.   Alipchenkov, V.M., et al., *A three-fluid model of two-phase dispersed-annular flow.* International Journal of Heat and Mass Transfer, 2004. **47**(24): p. 5323-5338.
24.   Wilcox, E.C. and A.M. Trout, *Analysis of thrust augmentation of turbojet engines by water injection at compressor inlet including charts for calculating compression processes with water injection.* NACA, 1951. **Technical report 1006**.
25.   White, A.J. and A.J. Meacock, *An Evaluation of the Effects of Water Injection on Compressor Performance.* Journal of Engineering for Gas Turbines and Power, 2004. **126**(4): p. 748-754.
26.   Hartel, C. and P. Pfeiffer, *Model Analysis of High-Fogging Effects on the Work of Compression.* ASME Conference Proceedings, 2003. **2003**(36851): p. 689-698.
27.   Abdelwahab, A., *An Investigation of the Use of Wet Compression in Industrial Centrifugal Compressors.* ASME Conference Proceedings, 2006. **2006**(42398): p. 741-750.

28. Fabbrizzi, M., et al., *An Experimental Investigation of a Single Stage Wet Gas Centrifugal Compressor.* ASME Conference Proceedings, 2009. **2009**(48869): p. 443-453.

29. Bettocchi, R., et al., *Set Up of an Experimental Facility for the Investigation of Wet Compression on a Multistage Compressor.* ASME Conference Proceedings, 2010. **2010**(44007): p. 673-683.

30. Hundseid, Ø., L.E. Bakken, and T. Helde, *A revised compressor polytropic performance analysis*, in *ASME Turbo Expo 2006: Power for Land, Sea and Air*2006, ASME: Barcelona, Spain.

31. Brenne, L., et al., *Performance Evaluation of a Centrifugal Compressor Operating under Wet-Gas Conditions*, in *34th Turbomachinery Symposium*, ASME, Editor 2005: Houston, Texas.

32. Hundseid, Ø., et al. *Wet Gas Performance of a Single Stage Centrifugal Compressor*. in *ASME Turbo Expo 2008: Power for Land, Sea and Air*. 2008. Berlin, Germany.

33. Ransom;, D., et al. *Mechanical Performance of a Two Stage Centrifugal Compressor under Wet Gas Conditions* in *Proceedings of the Fortieth Turbomachinery Symposium*. 2011. Houston, Texas.

34. Grüner, T.G., *Experimental investigation of the aerodynamics within a centrifugal compressor exposed to wet gas*, in *EPT*2012, NTNU: Trondheim.

35. Gyarmathy, G., *Foundations of a theory of the wet-steam turbine*1966: Translation Division, Foreign Technology Division.

36. Moore, J. and C.H. Sieverding, *Two-phase steam flow in turbines and separators: theory, instrumentation, engineering*1976: Hemisphere Pub. Corp.

37. Kleitz, A. and J.M. Dorey, *Instrumentation for wet steam.* Proceedings of the Institution of Mechanical Engineers Part C-Journal of Mechanical Engineering Science, 2004. **218**(8): p. 811-842.

38. Schleicher, E., M.J. Da Silva, and U. Hampel, *Enhanced local void and temperature measurements for highly transient multiphase flows.* Ieee Transactions on Instrumentation and Measurement, 2008. **57**(2): p. 401-405.

39. Wheeler, A.J., A.R. Ganji, and V.V. Krishnan, *Introduction to Engineering Experimentation*2009: Pearson Higher Education.

40. Udd, E. and J. William B. Spillman, *Fiber Optic Sensors: An Introduction for Engineers and Scientists*2011: John Wiley & Sons.

41. Verlaan, C., *Performance of novel mist eliminators*, in *Mechanical Engineering and Marine Technology*1991, Delft University of Technology.

42. Minisola, L., *Sviluppo di un modello per la previsione delle prestazioni della girante di un compressore centrifugo in condizioni di funzionamento bifase*, in *Energy engineering*2010, Sapienza Universita di Roma: Roma.

43. Spalding, D.B., *Combustion and mass transfer: a textbook with multiple-choice exercises for engineering students*1979: Pergamon Press.

44. Incropera, F.P. and D.P. DeWitt, *Fundamentals of heat and mass transfer*2007: John Wiley.

45. Sørvik, L.A., *Validation of Wet Gas Surge Phenomena*, in *Department of Energy and Process engineering*2012, NTNU: Trondheim.

46. Gruner, T.G. and L.E. Bakken, *Wet Gas Impeller Test Facility.* ASME Conference Proceedings, 2010. **2010**(44007): p. 705-712.

47. ASME, *Test uncertainty*, in *Performance Test Code 19.1*-2005.

48. Swanborn, R.A., *A new approach to the design of gas-liquid separators for the oil industry*, 1988, Delft University of Technology.

Appendix A   Error and Uncertainty

For uncertainty and treatment of errors the ASME PTC 10 refers to the PTC 19.1 Test Uncertainty [47]. To be able to say something quantitative about a result it is vital to perform an uncertainty analysis.

Types of errors and uncertainty in measurements

The total error δ_E consists of two components, the random error ε_E and the systematic error β_E, as seen in Eq 13-1. Random error is defined as the part of the total error that varies randomly in repeated measurements. This can arise from non-repeatability and uncontrolled test conditions. The systematic error is the part of the error that remains constant in the measurements. A cause of this can for instance be improper calibration of equipment. The mean, µ, of the population (an infinitely large sample) is defined in Eq 13-2 with N going to infinity. This means that with an infinite amount of tests the mean should not contain any random error, but each sample will. We can assume that the population will have a normal distribution. This is illustrated in Figure 13-1. The standard deviation, σ, tells us that for the normal distribution 68% of the population will be in the interval µ ± σ. The interval µ ± 2 σ is more frequently used and will contain 95% of the population (95% confidence interval).

$$\delta_{Ej} = \beta_{Ej} + \varepsilon_{Ej}$$

Eq 13-1

$$\mu = \frac{\sum_{j=1}^{\infty} x_j}{N}$$

Eq 13-2
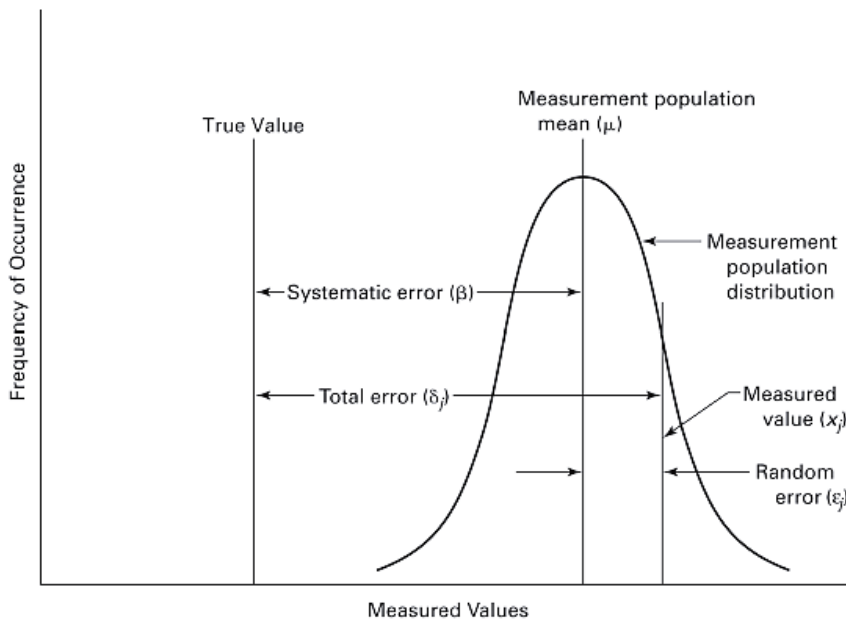
Figure 13-1 Error in measurements [47]

Since the standard deviation is not known, it has to be estimated from a sample of N measurements. For this finite sample, according to the sample mean and standard deviation is given as:

$$\bar{X} = \frac{\sum_{i=1}^{N} X_j}{N}$$

$$s_X = \sqrt{\sum_{i=1}^{N} \frac{(X_j - \bar{X})^2}{N-1}}$$

The sample standard deviation is only related to the sample and not the whole normal distribution. Therefore to estimate the true mean of the population, described as a range from the sample mean one must use the random standard uncertainty of the sample mean.

$$\xi_x = \frac{s_X}{\sqrt{N}}$$

This parameter tells us that the population mean, μ, is expected (with 95% confidence) to lie within ±2ξ from the sample mean $\bar{X}$.

The systematic error can be attributed to many specific systematic uncertainties β's. The elemental systematic standard uncertainty ψ_X by definition determines the variance of the possible β's at standard deviation level. This systematic standard uncertainty is often listed by the manufacturer for measurement instruments, if not the ASME PTC 19.1 relies upon engineering judgment to obtain this. It is important to notice that the systematic error relies upon the uncertainty of the entire instrument loop and not only the measurements. The combined standard uncertainty is the root-sum-square of the standard systematic uncertainty and the standard random uncertainty.

$$u_x = \sqrt{(\psi_x)^2 + (\xi_x)^2}$$

Uncertainty of a result

To see what effect this uncertainty will have on the results one must first describe the result by a certain number of independent parameters

$$F = f(\bar{X}_1, ..., \bar{X}_M)$$

These parameters are the average of a set of measurements of the independent parameters and are calculated by Eq 13-3. Then to see how each of these parameters affects the result the partial derivative of the result is taken with respect to each of the independent parameters.

$$\omega_j = \frac{\partial F}{\partial X_j}$$

The coefficient ω is the sensitivity coefficient and the subscript j, tells us that this coefficient is related to the j-th parameter. This sensitivity coefficient can also be calculated numerically.

$$\omega_j = \frac{\Delta F}{\Delta X_j}$$

Eq 13-9

The random absolute uncertainty of the result is then:

$$\xi_F = \sqrt{\sum_{j=1}^{M} (\omega_j \xi_{xj})^2}$$

Eq 13-10

Likewise the absolute systematic uncertainty is:

$$\psi_F = \sqrt{\sum_{j=1}^{M} (\omega_j \psi_{xj})^2}$$

Eq 13-11

The combined uncertainty is then:

$$u_F = \sqrt{(\psi_F)^2 + (\xi_F)^2}$$

Eq 13-12

With a bit of algebraic manipulation it may also be described as:

$$u_F = \sqrt{\sum_{j=1}^{M} \omega_j^2 (\psi_{xj}^2 + \xi_{xj}^2)}$$

Eq 13-13

By using the two standard deviations as the random error and the fixed error of the same value, this becomes the 95% confidence interval.

Differentiating the equation for the Mach number with respect to the radius:

$$\frac{1}{M^2}\frac{dM^2}{dr} = \frac{1}{C^2}\frac{dC^2}{dr} - \frac{1}{T}\frac{dT}{dr}$$
<div align="right">**Eq 13-14**</div>

The definition of stagnation temperature can be differentiated with respect to the radius:

$$\frac{1}{T_o}\frac{dT_o}{dr} = \frac{1}{T}\frac{dT}{dr} + \left(\frac{\frac{\gamma-1}{2}M^2}{1+\frac{\gamma-1}{2}M^2}\right)\frac{1}{M^2}\frac{dM^2}{dr}$$
<div align="right">**Eq 13-15**</div>

Combining the two equations above:

$$\frac{1}{C^2}\frac{dC^2}{dr} = \left(\frac{1}{1+\frac{\gamma-1}{2}M^2}\right)\frac{1}{M^2}\frac{dM^2}{dr} + \frac{1}{T_o}\frac{dT_o}{dr}$$
<div align="right">**Eq 13-16**</div>

Differentiating the equation for continuity:

$$\frac{1}{\rho}\frac{d\rho}{dr} + \frac{1}{C_R}\frac{dC_R}{dr} + \frac{1}{r} = 0$$
<div align="right">**Eq 13-17**</div>

An equation for radial equilibrium can be obtained from a balance of inertial, pressure and shear forces:

$$\frac{g}{\rho}\frac{dp}{dr} + \frac{c_f C^2 \cos\alpha}{h} = \frac{C_U^2}{r} + C_R\frac{dC_R}{dr}$$
<div align="right">**Eq 13-18**</div>

An equation for tangential equilibrium the equation can be obtained from a balance of the inertial and shear forces:

$$-\frac{c_f C^2 \sin\alpha}{h} = C_R\frac{dC_U}{dr} + \frac{C_R C_U}{r}$$
<div align="right">**Eq 13-19**</div>

The equation of state can be differentiated:

$$\frac{1}{p}\frac{dp}{dr} = \frac{1}{\rho}\frac{d\rho}{dr} + \frac{1}{T}\frac{dT}{dr}$$
<div align="right">**Eq 13-20**</div>

The last six equations are combined with the definition of alpha to result in seven equations. There are a total of seven unknowns, p, ρ, T, M, CU, CR and α. These equations can therefore be solved iteratively.

In the entrance of the cyclone, the cross section will increase, thus decreasing the velocity of the mixture. Using the conservation of mass equation the flow velocity will be reduced drastically.

$$v_2 = \frac{V_2}{A_2} = 130\frac{m^3}{h} \times \frac{1}{\pi(0,025)^2 m^2} \times \frac{1}{3600}\frac{h}{s} = 18,39\frac{m}{s}$$

Eq 13-21

The velocity of the flow before the cyclone is with a flow of 0,7m3/s and a pipe diameter of 11cm, 73,66m/s. Rearranging Bernoulli's equation for incompressible flow.

$$p_2 = p_1 + \frac{1}{2}\rho\left(v_1^2 - v_2^2\right)$$

Eq 13-22

The density at the compressor outlet was calculated by the ideal gas law to 1,23kg/m^3. The pressure in the cyclone before the swirl element can then be calculated.

$$P_2 = 1,2\times10^5\frac{N}{m^2} + \frac{1}{2}\times0,9\frac{kg}{m^3}(73,66^2 - 18,39^2)\frac{m^2}{s^2} = 1,22300\times10^5\frac{N}{m^2}$$

Eq 13-23

The pressure increase before the swirl element is then 23 mbar. The rest of the pipe will have a pressure decrease, as a result of the decreasing flow area due to the cyclone. Right before the swirl element the area of the cyclone has increased, so the area of the pipe minus the cyclone will be smaller than at the inlet of the cyclone. Using the continuity equation for incompressible flow the velocity will be:

$$v_2 = 73,66\frac{0,11^2 - 0,025^2}{0,11^2 - 0,05^2} = 88,05\frac{m}{s}$$

Eq 13-24

It is then possible to use Bernoulli's equation again for the pressure losses.

$$P_2 = 1,2\times10^5\frac{N}{m^2} + \frac{1}{2}\times0,9\frac{kg}{m^3}(73,66^2 - 88,05^2)\frac{m^2}{s^2} = 1,1895\times10^5\frac{N}{m^2}$$

Eq 13-25

The pressure decrease on the outside of the cyclone will then be 10,5 mbar. This will result in a total pressure difference of 33,5 mbar. Swanborn (1988) [48] estimates the pressure drop of such a cyclone to be less than 10mbar. This means that at the outlet, the two flows will meet with different velocities and pressures. There will be a lower pressure outside the cyclone, causing vortices around the end of the cyclone. Therefore the end of the cyclone has to be sufficiently long to prevent backflow from reaching the temperature sensing element. Another important prospect is the fact that with a temperature difference comes also a different pressure. This means that the temperature measured in the cyclone may not be the actual temperature of the gas outside.

Hei Erik.

Vi kunne vel tenkt oss å gjort en type leie avtale, med en konfidensialitets avtale.
Så bygger vi syklonene inn i ett rør stykke som passer inn i riggen deres. Så når dere er ferdig med syklonen så får vi den bare igjen.

Hvor lenge skal prosjektet pågå?
Vi kunne ringtes iløpet av morgen dagen så tar vi en prat.

Vennlig hilsen,
Fredrik Carlson
Process Engineer
Process Systems
Europe, Africa, Caspian and Russia

The Runge-Kutta fourth order is a high precision numerical method, where the next time-step is calculated with the following equation.

$$y_{i+1} = y_i + \tfrac{1}{6}\left(k_1 + 2k_2 + 2k_3 + k_4\right)$$

Eq 13-26

Where the k1, k2, k3 and k4 are slope increments in different places, calculated from Eq 13-27 to Eq 13-30.

$$k_1 = h \cdot y'(t_i, y_i)$$

Eq 13-27

$$k_2 = h \cdot y'(t_i + \frac{1}{2}h, y_i + \frac{1}{2}k_1)$$

Eq 13-28

$$k_3 = h \cdot y'(t_i + \frac{1}{2}h, y_i + \frac{1}{2}k_2)$$

Eq 13-29

$$k_4 = h \cdot y'(t_i + h, y_i + k_3)$$

Eq 13-30

```matlab
function T=Runge_Kutta_enthalpypred_new(tspan,T)
global RHO_M GAMMA Xs_surf Xs_inf

%-------------Constants-----------------------%
Nu=2;
lambda_ref=26.3;      %Air @ 1atm 300K (W/(m*K))%
rho_l=1000;           %Density (kg/m^3) @ standard pressure and
temp3%
cp_l=4185.5 ;         %Specific heat capacity (J/kg K) @ 1 atm
25C%
h_ev=40650;           %Heat of evaporation (J /mol) %

Dia=T(1);             %Inlet droplet diameter%
T_liq=T(2);           %Inlet droplet temperature%
T2=T(3);              %Inlet gas temperature%
Mv=18.02/1000;        %kg/mol%
Fr=1;

D_new=Dia;            %Prelocate for function%
h=tspan(2)-tspan(1);%Time step%

%-----------Equations are defined-------------%
F_xy1 = @(Dia) -Fr*((4*RHO_M*GAMMA)/(rho_l*Dia))...
    *log((Xs_inf-1)/(Xs_surf-1));            %Droplet
diameter%
F_xy2 = @(T_liq) ((6*Nu*Fr)/(rho_l*(D_new^2)*cp_l))*...
    ((Nu*lambda_ref*(T2-T_liq))-((2*(h_ev/Mv))*RHO_M*...
    GAMMA*log((Xs_inf-1)/(Xs_surf-1))));     %T_l%

%-----------Calculation loop------------------%
    k_11 = F_xy1(Dia);
    k_21 = F_xy1(Dia+0.5*h*k_11);
    k_31 = F_xy1(Dia+0.5*h*k_21);
    k_41 = F_xy1(Dia+k_31*h);

%-----------Diameter updated for 2nd Eq--------%
    D_new = Dia + (1/6)*(k_11+2*k_21+2*k_31+k_41)*h;
%-----------Calculation loop------------------%
    k_12 = F_xy2(T_liq);
    k_22 = F_xy2(T_liq+0.5*h*k_12);
    k_32 = F_xy2(T_liq+0.5*h*k_22);
    k_42 = F_xy2(T_liq+k_32*h);

    Tnew= T_liq + (1/6)*(k_12+2*k_22+2*k_32+k_42)*h;

%-----------Output variables------------------%
    T(1)=D_new;
    T(2)=Tnew;
```

```matlab
l=1.2;                      %Length%
w=1.015;                    %Width%
b=0.22;                     %Thickness%
r=0.19576058;              %Radius%
Ts=67+273.15;              %Surface temperature%
Tinf=24+273.15;            %Room temperature%

alpha=22.5*10^-6;          %Thermal diffusivity%
beta=1/Tinf;               %Volumetric thermal expansion
coefficient%
ny=15.89*10^-6;            %Kinematic viscosity%
g=9.81;                    %Gravitational acceleration

sigma=5.67*10^-8           %Stefan-Boltzmann constant%

l2=w*b/(2*w+2*b);

Ra1=(g*beta*(Ts-Tinf)*(l^3))/(alpha*ny);    %Rayleigh number%
Ra2=(g*beta*(Ts-Tinf)*(l2^3))/(alpha*ny);   %Reyleigh number%


Pr=0.707;                  %Prandtl number%

Nu1=0.68+((0.67*(Ra1^(1/4)))/((1+((0.492/Pr)^(9/16)))^(4/9)));
Nu2=0.54*Ra2^(1/4);        %Nusselt number%

k=26.3*10^-3;              %Thermal conductivity%

h1=(Nu1*k)/l;              %Local convection coefficient%
h2=(Nu2*k)/l2;             %Local convection coefficient%

A1=l*w*2+l*b*2-(pi*(r^2));      %Area%
A2=w*b;                        %Area%

q1=h1*A1*(Ts-Tinf);       %heat transfer rate free convection%
q2=h2*A2*(Ts-Tinf);       %heat transfer rate free convection%

qrad=sigma*(Ts^4)*(A1+A2)      %heat transfer rate radiation%

qtot=q1+q2+qrad           %Total heat transfer rate%
```

Appendix H   Matlab script Droplet Size

```
rho_l=1000                  %Density water%
rho_g=1.225                 %Density Air
sigma=0.0728                %Surface tension air-water
din(1)=50*10^(-6)           %Initial droplet diameter 'Guess'%
my=1.0020*10^-3             %Viscosity%
U=48                        %Velocity difference at nozzles%

for i=1:100
We(i)=12+18*((rho_l*sigma*din(i))/(my^2))^-0.37
din(i+1)=(We(i)*sigma)/(rho_g*U^2)
end
```

Appendix I Datasheet temperature sensors

The next pages show the datasheet for the temperature sensors.

A|S|L

HEIGHT OF PRECISION

F500 PRECISION THERMOMETER

ASL's F500 provides you with high accuracy, dual channel temperature measurement for Platinum Resistance Thermometers (PRT) and exploits the inherent advantages of AC bridge technology to maintain repeatable measurements with unique levels of performance and speed.

Features:

- Accuracy: ±0.005°C, ±5mK, over the full range (Typically ±0.001°C, ±1mK, at 0.01°C)
- Resolution: 0.001°C / 0.0001Ω
- Temperature ranges: -200°C to +962°C
- Display update rate: 500ms to full instrument performance
- 25R and 100R Internal reference resistors (user or auto selectable)
- Single, differential and alternate measurement
- 2 Channels as standard with optional 4 or 6 channels
- Expandable up to an additional 64 channels with multiplexers
- Store up to 72 calibrated probe data, unlimited when using Smart probes
- Stand alone Data logging with output to PC or USB Memory Stick
- Sequential Channel scan
- Common Inputs for both 'SMART' and passive probes
- SMART probe review and editor
- Coefficient generation from data pairs
- Individual probe Over Temperature (Tmax, Tmin) visual and audible warning
- Anti-reflective LCD backlit display with numeric, statistical or graphical information
- Self calibrating against traceable external references
- USB interface as standard with optional, RS232, IEEE or LAN interfaces

The F500 comes with two channels as standard, but four and six channel variations are available with each channel able to work with up to 72 user-defined probes. It can also provide a sequential channel scan with a data logging function that can also be sent to PC or USB Memory Stick. The F500 also offers single, differential and alternative measurement modes with the ability to provide direct comparison calibration.

Using calibrated probes with the F500 you can choose between storing the calibration data into the memory of the instrument or if using ASL 'SMART' probes the data can be reviewed and edited therefore easy calibration. The F500 can also generate coefficients from reference temperature / resistance data pairs.

The F500 has 25Ω and 100Ω Internal Standard resistors and with an extended range of 0-500 ohms is capable of measuring temperature ranges to meet ITS90, CVD, EN60751 & IEC751 standards and results are delivered via an anti-reflective LCD backlit display with large numeric, Average, Std Dev, Min, Max and n sample count statistical or graphical information. It also comes with USB interface as standard, but optional RS232, IEEE or LAN interfaces are also available.

To ensure long term reliability the F500 uses surface mount technology with no mechanical relays or potentiometers.

F500 Specification	
Temperature Range:	-200°C to +962°C
Resistance range:	0 to 500Ω
Instrument Accuracy:	+/-0.005°C, +/-5mK over the full range (Typically ±0.001°C, ±1mK, at 0.01°C)
Internal Reference: **TCR:** **Stability:**	25Ω and 100Ω (user, auto selectable) +/-0.1ppm/ °C +/-5ppm / year
Resolution:	0 to 0.001°C/°F/K 0.0001Ω (user selectable)
Display update rate:	500ms to full instrument performance
Probe Current:	Industry standard 1mA, 5mA constant current source (Auto selectable)
Probe Types:	Industrial PRTs and SPRTs with Ro = 25Ω and 100Ω up to an alpha of 0.00392
Data entry format:	ITS90 coefficients, Callender Van Dusen coefficients EN60751 and IEC751 and data pairs for un-calibrated probes.
Thermometer Input: **Connectors:**	2 (front panel), 4 or 6 (rear panel) 5 pin industrial DIN sockets can be used with passive or proprietary 'Smart connector'. Expandable up to an additional 64 channels with SB500 multiplexers
Data logging:	Sequential scan of all channels, log up to 8,000 individual time and date stamped readings to internal memory, export logged data direct to PC or USB Memory Stick
Cable Length:	maximum 30 metres of 4-core 19/0.15 SPC/PTFE screened cable.
Optional Interfaces:	RS232, IEEE-488.2 or LAN Ethernet
Operating Conditions:	15°C to 35°C, < 80% RH non condensing (15°C to 25°C for full range accuracy)
Power Requirements:	90–264VAC universal IEC320 input on rear panel, 47-63Hz, 25VA Max
Dimensions / Weight:	260mm (w) x 80mm (H) x 270mm (D) 2.7Kgs

Appendix J Datasheet torque meter

The next pages show the datasheet for the torque meter.

T12

Digital Torque Transducer

smart torque® by HBM
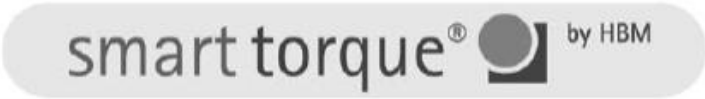
Special features

- Nominal (rated) torques of 100 N·m, 200 N·m, 500 N·m, 1 kN·m, 2 kN·m, 3 kN·m, 5 kN·m and 10 kN·m
- Nominal (rated) speeds from 10,000 rpm to 18,000 rpm
- Wide measurement frequency range up to 6 kHz (−3 dB)
- Fast digital transmission of measurement signals: 4,800 measured values/sec
- High resolution of 19 bit (integral method)
- Monitoring functions
- Extensive options

Block diagram signal flow

Low pass LP1: 0.05 Hz ... 4000 Hz
Low pass LP2: 0.05 Hz ... 100 Hz

Low pass LP: 0.1 Hz ... 80 Hz

Frequency output (10±5 kHz, 60±30 kHz)

Analog output (± 10V)

CANbus

Profibus (optional)

Frequency/ Pulse output

Rotor

Stator

FPGA

Torque

Temperature

Rotational speed/ Angle of rotation: N0, N1, N2

Specifications

Type						T12				
Accuracy class						0.03				
Torque measuring system										
Nominal (rated) torque M$_{nom}$	N·m	100	200	500						
	kN·m				1	2	3	5	10	
for reference only	kft-lb	75	150	375	750	1,500	2,250	3,750	7,500	

Nominal (rated) sensitivity (range between torque = zero and M$_{nom}$)		
Frequency output 10 kHz/60 kHz	kHz	5/30
Voltage output	V	10
Sensitivity tolerance (deviation of the actual output quantity at M$_{nom}$ from the nominal (rated) sensitivity)		
Fieldbusses	%	± 0.05
Frequency output	%	± 0.05
Voltage output	%	± 0.1
Output signal at torque = zero		
Frequency output 10 kHz/60 kHz	kHz	10/60
Voltage output	V	0
Nominal (rated) output signal		
Frequency output		
with positive nominal (rated) torque 10 kHz/60 kHz	kHz	15/90 (5 V symmetric [1])
with negative nominal (rated) torque 10 kHz/60 kHz	kHz	5/30 (5 V symmetric [1])
Voltage output		
with positive nominal (rated) torque	V	+10
with negative nominal (rated) torque	V	−10
Low-pass filter LP1	Hz	0.05 ... 4,000 (4th order Bessel, −1 dB); factory settings 1,000 Hz
Low-pass filter LP2	Hz	0.05 ... 100 (4th order Bessel, −1 dB); factory settings 1 Hz
Load resistance		
Frequency output	kΩ	≥ 2
Voltage output	kΩ	≥ 10
Long-term drift over 48 h		
Voltage output	mV	± 3
Measurement frequency range		
Frequency output/Voltage output	Hz	0 ... 4,000 (−1 dB)
	Hz	0 ... 6,000 (−3 dB)
Group delay time (Low pass LP1: 4 kHz)		
Frequency output 10 kHz/60 kHz	µs	320/250
Voltage output	µs	500
Scale range		
Frequency output/Voltage output	%	10 ... 1,000 (of M$_{nom}$)
Resolution		
Frequency output 10 kHz/60 kHz	Hz	0.03/0.25
Voltage output	mV	0.33
Residual ripple		
Voltage output	mV	3
Temperature influence per 10 K in the nominal (rated) temperature range		
on the output signal, related to the actual value of signal span		
Fieldbusses	%	± 0.03
Frequency output	%	± 0.03
Voltage output	%	± 0.1
on the zero signal, related to the nominal (rated) sensitivity		
Fieldbusses	%	± 0.02 (± 0.01 optional)
Frequency output	%	± 0.02 (± 0.01 optional)
Voltage output	%	± 0.1
Maximum modulation range [2]		
Frequency output 10 kHz/60 kHz	kHz	4 ... 16/24 ... 96
Voltage output	V	−10.2 ... +10.2
Power supply		
Nominal (rated) supply voltage (DC) (separated extra low voltage)	V	18 ... 30
Current consumption in measuring mode	A	< 1 (typ. 0.5)
Current consumption in start-up mode	A	< 4

[1] RS-422 complementary signals, observe terminating resistance.
[2] Output signal range with a repeatable relationship between torque and output signal.

LXXVIII

Appendix K Datasheet pressure sensors

The next pages show the datasheet for the pressure sensors.

DIFFERENTIAL PRESSURE TRANSMITTER
PRE-28
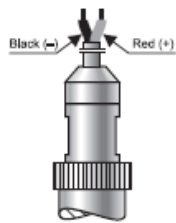
PK type
Electrical cable connection
Degree of protection IP-67
The cable electrical connection, contact with the atmosphere through the capillary inside the cable. The cable length 3m (other cable lengths available, if required)

PD type
DIN 43650 connector
Degree of protection IP-65

PZ type
Electrical connection in a steel field casing with a packing gland M20×1,5
Degree of protection IP-66
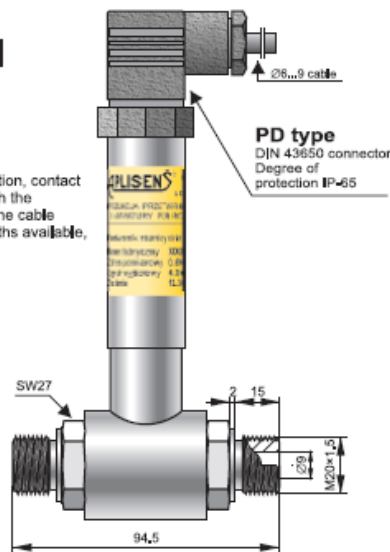
Transmitter PRE-28
Process connection **P type**
Static pressure limit 40 bar
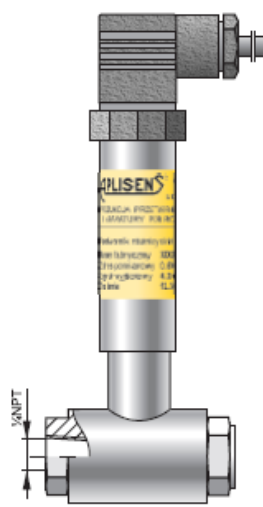
Transmitter PRE-28
Version with **PN type** process connection.
Static pressure limit 40 bar
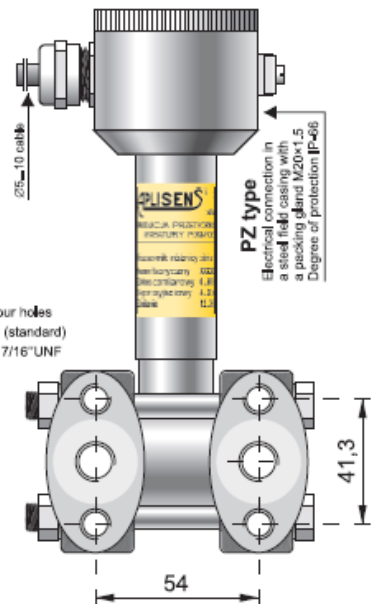
Transmitter PRE-28 — version with **type C** process connection to be mounted together with a valve manifold. Static pressure limit 250 or 320 bar

✓ **Overloads up to 420 bar total static pressure**
✓ **Accuracy 0.25%**
✓ **Any range from 0…16 mbar up to 0…25 bar**

✓ **ATEX Intrinsic safety (Gas and Dust)**
✓ **Marine certificate DNV**

Application
The PRE-28 transmitter is applicable to the measurement of dofferential pressure of gases, vapours and liquids.

Construction
The active element is a piezoresistance silicon sensor separated from the medium by separating diaphragm and a specially selected type of manometric fluid. The special desing of theactive sensing element ensures withstanding the pressure surges and overloads of up to 320bar. The electronics is placed in a casing with a degree of protection IP65, IP67, depending on the type of electrical connection applied.

Calibration
Potentiometers can be used to shift the zero position and the range by up to 10%, without altering the settings.

Installation
The transmitter with P type process connection is not heavy, so it can be installed directly onto impulse lines. For fitting in any desired position on a ∅25 pipe the Aplisens mounting bracket (Fi25 mounting bracket, page 65) is recommended.

The version with C type process connection can be fitted directly to a 3- or 5-valve manifold. The factory-mounted transmitters with VM type valve manifold (page 62) are recommended. A transmitter without a valve manifold can be fitted in any position on a 2" pipe or on a wall using the C-2" mounting bracket (page 65).

When the special process connections are required for the measurement of levels and pressures (e.g. at food and chemical industries), the transmitter is provided with an Aplisens diaphragm seal. The differential pressure transmitters with diaphragm seals are described in detail in the further part of the catalogue.

Technical data

Materials:	Wetted parts:		type P process conn. 316Lss
			type C process conn. 316ss
	Diaphragm	Hastelloy C 276
	Casing	304ss
	Option:	316ss

Hysteresis, repeatability	0,05%
Thermal compensation range:	0÷70 C
Operating temperature range:	-25÷80 C
Medium temperature range:	-25÷120 C (direct measurement)
	Over 120C — measurement with the use of impulse line or diaphragm seals

CAUTION: the medium must not be allowed to freeze in the impulse line or close to the process connection of the transmitter.

Technical data

Any measuring range 0...16 mbar ÷ 0...25 bar

	Measuring Range			
	100 mbar	**1 bar**	**2 bar**	**25 bar**
Overpressure Limit Static Pressure Limit (repeated, without hysteresis)	250 bar (option 420 bar) (40 bar for P type process connection)			
Accuracy	0.4%	0.25%		
Long term stability	0.2% / year	0.1% / year		
Thermal error	Typically 0.3% / 10℃ max 0.4% / 10℃	Typically 0.2% / 10℃ max 0.3% / 10℃		
Zero shift error for static pressure*	0.1% / 10 bar			

* Zeroing the transmitter in conditions of static pressure can eliminate this error.

Output signal 4...20 mA, two wire transmission
0…10 V, three wire transmission

Power supply 10.5...36 V DC (EEx 12...28 V)
    – two wire transmission
15...30 V DC – three wire transmission

Error due to supply voltage changes 0.005% (FSO) / V

Load resistance (for current output) $R[\Omega] \leq \dfrac{U_{sup}[V] - 10.5V}{0.02A} \, 0.85$

Load resistance (for supply output) $R \geq 5\,k\Omega$

Electrical diagrams

4–20 mA output signal

0-10 V output signal
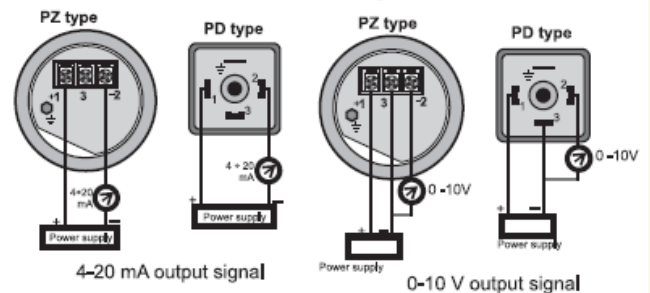
Ordering procedure

Model	Code		Description
PRE-28			Differential pressure transmitter.
Versions * *) more than one option is available	/EExia..		Ex II 1/2G Ga/Gb Ex ia IIC T4/T5/T6, I M1 Ex ia I, II 1D Ex ia D20 T105C (only for transmitters with 4..20mA output)
	/Tlen... /MR...		version for oxygen service (sensor filled with Fluorolube fluid). Marine Certificate DNV
Measuring range	/..........÷............ [required units]		Measuring range in relation to 4mA and 20mA (or 0 and 10V) output. Units: bar, MPa, kPa, etc.
Output signal	⇒	(without marking)..	4...20mA (power supply 10,5÷36VDC)
		/0...10V...	0..10V DC (power supply 15÷30VDC)
		/(other)..	other output signal and power supply (e.g for NE or NN version)
Casing, Electrical connection,	⇒	/PD... PZ.. PZ/316.. PK .... (if other length of cable is required, please specify it /K=....[m])	Housing IP65 with DIN43650 connector PG-11 packing gland. 304SS housing, Ip66, packing gland M20x1,5. 316SS housing, Ip66, packing gland M20x1,5. Housing IP67 with thread M12x1 and connector 304SS housing, IP67, cable electrical connection, 3m of cable
Process connections	⇒	/C.. /P.. /PN.. /code of diaphragm seal...........	Thread 1/4NPT F on the cover flanges, diaphragms material Hastelloy C 276, cover flanges material SS316L. Allows mounting with a valve manifold. Thread M20x1,5 (male) with Ø9hole, diaphragms material Hastelloy C 276, wetted parts SS316L Thread 1/4"NPT (female), diaphragms material Hastelloy C 276, wetted parts SS316L Diaphragm seal (see chapter of diaphragm seals) mounted on Hi side of transmitter, Lo side 1/4NPT Female
Accessories	⇒	/C-2".. /FI25.. /RedSpaw P.................................... /RedSpaw C.................................... /Red d/P ½"......................	Mounting bracket for 2" pipe (to C process conn.), mat. zinced steel Mounting bracket for 2" pipe (to P process conn.), mat. stainless steel Connector to weld impulse pipes dia. 12 and 14 mm, material 15HM(SO) or SS 316(S) . Only process connection P type, Connector to weld impulse pipes dia. 12 and 14 mm, material 15HM. Only process connection C type, Adapter for differential pressure transmitters with C type process connection, output thread 1/2NPT F. Material 316 LSS
Other specification	/...		Description of required parameters
The most typical specification is marked by "⇒" mark.			

Example: Differential pressure transmitter, version EExia, measuring range 0..160mbar, output signal 4..20mA, C type process connection, electrical process connection with DIN43650 connector

PRE-28/EExia/0÷160mbar/PD/C

LD300 Series

301 - 302 - 303

PRESSURE TRANSMITTERS

FOR PRESSURE, LEVEL AND FLOW APPLICATIONS

CE

- ± 0.04% High Accuracy

- ± 0.2% of URL Stability Guarantee for 12 Years

- 120:1 Rangeability

- Non-volatile Flow Totalizer

- Tank Linearization

- 100 ms Total Response Time

- PID Control Capability

- Bi-directional Flow Measurement

- Advanced Diagnostics

- Largest Library of Function Block Execution Capacity

- Instantiable Function Blocks

- Supported by DD, EDDL and FDT/DTM

- Three Technology Options

CEPEL
OCP-0007

INMETRO

CSA®

Ex

EXAM
BBG Prüf- und Zertifizier GmbH

FM
APPROVED

N

Ex
NEPSI

Fieldbus Foundation

I'VE GOT PROFIBUS CAPABILITY

PROFIBUS®

FDT

EDDL
ELECTRONIC DEVICE DESCRIPTION LANGUAGE

smar

Temperature Limits	Ambient: -40 to 85 °C (-40 to 185 °F)
	Process: -40 to 100 °C (-40 to 212 °F) (Silicone Oil)
	                  0 to 85 °C (32 to 185 °F) (Halocarbon and Fluorolube Oil)
	           -20 to 85 °C (-4 to 185 °F) (Krytox Oil and Fomblim Oil)
	           -25 to 85 °C (-13 to 185 °F) (Viton O'Ring)
	           -40 to 150 °C (-40 to 302 °F) (LD301L)
	Storage: -40 to 100 °C (-40 to 212 °F)
	Digital Display: -20 to 80 °C (-4 to 176 °F)
	           -40 to 85 °C (-40 to 185 °F) (without damage)

Turn-on Time	**HART®:** Performs within specifications in less than 5 seconds after power is applied to the transmitter. **FOUNDATION™ Fieldbus and PROFIBUS PA:** Performs within specifications in less than 10 seconds after power is applied to the transmitter.
Configuration	**HART®:** By digital communication (HART® protocol) using the configuration software CONF401, DDCON or HPC301 and HPC401 for Palms. It can also be configured using DD and FDT/DTM tools, and can be partially configured through local adjustment. **FOUNDATION™ Fieldbus and PROFIBUS PA:** Basic configuration may be done using the local adjustment magnetic tool if device is fitted with display. Complete configuration is possible using configuration tools.
Volumetric Displacement	Less than 0.15 cm³ (0.01 in³)
Overpressure and Static Pressure Limits	From 3.45 kPa abs. (0.5 psia)* to: 0.5 MPa (72.52 psi) for range 0 8 MPa (1150 psi) for range 1 16 MPa (2300 psi) for ranges 2, 3 & 4 32 MPa (4600 psi) for models H & A5 40 MPa (5800 psi) for model M5 52 MPa (7500 psi) for model M6 *except the LD300A model* Flange Test Pressure: 60 MPa (8570 psi) For ANSI/DIN Level flanges (LD300L models): 150lb: 6 psia to 230 psi (-0.6 to 16 bar) at 38 °C (100.8 °F) 300lb: 6 psia to 600 psi (-0.6 to 41 bar) at 38 °C (100.8 °F) 600lb: 6 psia to 1200 psi (-0.6 to 83 bar) at 38 °C (100.8 °F) PN10/16: -60 kPa to 1.4 MPa at 120 °C (248 °F) PN25/40: -60 kPa to 4 MPa at 120 °C (248 °F) The above pressures will not damage the transmitter, but a new calibration may be necessary.
Humidity Limits	0 to 100% RH
Damping Adjustment	User configurable from 0 to 128 seconds (via digital communication).

Performance Specifications

Reference Conditions	Span starting at zero, temperature of 25 °C (77 °F), atmospheric pressure, power supply of 24 Vdc, silicone oil fill fluid, isolating diaphragms in 316L SST and digital trim equal to lower and upper range values.

Accuracy	**For range 0, differential and gage models, diaphragms in SST 316L, fill fluid in Silicone or Halocarbon:**
	    0.1URL ≤ span ≤ URL: ± 0.2% of span
	    0.05URL ≤ span ≤ 0.1 URL: ± 0.1 [1 + 0.1 URL/span]% of span
	
	For ranges 1, 2, 3 and 4:
	    0.1 URL ≤ span ≤ URL: ± 0.075% of span
	    0.025 URL ≤ span ≤ 0.1 URL: ± 0.0375 [1+0.1 URL/span]% of span
	    0.0085 URL ≤ span ≤ 0.025 URL: ± [0.0015+0.00465 URL/span]% of span
	
	For ranges 5 and 6, absolute models; diaphragms in Tantalum or Monel; or fill fluid in Fluorolube:
	    0.1 URL ≤ span ≤ URL: ± 0.1% of span
	    0.025 URL ≤ span ≤ 0.1 URL: ± 0.05 [1+0.1 URL/span]% of span
	    0.0085 URL ≤ span ≤ 0.025 URL: ± [0.01+0.006 URL/span]% of span
	
	For absolute models, range 1:
	    ± 0.2% of span
	    Linearity, hysteresis and repeatability effects are included.

Stability	± 0.4% of URL for 12 months for range 0, at 20 °C temperature change and up to 100 kPa (1 bar) of static pressure ± 0.1% of URL for 24 months for ranges 2, 3, 4, 5 & 6 ± 0.2% of URL for 12 months for range 1 & L models ± 0.25% of URL for 5 years, at 20 °C temperature change and up to 7 MPa (1000 psi) of static pressure

Temperature Effect	± (0.1%URL + 0.3% span) per 20 °C for range 0
	± (0.02% URL+ 0.1% span) per 20 °C (36 °F) for ranges 2, 3, 4, 5 & 6
	± (0.05% URL+ 0.15% span) per 20 °C (36 °F) for range 1
	For LD300L:
	    6 mmH$_2$O per 20 ºC for 4" and DN100
	    17 mmH$_2$O per 20 ºC for 3" and DN80
	Consult for other flange dimensions and fill fluid.

Static Pressure Effect	**Zero error:** ± 0.1% URL per 7 MPa (1000 psi) for ranges 2, 3, 4 & 5 ± 0.1% URL per 3.5 MPa (500 psi) for L models ± 0.1% URL per 1.7 MPa (250 psi) for range 1 ± 0.2% URL per 0.5 MPa (5 bar) for range 0 The zero error is a systematic error that can be eliminated by calibrating at the operating static pressure. **Span error:** Correctable to ± 0.2% of reading per 7 MPa (1000 psi) for ranges 2, 3, 4 & 5 or 3.5 MPa (500 psi) for range 1 and L models. Correctable for ± 0.2% of reading per 0.5MPa (5 bar) for range 0.
Power Supply Effect	± 0.005% of calibrated span per volt
Mounting Position Effect	Zero shift of up to 250 Pa (1 inH2O) which can be calibrated out. No span effect.
Electro-Magnetic Interference Effect	Approved according to IEC 61000-6-2, IEC 61000-6-4 and IEC 61326:2002.

kulite®

5 VDC OUTPUT IS® PRESSURE TRANSDUCER
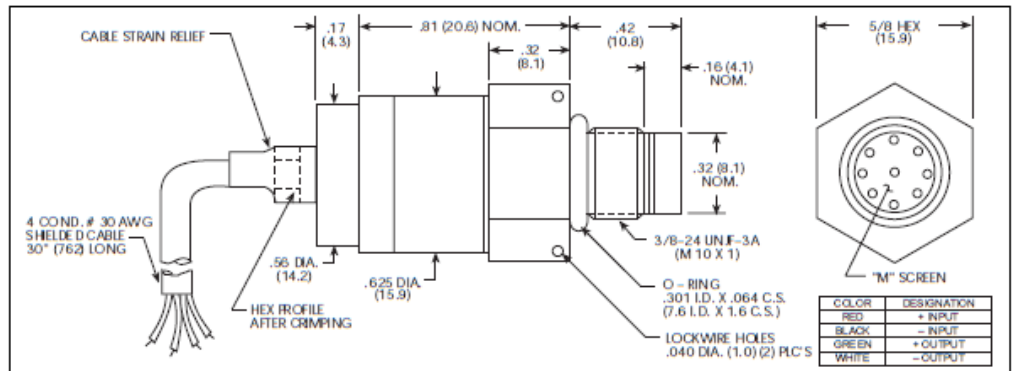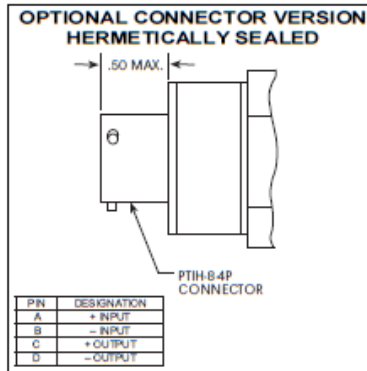
ETM-375 (M) SERIES ETL-375 (M) SERIES

- 5 VDC Output
- Hybrid Microelectronic Regulator-Amplifier
- Flush Diaphragm
- All Welded Construction
- Secondary Containment On Absolute And Sealed Units
- Flight Qualified
- 3/8-24 UNJF or M10 X 1 Thread
- 4 Wire (ETM-375)   3 Wire (ETM-300-375)

ETM-375 series transducers are miniature, threaded flush diaphragm instruments. They utilize a flush metal diaphragm as a force collector. Force is transferred to a solid state piezoresistive sensing element via a thin intervening film of non-compressible silicone oil. This sensing sub-assembly is protected from mechanical damage by a solid screen which has been shown to have minimal influence of the frequency response of the sensor. For applications where a true flush diaphragm is needed, Kulite will supply these transducers without the screen. The ETL Series uses Kulite's Patented Leadless Technology.

Incorporation of a Kulite proprietary electronics module within the main body of this product allows for operation from an unregulated power supply ranging from 13 to 32 VDC. Standard output is a stable, low noise 0 to 5 VDC signal.

OPTIONAL CONNECTOR VERSION HERMETICALLY SEALED

.50 MAX.

PTIH-8-4P CONNECTOR

PIN	DESIGNATION
A	+ INPUT
B	– INPUT
C	+ OUTPUT
D	– OUTPUT

CABLE STRAIN RELIEF

.17 (4.3)
.81 (20.6) NOM.
.32 (8.1)
.42 (10.8)
.16 (4.1) NOM.
.32 (8.1) NOM.
5/8 HEX (15.9)

4 COND. # 30 AWG SHIELDED CABLE 30" (762) LONG

.56 DIA. (14.2)

.625 DIA. (15.9)

HEX PROFILE AFTER CRIMPING

3/8-24 UNJF-3A (M 10 X 1)

O – RING .301 I.D. X .064 C.S. (7.6 I.D. X 1.6 C.S.)

LOCKWIRE HOLES .040 DIA. (1.0) (2) PLC'S

"M" SCREEN

COLOR	DESIGNATION
RED	+ INPUT
BLACK	– INPUT
GREEN	+ OUTPUT
WHITE	– OUTPUT

INPUT										
Pressure Range	1.7	3.5	7	17	35	70	170	350	700	1400 BAR
	25	50	100	250	500	1000	2500	5000	10000	20000 PSI
Operational Mode	Absolute, Gage, Sealed Gage									
Over Pressure	3.5	7	14	35	52	105	210	525	1050	2100 BAR
	50	100	200	500	750	1500	3000	7500	15000	30000 PSI
Burst Pressure	3 Times Rated Pressure to a Max. of 35000 PSI (2400 BAR)									
Pressure Media	Any Liquid or Gas Compatible With 17-4PH or 316SS and Selected O-Ring									
Rated Electrical Excitation	13 - 32 VDC (Other Inputs Available on Special Order)									
Maximum Electrical Current	25 ma									
OUTPUT Output Impedance	200 Ohms (Typ.)									
Full Scale Output (FSO)	5 V ± 3%									
Bandwidth (–3dB)	DC to 5 KHz									
Residual Unbalance	0 to 100 mV (ETM-375)					200 mV ± 50 mV (ETM-300-375)				
Combined Non-Linearity, Hysteresis and Repeatability	± 0.1% FS BFSL (Typ.) (± 0.25% FS Max.) BFSL									
Hysteresis	± 0.1% FSO (Typ.)									
Repeatability	± 0.1% FSO (Typ.)									
Resolution	Infinitesimal									
Natural Frequency (KHz) (Typ.)	120	210	285	425	550	720	910	1120	1350	1600
Acceleration Sensitivity % FS/g Perpendicular	1.9×10^{-3}	1.0×10^{-3}	5.2×10^{-4}	2.2×10^{-4}	1.1×10^{-4}	6.2×10^{-5}	2.6×10^{-5}	1.5×10^{-5}	8.6×10^{-6}	5.2×10^{-6}
Transverse	1.9×10^{-5}	1.0×10^{-5}	5.2×10^{-7}	2.2×10^{-7}	1.1×10^{-7}	6.2×10^{-8}	2.6×10^{-8}	1.5×10^{-8}	8.6×10^{-9}	5.2×10^{-9}
Insulation Resistance	100 Megohm Min. at 50 VDC									
ENVIRONMENTAL Operating Temperature Range	–65° F to +250° F (–55° C to +120° C)									
Compensated Temperature Range	0° F to +212° F (–18° C to +100° C) Other Ranges Quoted on Request									
Thermal Zero Shift	± 1% FSO/100° F (55° C) (Typ.)									
Thermal Sensitivity Shift	± 1% FSO/100° F (55° C) (Typ.)									
Linear Vibration	100g Peak, Sine up to 5000 Hz									
Altitude	Unaffected									
Humidity	100% Relative Humidity									
Mechanical Shock	100g 11 msec., 5000g 100µ sec.									
PHYSICAL Electrical Connection	4 Conductor 30 AWG Shielded Cable 30" (762) Long									
Weight	24.5 Grams (Max.) Excluding Cable									
Sensing Principle	Fully Active Four Arm Wheatstone Bridge Dielectrically Isolated Silicon on Silicon									
Mounting Torque	80 Inch-Pounds (Max.)									

Note: Custom pressure ranges, accuracies and mechanical configurations available.
Continuous development and refinement of our products may result in specification changes without notice - all dimensions nominal.

Appendix L HAZOP

The next pages show the HAZOP for the compressor test rig.

Risk Assessment Report

[Wet gas impeller test facility]

Prosjekttittel	
Prosjektleder	Lars Erik Bakken
Enhet	NTNU
HMS-koordinator	Erik Langørgen
Linjeleder	Olav Bolland
Plassering	
Romnummer	
Riggansvarlig	[Trond Grüner]
Risikovurdering utført av	Lars Andreas Øvrum Sørvik, Erik Mele, Dag Remi Reitan.

TABLE OF CONTENTS

1   INTRODUCTION

An open-loop facility is designed for impeller testing in a single-stage configuration with a direct axial inlet. The facility is adapted for different impeller and diffuser geometries as well as implementation of inlet configurations.

The test facility consists of a high-speed electric motor capable of 450 kW at 11,000 rpm, a bearing pedestal, and a compressor section. The latter includes an shrouded backswept impeller, an integrated diffuser, and a symmetrical circular volute section. All of the components is mounted on a single rigid frame. The rotational speed can be changed by controlling the frequency converter. A discharge throttle valve is used for volume flow regulation.

A single nozzle module has been mounted in the centre of the inlet pipe 0.6 m upstream of the impeller inlet. The nozzle is supplied with pressurized water at a maximum of 16 bar. The liquid flow rate is adjusted by the operating pressure of the pump and a needle valve for fine tuning. Compressor geometry and tube arrangement for the rig facility are presented in Table 1.

Table 1

Impeller		
Outlet diameter	D_2	455mm
Hub diameter	D_H	176-180mm
Shroud diameter	D_S	251,7mm
Outlet width	b_2	14mm
Number of blades	N	18
Exit blade angle	B_2	50°
Diffuser		
Diffusion ratio	D_3/D_2	1,7
With	b_3	14mm

The experiments are conducted in the wet gas impeller test facility at the Norwegian University of Science and Technology (NTNU) in Trondheim, Norway[1].

2   ORGANISATION

Rolle	NTNU	Sintef
Lab Ansvarlig:	Morten Grønli	Harald Mæhlum
Linjeleder:	Olav Bolland	Mona J. Mølnvik
HMS ansvarlig:	Olav Bolland	Mona J. Mølnvik
HMS koordinator	Erik Langørgen	Harald Mæhlum
HMS koordinator	Bård Brandåstrø	
Romansvarlig:	Erik Langøren	
Prosjekt leder:	Lars Andreas Øvrum Sørvik, Erik Mele	
Ansvarlig riggoperatører:	Trond Grüner	

3   RISK MANAGEMENT IN THE PROJECT

Hovedaktiviteter risikostyring	Nødvendige tiltak, dokumentasjon	DATE
Prosjekt initiering	Prosjekt initiering mal	
Veiledningsmøte Guidance Meeting	Skjema for Veiledningsmøte med pre-risikovurdering	
Innledende risikovurdering Initial Assessment	Fareidentifikasjon – HAZID Skjema grovanalyse	
Vurdering av teknisk sikkerhet Evaluation of technical security	Prosess-HAZOP Tekniske dokumentasjoner	
Vurdering av operasjonell sikkerhet Evaluation of operational safety	Prosedyre-HAZOP Opplæringsplan for operatører	
Sluttvurdering, kvalitetssikring Final assessment, quality assurance	Uavhengig kontroll Utstedelse av apparaturkort Utstedelse av forsøk pågår kort	

4   DRAWINGS, PHOTOS, DESCRIPTIONS OF TEST SETUP

Attachments:
Process and Instrumentation Diagram (PID)
Shall contain all components in the experimental setup
Component List with specifications
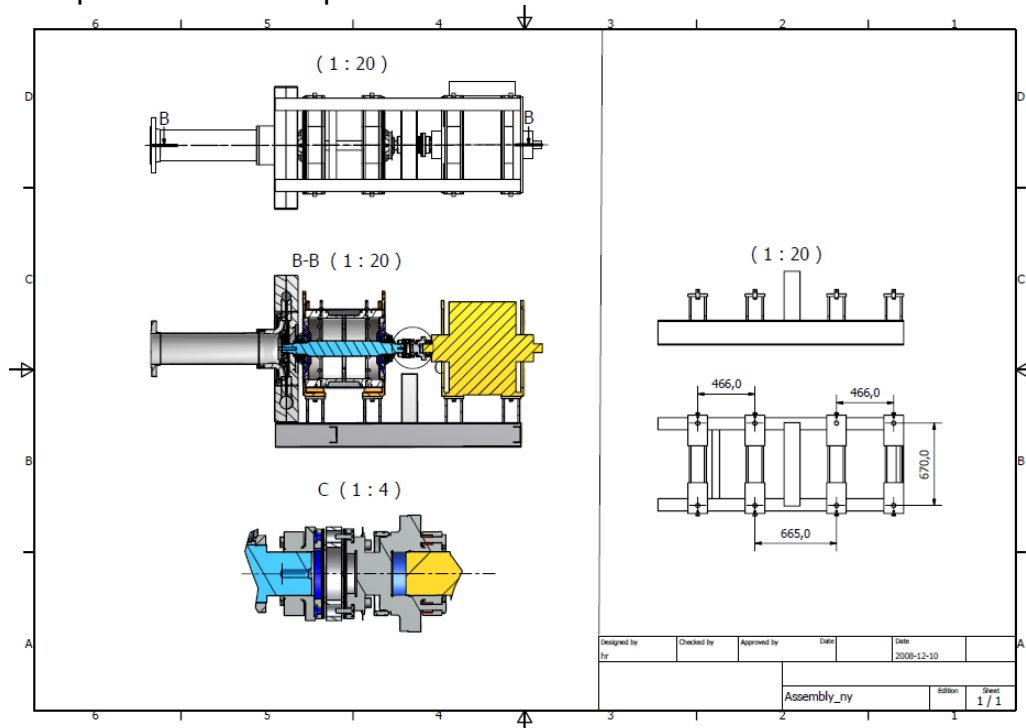
The compressor is driven by an electrical motor with maximum power of 450 kW at 11000 rpms. The Operator of the rig is present in the control room. The frequency converter which is used to change the rotational speed of the machine and the water pump can be controlled from here. Unfortunately, the manual throttling valve

downstream the compressor cannot be closed from the control room. Therefore, in order for attain transient conditions, the regulation of volume flow is done manually.

To ensure that the injection of water provides an equal distribution, 16 nozzles is distributed uniformly over the circumference of the tube.

The water pump is capable of flows up to 50kg/s at 16bar.

5 EVACUATION FROM THE EXPERIMENT AREA

Evacuate at signal from the alarm system or local gas alarms with its own local alert with sound and light outside the room in question, see 6.2
Evacuation from the rigging area takes place through the marked emergency exits to the meetingpoint, (corner of Old Chemistry Kjelhuset or parking 1a-b.)
Action on rig before evacuation:
(Shut off the air and water supply. Power off the electrical supply.)

6 WARNING

6.1 Before experiments

E-mail with information about the test run duration, (hour) and the involved to
 HMS koordinator NTNU/SINTEF
Erik.langorgen@ntnu.no
Baard.brandaastro@ntnu.no
Project Managers on neighboring units alerted for clarification around the use of the exhaust system without fear or interference of any kind, see rig matrix.

All experiments should be planned and put into the activity calendar for the lab.
Experiment leader must get confirmation that the experiments are coordinated with other activity before start up.

6.2 Nonconformance

FIRE
Fire you are not able to put out with locally available fire extinguishers, activate, the nearest fire alarm and evacuate area. Be then available for fire brigade and building caretaker to detect fire place.
If possible, notifie:

NTNU	SINTEF
Labsjef Morten Grønli, tlf: 918 97 515	Labsjef Harald Mæhlum tlf 930 149 86
HMS: Erik Langørgen, tlf: 91897160	Forskningssjef Mona J Mølnvik tlf 930 08 868
Instituttleder: Olav Bolland: 91897209	

GASALARM
At a gas alarm, close gas bottles immediately and ventilated the area. If the level of gas concentration not decrease within a reasonable time, activate the fire alarm and

evacuate the lab. Designated personnel or fire department checks the leak to determine whether it is possible to seal the leak and ventilate the area in a responsible manner.

Alert Order in the above paragraph.

PERSONAL INJURY
- First aid kit in the fire / first aid stations
- Shout for help
- Start life-saving first aid•

CALL 113 if there is any doubt whether there is a serious injury

Other Nonconformance (AVVIK)

NTNU:

Reporting form for nonconformance at:
 http://www.ntnu.no/hms/2007_Nettsider/HMSRV0401_avvik.doc

SINTEF:

Synergi

7   ASSESSMENT OF TECHNICAL SAFETY

7.1   HAZOP

See Chapter 14 "Guide to the report template".

Explosive zones

Zone 0	Always explosive area, for instance vessels with pressurized gas, or flamable liquid
Zone 1	Occasionally explosive zone, for instance fuel stations
Zone 2	Secondary emission discharge site, may be explosive due to accidents

Attachments:, skjema: Hazop_mal

Conclusion: The testrig is not classified as any of the descriptions above, it is not necessary to take EX precautions

7.2   Flammable, reactive and pressurized substances and gas

Contains the experiments Flammable, reactive and pressurized substances and gas

No	

Attachments: Hazop template

7.3   Pressurized equipment

Contain the set up pressurized equipment?

Yes	Equipment have to undergo pressure testes in accordance with the norms and be documented

Attachements:

7.4 Effects on the environment (emissions, noise, temperature, vibration, smell)

Yes	

Conclusion: The experimens will generate large amounts of noise and vibrations. Therefore, experiments at high speeds are scheduled after normal work hours. An eventual oil leakage will be minor and will be handled locally.

7.5 Radiation

See Chapter 14 "Guide to the report template".

No	

7.6 Usage and handling of chemicals.

See Chapter 14 "Guide to the report template".

No	

7.7 El safety (need to deviate from the current regulations and standards.)

Yes	Stay clear of perimeter during operational hours

8   ASSESSMENT OF OPERATIONAL SAFETY

Ensures that established procedures cover all identified risk factors that must be taken care of through procedures. Ensures that the operators and technical performance have sufficient expertise.

8.1 Prosedure HAZOP

See Chapter 14 "Guide to the report template".
The method is a procedure to identify causes and sources of danger to operational problems.
Attachments:: HAZOP_MAL_Prosedyre
Conclusion:

8.2 Operation and emergency shutdown procedure

See Chapter 14 "Guide to the report template".
The operating procedure is a checklist that must be filled out for each experiment.
 Emergency procedure should attempt to set the experiment set up in a harmless state by unforeseen events.
Attachments: "Procedure for running experiments
Emergency shutdown procedure:

8.3 Training of operators

A Document showing training plan for operators
  What are the requirements for the training of operators?
  • *What it takes to be an independent operator*
  •*Job Description for operators*
 Attachments:: Training program for operators

8.4 Technical modifications

- Technical modifications made by the Operator
  o (for example: Replacement of components, equal to equal)
  - • Technical modifications that must be made by Technical staff:
  o (for example, modification of pressure equipment).

Conclusion:

8.5 Personal protective equipment

- Mandatory use of eye protection in the rig zone
- Mandatory use of hearing protection.

Conclusion:.

8.5.1 General Safety

- The area around the staging attempts shielded.
- Gantry crane and truck driving should not take place close to the experiment.
- Gas cylinders shall be placed in an approved carrier with shut-off valve within easy reach.
- Monitoring, can experiment run unattended, how should monitoring be?

Conclusion:
Is Operator allowed to leave during the experiment?

8.6 Safety equipment

- Have portable gas detectors to be used during test execution?
- Warning signs, see the Regulations on Safety signs and signaling in the workplace

8.7 Special actions.

For example:
- Monitoring.
- Safety preparedness.
- Safe Job Analysis of modifications, (SJA)
- Working at heights
- Flammable / toxic gases or chemicals

9 QUANTIFYING OF RISK - RISK MATRIX

See Chapter 14 "Guide to the report template".
The risk matrix will provide visualization and an overview of activity risks so that management and users get the most complete picture of risk factors.

IDnr	Aktivitet-hendelse	Frekv-Sans	Kons	RV
xx	*Rotating shaft, locked room*	1	C1	C1
	Much noise, people without protective gear enter the rig site *Barriers and running experiments outside working hours*	1	B1	B1

Conclusion : *Participants will make a comprehensive assessment to determine whether the remaining risks of the activity / process is acceptable. Barriers and driving outside working hours e.g.*

10 CONCLUSJON

The rig is built in good laboratory practice (GLP).
What technical changes or changes in operating parameters will require new risk assessment?
(Other media, pressure, mechanical intervention)

Experiment unit card get a period of **XX months**
Experiment in progress card get a period of **XX months**

11 REGULATIONS AND GUIDELINES

Se http://www.arbeidstilsynet.no/regelverk/index.html

- Lov om tilsyn med elektriske anlegg og elektrisk utstyr (1929)
- Arbeidsmiljøloven
- Forskrift om systematisk helse-, miljø- og sikkerhetsarbeid (HMS Internkontrollforskrift)
- Forskrift om sikkerhet ved arbeid og drift av elektriske anlegg (FSE 2006)
- Forskrift om elektriske forsyningsanlegg (FEF 2006)
- Forskrift om utstyr og sikkerhetssystem til bruk i eksplosjonsfarlig område NEK 420
- Forskrift om håndtering av brannfarlig, reaksjonsfarlig og trykksatt stoff samt utstyr og anlegg som benyttes ved håndteringen
- Forskrift om Håndtering av eksplosjonsfarlig stoff
- Forskrift om bruk av arbeidsutstyr.
- Forskrift om Arbeidsplasser og arbeidslokaler
- Forskrift om Bruk av personlig verneutstyr på arbeidsplassen
- Forskrift om Helse og sikkerhet i eksplosjonsfarlige atmosfærer
- Forskrift om Høytrykksspyling
- Forskrift om Maskiner
- Forskrift om Sikkerhetsskilting og signalgivning på arbeidsplassen
- Forskrift om Stillaser, stiger og arbeid på tak m.m.
- Forskrift om Sveising, termisk skjæring, termisk sprøyting, kullbuemeisling, lodding og sliping (varmt arbeid)
- Forskrift om Tekniske innretninger
- Forskrift om Tungt og ensformig arbeid
- Forskrift om Vern mot eksponering for kjemikalier på arbeidsplassen (Kjemikalieforskriften)
- Forskrift om Vern mot kunstig optisk stråling på arbeidsplassen
- Forskrift om Vern mot mekaniske vibrasjoner
- Forskrift om Vern mot støy på arbeidsplassen

Veiledninger fra arbeidstilsynet
se: http://www.arbeidstilsynet.no/regelverk/veiledninger.html

12 DOCUMENTATION

- Tegninger, foto, beskrivelser av forsøksoppsetningen
- Hazop_mal
- Sertifikat for trykkpåkjent utstyr
- Håndtering avfall i NTNU
- Sikker bruk av LASERE, retningslinje
- HAZOP_MAL_Prosedyre
- Forsøksprosedyre
- Opplæringsplan for operatører
- Skjema for sikker jobb analyse, (SJA)
- Apparaturkortet
- Forsøk pågår kort

13   GUIDANCE TO RISK ASSESSMENT TEMPLATE

Kap 7 Assessment of technical safety.
Ensure that the design of the experiment set up is optimized in terms of technical safety.
Identifying risk factors related to the selected design, and possibly to initiate re-design to ensure that risk is eliminated as much as possible through technical security.
This should describe what the experimental setup actually are able to manage and acceptance for emission.

7.1 HAZOP
The experimental set up is divided into nodes (eg motor unit, pump unit, cooling unit.). By using guidewords to identify causes, consequences and safeguards, recommendations and conclusions are made according to if necessary safety is obtained. When actions are performed the HAZOP is completed.
(e.g. "No flow", cause: the pipe is deformed, consequence: pump runs hot, precaution: measurement of flow with a link to the emergency or if the consequence is not critical used manual monitoring and are written into the operational procedure.)

7.2 Flammable, reactive and pressurized substances and gas.
According to the Regulations for handling of flammable, reactive and pressurized substances and equipment and facilities used for this:

Flammable material: Solid, liquid or gaseous substance, preparation, and substance with occurrence or combination of these conditions, by its flash point, contact with other substances, pressure, temperature or other chemical properties represent a danger of fire.
Reactive substances: Solid, liquid, or gaseous substances, preparations and substances that occur in combinations of these conditions, which on contact with water, by its pressure, temperature or chemical conditions, represents a potentially dangerous reaction, explosion or release of hazardous gas, steam, dust or fog.
Pressurized : Other solid, liquid or gaseous substance or mixes havinig fire or hazardous material response, when under pressure, and thus may represent a risk of uncontrolled emissions

Further criteria for the classification of flammable, reactive and pressurized substances are set out in Annex 1 of the Guide to the Regulations "Flammable, reactive and pressurized substances"
http://www.dsb.no/Global/Publikasjoner/2009/Veiledning/Generell%20veiledning.pdf
http://www.dsb.no/Global/Publikasjoner/2010/Tema/Temaveiledning_bruk_av_farlig_stoff_Del_1.pdf

Experiment setup area should be reviewed with respect to the assessment of Ex zone
• Zone 0: Always explosive atmosphere, such as inside the tank with gas, flammable liquid.
• Zone 1: Primary zone, sometimes explosive atmosphere such as a complete drain

point
• Zone 2: secondary discharge could cause an explosive atmosphere by accident, such as flanges, valves and connection points

7.4 Effects on the environment
With pollution means: bringing solids, liquid or gas to air, water or ground, noise and vibrations, influence of temperature that may cause damage or inconvenience effect to the environment.
Regulations: http://www.lovdata.no/all/hl-19810313-006.html#6
NTNU guidance to handling of waste:http://www.ntnu.no/hms/retningslinjer/HMSR18B.pdf

7.5 Radiation
Definition of radiation

Ionizing radiation: Electromagnetic radiation (in radiation issues with wawelength <100 nm) or rapid atomic particles (e.g. alpha and beta particles) with the ability to stream ionized atoms or molecules.
Non ionizing radiation: Electromagnetic radiation (wavelength >100 nm), og ultrasound$_1$ with small or no capability to ionize.
Radiation sources: All ionizing and powerful non-ionizing radiation sources.
Ionizing radiation sources: Sources giving ionizing radiation e.g. all types of radiation sources, x-ray, and electron microscopes.
Powerful non ionizing radiation sources: Sources giving powerful non ionizing radiation which can harm health and/or environment, e.g. class 3B and 4. MR$_2$ systems, UVC$_3$ sources, powerful IR sources$_4$.
$_1$Ultrasound is an acoustic radiation ("sound") over the audible frequency range (> 20 kHz). In radiation protection regulations are referred to ultrasound with electromagnetic non-ionizing radiation. $_2$MR (e.g. NMR) - nuclear magnetic resonance method that is used to "depict" inner structures of different materials. $_3$UVC is electromagnetic radiation in the wavelength range 100-280 nm. $_4$IR is electromagnetic radiation in the wavelength range 700 nm - 1 mm.

For each laser there should be an information binder (HMSRV3404B) which shall include:
• General information
• Name of the instrument manager, deputy, and local radiation protection coordinator
• Key data on the apparatus
• Instrument-specific documentation
• References to (or copies of) data sheets, radiation protection regulations, etc.
• Assessments of risk factors
• Instructions for users
• Instructions for practical use, startup, operation, shutdown, safety precautions, logging, locking, or use of radiation sensor, etc.
• Emergency procedures
See NTNU for laser: http://www.ntnu.no/hms/retningslinjer/HMSR34B.pdf

7.6 Usage and handling of chemicals.
In the meaning chemicals, a element that can pose a danger to employee safety and health
See: http://www.lovdata.no/cgi-wift/ldles?doc=/sf/sf/sf-20010430-0443.html

Safety datasheet is to be kept in the HSE binder for the experiment set up and registered in the database for chemicals.

Kap 8 Assessment of operational procedures.

Ensures that established procedures meet all identified risk factors that must be taken care of through operational barriers and that the operators and technical performance have sufficient expertise.

8.1 Prosedure Hazop

Procedural HAZOP is a systematic review of the current procedure, using the fixed HAZOP methodology and defined guidewords. The procedure is broken into individual operations (nodes) and analyzed using guidewords to identify possible nonconformity, confusion or sources of inadequate performance and failure.

8.2 Procedure for running experiments and emergency shutdown.

Have to be prepared for all experiment setups.

The operating procedure has to describe stepwise preparation, startup, during and ending conditions of an experiment. The procedure should describe the assumptions and conditions for starting, operating parameters with the deviation allowed before aborting the experiment and the condition of the rig to be abandoned.

Emergency procedure describes how an emergency shutdown have to be done, (conducted by the uninitiated),

what happens when emergency shutdown, is activated. (electricity / gas supply) and

which events will activate the emergency shutdown (fire, leakage).

Kap 9 Quantifying of RISK

Quantifying of the residue hazards, Risk matrix
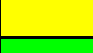
To illustrate the overall risk, compared to the risk assessment, each activity is plo tted with values for the probability and consequence into the matrix. Use task IDnr.

Example: If activity IDnr. 1 has been given a probability 3 and D for consequence the risk value become D3, red. This is done for all activities giving them risk values.

In the matrix are different degrees of risk highlighted in red, yellow or green. When an activity ends up on a red risk (= unacceptable risk), risk reducing action has to be taken

CONSEQUENSES		Svært liten	Liten	Middels	Stor	Svært Stor
	Svært alvorlig	E1	E2	E3	E4	E5
	Alvorlig	D1	D2	D3	D4	D5
	Moderat	C1	C2	C3	C4	C5
	Liten	B1	B2	B3	B4	B5
	Svært liten	A1	A2	A3	A4	A5
		PROBABILITY				

The principle of the acceptance criterion. Explanation of the colors used in the matrix

Farge		Beskrivelse
Rød		Unacceptable risk Action has to be taken to reduce risk
Gul		Assessment area. Actions has to be concidered
Grønn		Acceptable risk. Action can be taken based on other criteria

Attachment to Risk Assessment report

[Wet gas impeller test facility]

Prosjekttittel	
Prosjektleder	Lars Erik Bakken
Enhet	NTNU
HMS-koordinator	Erik Langørgen
Linjeleder	Olav Bolland
Plassering	
Romnummer	
Riggansvarlig	[Trond Grüner]
Risikovurdering utført av	Lars Andreas Øvrum Sørvik, Erik Mele

TABLE OF CONTENTS

• ATTACHMENT A HAZOP MAL

Project: Impeller rig						Page	
Node: 1 DRIVERSYSTEM						1	

Driver system: frekvensomformer, el.motor, lagerbukk og smøreenhet, (oljeaggregat)

Ref #	Guideword	Causes	Consequences	Safeguards	Rec#	Recommendations	Action
1	No flow	Oljeaggregat går ikke	Varmgang, lagerhavari	Varsellampe "alarm" Registrering av flow Temperaturmåling "shut down" ved overtemp. PLS overvåkning el.motor starter ikke Manuell resettfunksjon	Systemuttestin g med manuell overvåkning, min to personer		Varsellampe styres av pls. Registrering av flow i pls. Pls styrer start av impellermotor.
		Tom for olje	-"- oljepumpehavari	Nivåmåling oljetank		Oljenivåsignal tas inn i styreprogram	Forsvinner oljestrømmen under drift eller overtemp, må pls resettes Nivåmåling i pls. Styrer start av oljeaggregat
2	Reverse flow	Koblingsfeil	Lekkasje Oljepumpehavari Motor vil ikke starte		systemtestin g	Lekkasjesøk inngår i driftsprosedyre	
		Slangebytte	-"-	Ulike slangefittings			OK (tgg)

Project: Impeller rig
Node: 1 DRIVERSYTEM

	Page
	1

Driver system: frekvensomformer, el.motor, lagerbukk og smøreenhet, (oljeaggregat)

Ref #	Guideword	Causes	Consequences	Safeguards	Rec#	Recommendations	Action
3	More flow	Feil trykkinnstilling	Lekkasje	Manometerovervåking		Trykkontroll inngår i driftsprosedyre Trykkmåling tas inn i systemovervåking	Trykkontroll inngår i driftsprosedyre (manometer)lav nivå olje er i systemovervåk ning
4	Less flow	Tett filter	Varmgang i lager	trykkbryter		Trykkbryter signal legges inn i systemovervåknin g Kontroll av filter tas inn i driftsprosedyre	Trykkmåling i filter. Ivaretas av pls.
5	More level	overfylling	oljesøl	nivåglass		driftsprosedyre	Påpasselighet ved fylling
6	Less level	For lite olje	Varmgang	Temperaturkontroll Signal fra temperaturkontroll ligger i systemovervåkning Nivåbryter i oljetank		Signal tas inn i systemovervåking	Nivåmåling ok. Pls styrer drift av smøreaggregatet og impellermotore n.
7	More pressure	Se ref 3					

Project: Impeller rig
Node: 1 DRIVERSYTEM

Page 1

Driver system: frekvensomformer, el.motor, lagerbukk og smøreenhet, (oljeaggregat)

Ref #	Guideword	Causes	Consequences	Safeguards	Rec#	Recommendations	Action #
8	Less pressure	Se ref 4					
9	More temperature	Manglende smøring	Varmgang motor	Se Ref:1, 4, 6, 8			Pls styrer tempmåling. Først lysalarm, deretter shutdown
		Manglende kjøling	Varmgang frekvensomforme r	6 stk temperaturfølere koblet til systemovervåking			Varsellys på ved testrigg og i kontrollrom Frekvensomform er plasseres med tilgang på kjøleluft
		Varmgang frekvensomforme r	Temperaturovervåknin g i frekvensomformer	Lastbegrensing i frekvensomformer			
		For høy last	Varmgang motor	Lastbegrensing i frekvensomformer			Tempmåling i omformer ok. Ferdig programmert i softwaren.
			Varmgang frekvensomforme	Lastbegrensing i frekvensomformer			

Project: Impeller rig
Node: 1 DRIVERSYSTEM

Page
1

Driver system: frekvensomformer, el.motor, lagerbukk og smøreenhet, (oljeaggregat)

Ref #	Guideword	Causes	Consequences	Safeguards	Rec#	Recommendations	Action #
10	Less temperature	NA	Mekanisk overlast r				
11	More viscosity	Feil oljetype	Ref: 4			Oljetype ivaretas i driftsprosedyre	OK (tgg)
12	Less viscosity	Feil oljetype	Ref: 3			Oljetype ivaretas i driftsprosedyre	OK (tgg)
13	Composition Change	NA					
14	Contamination	Støv inn i frekvensomforme r	Kortslutning varmgang Kortslutning varmgang	Industritype motor Filterduk		Jevnlig støvsuging	Inn i driftsprosedyre
15	Relief, (trykkavlastning)	Støv inn i motor	Kortslutning varmgang	Overtrykksventil i aggregat			ok
16	Instrumentation	Uheldig rask Turtallsøkning		Frekvensomformer og el.motor er tilpasset hverandre		"Ramp time" på frekvensomforme r.	ok

4

Driver system: frekvensomformer, el.motor, lagerbukk og smøreenhet, (oljeaggregat)

Ref #	Guideword	Causes	Consequences	Safeguards	Rec#	Recommendations	Action #
17	Sampling	NA	NA				
18	Corrosion/erosion	NA					
19	Service failure	Strømutfall PC utfall	Motorstopp Fullt turtall på motor	Utstyret tåler dette Nødstoppbrytere blir plassert hensiktsmessig		Nødstopp styrer kontaktor og rele. Må resettes for hver gang strømmen har vært borte.	
		Olje tilførsel Mekanisk havari	Ref:3 og 4 driftsstopp	Beskyttelses deksel rundt roterende deler		Deksel reduserer utkast av komponenter	
				Uvedkommende skal ikke oppholde seg ved testrigg under drift		Beskrives i driftsprosedyre	
20	Abnormal operation,	Strømutfall PC utfall Nødavstegning Feilsøking	Ingen Ref:19 Ingen Ingen			Benytt SJA	Utføres med GLP

Project: Impeller rig
Node: 1 DRIVERSYTEM

	Page
	1

Driver system: frekvensomformer, el.motor, lagerbukk og smøreenhet, (oljeaggregat)

Ref #	Guideword	Causes	Consequences	Safeguards	Rec#	Recommendations	Action
21	Maintenance	Demontasje Montasje	ingen	Lab rutiner for dette. Vedlikeholdspeosedyre		Benytt SJA	Utføres med GLP
	Ignition		Ingen HC i forbindelse med rigg	Lab rutiner for koordinering av forsøkskjøring			OK
	Spare equipment	NA	rigg				
	Safety	Høy lyd	hørselsskade	Hørselsvern Skilting Støysoner Tidsregulert forsøkskjøring Labrutiner for koordinering av forsøkskjøring		Beskrives i driftsprosedyre	OK

NTNU

Project: Impeller rigg
Node: 2
Kompressorsystem

Page

SINTEF

Ref #	Guideword	Causes	Consequences	Safeguards	Rec#	Recommendations	Action
1	No flow	Motor går ikke Ventil stengt	ingen For høy temperatur	Temperatur måler inn i systemovervåking		Temperatur grenser settes i systemovervåking Alarmlampe ved for høy temperatur	OK Lampe, stopp ved høy høy nivå
		nnløp blokkert	Se pkt: "ventil stengt"	Kontroll tas inn i driftsprosedyre Gitter i front av innløp		Egen oppstartsprosedyre lages	
2	Reverse flow	Betjeningsfeil Programeringsfeil koblingsfeil	ingen	Turtallskontroll i frekvensomformer		Dreieretning kontrolleres i oppstartsprosedyre	OK
3	More flow	Turtall ut over driftsparameter	Ødelagt impeller	Turtallssperre i frekvensomformer		Kun ett program og fil for driftsoppsett	Ett oppsett lagret på server
4	Less flow	Ref:1					
5	More level	NA					
6	Less level	NA					

Ref #	Guideword	Causes	Consequences	Safeguards	Rec#	Recommendations	Action #
7	More pressure	Blokkert utløp, stengt ventil	Ref:1	Trykkføler med HH alarm til systemovervåkning		Behov vurderes i årsaksdiagram	Utløpstrykk måles i pls. Overtrykk medfører aut. nedstengning
8	Less pressure	Ref:1					
9	More temperature	Ref:1	Varm overflatetetemperatur på komponenter Fare for brannskader på personell			Isolering eller skjerming av varme komponenter	OK
10	Less temperature	NA					
11	More viscosity	NA					
12	Less viscosity	NA					
13	Composition	NA					

Project: Impeller rigg					Page		
Node: 2							
Kompressorsystem							

Ref #	Guideword	Causes	Consequences	Safeguards	Rec#	Recommendations	Action #
	Change						
14	Contamination	NA					
15	Relief	NA					
16	Instrumentation	Uheldig plassering av temperaturmåler Feilmontasje	Feil måling av utløpstemperatur Feil mengde måling Feil målinger	Plassering av temperatur transmitter Følg leverandørens spesifikasjoner Korrekt montasje av kabler		Kontroller leverandørens anbefalinger Beskrives i driftsprosedyrer Kontrolleres og kalibreres før drift	Benytter ASME standard, OK
17	Sampling	NA					
18	Corrosion/erosion	NA					
19	Service failure	Bortfall av måleinstrumenter Kabelbrudd Mekanisk havari	Bortfall av feilmeldinger og nedstengningsfunksjoner Økonomisk og tidsplan	Manuell overvåkning og nødstopp Solid		Nullpunkt legges til verdi over null	Programmert i pls. Alarm og shutdown.

Ref #	Guideword	Causes	Consequences	Safeguards	Rec#	Recommendations	Action
			overskridelser Trond blir ikke Dr Grüner	kompressorhus, lav sannsynlighet for personskade			
20	Abnormal operation	Nødstopp Ref:1 og node 1	ingen				Nødstopp kutter all strøm til motor.
21	Maintenance	Inspeksjon av kompressor	feilmontasje	Styrepinner Utføres av kvalifisert personell Støy fra frekvensomformer indikerer at strøm er slått på		Inspeksjon dokumenteres i prosedyre Hovedsikring låses ut SJA på vedlikehold	Ivaretatt vedlikeholdsprosedyre
22	Ignition	NA					
23	Spare equipment	NA					
24	Safety	Ref: 21 og node 1		Nødstopp bryter, solid kompressorhus Prosedyrer			2 separate nødstoppbrytere

Project: Impeller rigg					Page		
Node: 2 Kompressorsystem							
Ref #	Guideword	Causes	Consequences	Safeguards	Rec#	Recommendations	Action #
				Verneutstyr Skilting og varsling			

- **ATTACHMENT B PRØVESERTIFIKAT FOR LOKAL TRYKKTESTING**

Trykktesten skal utføres I følge NS-EN 13445 del 5 (Inspeksjon og prøving).
Se også prosedyre for trykktesting gjeldende for VATL lab

Trykkpåkjent utstyr: ……………………….

Benyttes i rigg: ……………………………………….

Design trykk for utstyr: …………………..bara

Maksimum tillatt trykk: …………………..bara
(i.e. burst pressure om kjent)

Maksimum driftstrykk i denne rigg: …………………..bara

Prøvetrykket skal fastlegges i følge standarden og med hensyn til maksimum tillatt trykk.

Prøvetrykk: …………….bara   (………. x maksimum driftstrykk)
                    I følge standard

Test medium: _____

Temperatur: _____°C

Start: Tid: _____

          Trykk: _____bara

Slutt: Tid: _____

          Trykk: _____bara

Eventuelle repetisjoner fra atm. trykk til maksimum prøvetrykk:…………….

Test trykket, dato for testing og maksimum tillatt driftstrykk skal markers på (skilt eller innslått)

_____   _____
Sted og dato   Signatur

NTNU   ◉ SINTEF

- **ATTACHMENT F HAZOP TEMPLATE PROCEDURE**

Project:
Node: 1

Page

Ref #	Guideword	Causes	Consequences	Safeguards	Recommendations	Action	Date Sign
	Not clear procedure	Procedure is to ambitious, or confusingly					
	Step in the wrong place	The procedure can lead to actions done in the wrong pattern or sequence					
	Wrong actions	Procedure improperly specified					
	Incorrect information	Information provided in advance of the specified action is wrong					
	Step missing	Missing step, or step requires too much of operator					
	Step unsucessful	Step has a high probability of failure					
	Influence and effects from other	Procedure's performance can be affected by other sources					

Experiment, name, number:	Date/ Sign
Project Leader:	
Experiment Leader:	
Operator, Duties:	

	Conditions for the experiment:	Completed
	Experiments should be run in normal working hours, 08:00-16:00 during winter time and 08.00-15.00 during summer time. Experiments outside normal working hours shall be approved.	
	One person must always be present while running experiments, and should be approved as an experimental leader.	
	An early warning is given according to the lab rules, and accepted by authorized personnel.	
	Be sure that everyone taking part of the experiment is wearing the necessary protecting equipment and is aware of the shut down procedure and escape routes.	
	Preparations	**Carried out**
	Post the "Experiment in progress" sign.	
	Start up procedure	
	During the experiment	
	Control of temperature, pressure e.g.	
	End of experiment	
	Shut down procedure	
	Remove all obstructions/barriers/signs around the experiment.	
	Tidy up and return all tools and equipment.	
	Tidy and cleanup work areas.	
	Return equipment and systems back to their normal operation settings (fire alarm)	
	To reflect on before the next experiment and experience useful for others	
	Was the experiment completed as planned and on scheduled in professional terms?	
	Was the competence which was needed for security and completion of the experiment available to you?	
	Do you have any information/ knowledge from the experiment that you should document and share with fellow colleagues?	

- **ATTACHMENT H TRAINING OF OPERATORS**

Experiment, name, number:	Date/ Sign
Project Leader:	
Experiment Leader:	
Operator	

	Knowledge to EPT LAB in general	
	Lab - Access -routines and roules -working hour	
	Knowledge about the evacuation procedures.	
	Activity calendar for the Lab	
	Knowledge to the experiments	
	Procedures for the experiments	
	Emergency shutdown.	
	Nearest fire and first aid station.	

Operatør	**HMS responsible**
Dato	**Dato**
Signert	**Signert**

14   ATTACHMENT I FORM FOR SAFE JOB ANALYSIS

SJA tittel:		
Dato:	Sted:	
Kryss av for utfylt sjekkliste:		

Deltakere:		
SJA-ansvarlig:		

Arbeidsbeskrivelse: (Hva og hvordan?)

Risiko forbundet med arbeidet:

Beskyttelse/sikring: (tiltaksplan, se neste side)

Konklusjon/kommentar:

Anbefaling/godkjenning:	Dato/Signatur:	Anbefaling/godkjenning:	Dato/Signatur:
SJA-ansvarlig:		Områdeansvarlig:	
Ansvarlig for utføring:		Annen (stilling):	

HMS aspekt	Ja	Nei	Ikke aktuelt	Kommentar / tiltak	Ansv.
Dokumentasjon, erfaring, kompetanse					
Kjent arbeidsoperasjon?					
Kjennskap til erfaringer/uønskede hendelser fra tilsvarende operasjoner?					
Nødvendig personell?					
Kommunikasjon og koordinering					
Mulig konflikt med andre operasjoner?					
Håndtering av en evnt. hendelse (alarm, evakuering)?					
Behov for ekstra vakt?					
Arbeidsstedet					
Uvante arbeidsstillinger?					
Arbeid i tanker, kummer el.lignende?					
Arbeid i grøfter eller sjakter?					
Rent og ryddig?					
Verneutstyr ut over det personlige?					
Vær, vind, sikt, belysning, ventilasjon?					
Bruk av stillaser/lift/seler/stropper?					
Arbeid i høyden?					
Ioniserende stråling?					
Rømningsveier OK?					
Kjemiske farer					
Bruk av helseskadelige/giftige/etsende kjemikalier?					
Bruk av brannfarlige eller eksplosjonsfarlige kjemikalier?					
Må kjemikaliene godkjennes?					
Biologisk materiale?					
Støv/asbest?					
Mekaniske farer					
Stabilitet/styrke/spenning?					
Klem/kutt/slag?					
Støy/trykk/temperatur?					
Behandling av avfall?					
Behov for spesialverktøy?					
Elektriske farer					
Strøm/spenning/over 1000V?					
Støt/krypstrøm?					
Tap av strømtilførsel?					
Området					
Behov for befaring?					
Merking/skilting/avsperring?					
Miljømessige konsekvenser?					
Sentrale fysiske sikkerhetssystemer					
Arbeid på sikkerhetssystemer?					
Frakobling av sikkerhetssystemer?					
Annet					

15 ATTACHMENT J APPARATURKORT UNITCARD

Apparatur/unit

Dette kortet SKAL henges godt synlig på apparaturen!*This card MUST be posted on a visible place on the unit!*

Faglig Ansvarlig (Scientific Responsible)	**Telefon mobil/privat** (Phone no. mobile/private)
Apparaturansvarlig (Unit Responsible)	**Telefon mobil/privat** (Phone no. mobile/private)

Sikkerhetsrisikoer (Safety hazards)
Sikkerhetsregler Safety rules)
Nødstopp prosedyre Emergency shutdown)

Her finner du (Here you will find):

Prosedyrer (Procedures)
Bruksanvisning (Users manual)

Nærmeste (nearest)

Brannslukningsapparat (fire extinguisher)	
Førstehjelpsskap (first aid cabinet)	

NTNU
Institutt for energi og prosessteknikk

SINTEF Energi
Avdeling energiprosesser

Dato

Dato

_____

_____

Signert

Signert

_____

_____

16 ATTACHMENT K FORSØK PÅGÅR KORT

Forsøk pågår!
Experiment in progress!

Dette kort skal settes opp før forsøk kan påbegynnes This card has to be posted before an experiment can start

Ansvarlig / Responsible	Telefon jobb/mobil/hjemme
Operatører/Operators	Forsøksperiode/Experiment time(start – slutt)
Prosjektleder	Prosjekt

Kort beskrivelse av forsøket og relaterte farer
 Short description of the experiment and related hazards

NTNU
Institutt for energi og prosessteknikk

SINTEF Energi
Avdeling energiprosesser

Dato

Dato

_____

_____

Signert

Signert

_____

_____

1. Grüner, T.G.a.L.E.B., *Aerodynamic instability investigation of a centrifugal compressor exposed to wet gas.* 2010.

		utarbeidet av	Nummer	dato
EPT HMS-håndbok	**4.5.8 Apparaturkort**	E. Langørgen	HMSEPT-458	10/28/2009
		Godkjent av	side	erstatter
			1 av1	

Apparaturkort

UTSTYRSENHET/INSTRUMENT
(Unit/Instrument)
Impeller-rigg

Apparaturansvarlig (navn/tlf jobb/hjemme) varsles hvis noe er galt
(Instrument responsible – alert if anything goes wrong)
Trond G Grüner 99011717 / 735 92797

Linjeleder eller stedlig representant
(Research manager or local representative)
Morten Grønli

Godkjente (opplærte) operatører
Trond G. Grüner
Lars E. Bakken

Sikkerhetsrisikoer
(Safety hazards)
Støy ved drift.
|

Sikkerhetsregler
(Safety rules/precautions)
Området er avgrenset. Ingen adgang for uvedkommende.
Bruk av verneutstyr i hht forsøk pågår skilt. (støy, meget høy støy)

Slik slås utstyret av i et krisetilfelle
(Emergency turn-off-procedure)
Nødstopp i impeller rom benyttes.

Her finner du :
(Here you will find:)
- First aid suitcase, HMS skap ved heis I 1. Etg.
- Fire extinguisher Slangepost ved slusa.

NTNU
ENERGI OG PROSESSTEKNIKK
Dato:.....7/11-09

Signert:...............
(Dette kortet skrives ut/kopieres på lysegrønt papir, "Colorit lime green" 140/160 g)

Impeller rigg

WARNINGS FOR THIS ZONE

Restricted area
Give attention to "Experiment in progress" sign
Containing one gas bottle

PÅBUDT VERNEUTSTYR I SONE
PERSONAL PROTECTIVE EQUIPMENT
MANDATORY IN ZONE

	Trykk start på skapdør	
	Slå over hovedbryter til impellerrig Q1	
4	Velg flowmåler, blendeplate eller turbinmåler (1: 0,3-1,2 kg/s xxxs) Labview	
5	Motor kjøres trinnvis opp til 3000 rpm. Drift under 3000 rpm unngås.	
#	**Drift**	*Utført*
1	Periodevis kontroll av utløpstemperatur og trykk	
2	Periodevis kontroll av oljetrykk	
	Periodevis kontroll av oljelekkasje	
	Periodevis kontroll av vikling og lagertemperatur	
	Pumpefilter skal jevnlig undersøkes	
	Manuell kontroll av temperatur på blokka	
	Periodevis kontroll av utluft	
	Vær obs på unormal støy og vibrasjon	
	Unngå ugunstige turtall, (kvin og vibrasjon)	

#	**Ved injeksjon av vann**	*Utført*
	Sjekk om tilstrekkelig med vann på tank	
1	Kontroller vannlinje, Åpne ventiler,	
	Start pumpe – kontroll av innløpstrykk*	
	Juster mengde rolig opp til ønsket vannmengde	
	Slå av pumpe, steng ventil etter at frekvens er 0 Hz	
	Steng ventiler….	
	Etter vanninjeksjon kjøres impeller i min 10 min uten vann	

#	**Nedstegning**	*Utført*
	Utløpsventil åpnes fullt	
	Motor stanses ved kontrollert nedkjøring	
	Slå av oljesmøring	
	Slå av frekvensomformer	

Nødstopp

Nødstopp benyttes ved behov for akutt stopp eller mistanke om uheldig drifttilstand som kan medføre skade på personell og/eller utstyr. Ved PC-utfall benyttes nødstopp. Reset aktiveres før igangkjøring.